



**UNIVERSITY
OF TRENTO - Italy**
DEPARTMENT OF INDUSTRIAL ENGINEERING

XXVI cycle

Doctoral School in Materials Science and Engineering

Effect of process parameters on the dimensional and geometrical precision of PM steel parts

**PhD student:
Melania Pilla**

**Tutors:
Ilaria Cristofolini
Alberto Molinari**

Year 2013

Contents

1	Introduction	5
2	Context and objective of the work.....	7
2.1	Dimensional and geometrical tolerances.....	7
2.1.1	Dimensional tolerances	7
2.1.2	Geometrical tolerances	8
2.1.2.1	Tolerances controlling the intrinsic shape of the features defining the parts	8
2.1.2.1.1	Flatness.....	8
2.1.2.1.2	Cylindricity.....	8
2.1.2.2	Orientation tolerance	9
2.1.2.2.1	Perpendicularity	9
2.1.2.2.2	Parallelism	9
2.1.2.3	Location tolerance.....	10
2.1.2.3.1	Concentricity-coaxiality	10
2.1.3	Typical tolerances for parts produced by PM conventional process	10
2.2	Parameter that affect the dimensions and the geometrical characteristics in PM technology	11
2.3	The objective of the present work	13
2.4	References	14
3	Experimental procedure.....	15
3.1	Measurement of the dimensions and geometrical characteristics.....	15
3.1.1	Introduction.....	15
3.1.2	Measurement procedure, a real part program	17
3.1.3	Characterization	19
3.2	References	19
4	Results	20
4.1	Powders.....	20
4.1.1	Swelling system	20
4.1.1.1	The DoE plan.....	20
4.1.1.2	Densification and microstructure	21
4.1.1.3	Dimensions in green and sintered state	23
4.1.1.4	Dimensional variation.....	25
4.1.1.5	Analysis of variance	26
4.1.1.6	Geometrical characteristics in green and sintered state.....	28
4.1.2	Shrinking system.....	31

4.1.2.1	Analysis of density and microstructure	31
4.1.2.2	Dimensions in green and sintered state.....	33
4.1.2.3	Dimensional variation.....	35
4.1.2.4	ANOVA analysis	36
4.1.2.5	Geometrical characteristics:.....	40
4.1.3	Conclusions.....	42
4.1.4	References	42
4.2	Compaction	44
4.2.1	The pulley	44
4.2.1.1	The steps of compaction	44
4.2.1.2	Dimensions in the green state.....	45
4.2.1.3	Density distribution	46
4.2.1.4	Geometric characteristics.....	48
4.2.2	The ring-shaped part	50
4.2.2.1	The steps of compaction	50
4.2.2.2	Dimensions in green state	52
4.2.2.3	Geometrical characteristics.....	54
4.2.2.4	Density distribution	55
4.2.2.5	Compaction cycle.....	56
4.2.3	Conclusions.....	59
4.2.4	References	59
4.3	Sintering.....	60
4.3.1	Fe-3%Cr-0.5%Mo-0.5%C.....	60
4.3.1.1	Density and microstructure.....	60
4.3.1.2	Dimensions in the green and sintered state, and dimensional variation.....	63
4.3.1.3	Geometrical characteristics.....	64
4.3.2	AISI 316L	67
4.3.2.1	Density and microstructure.....	67
4.3.2.2	Dimensions in green and sintering state, and dimensional variation	68
4.3.2.3	Geometrical characteristics.....	70
4.3.2.4	Study of the flatness	74
4.3.3	Conclusions.....	76
4.3.4	References	76
4.4	Post-sintering operation.....	78
4.4.1	Displacement control sizing.....	78

4.4.1.1	Dimensions and conicity	78
4.4.2	Force control sizing	79
4.4.2.1	Dimensions and conicity	79
4.4.2.2	Geometrical characteristics	81
4.4.2.3	Dimensional precision	82
4.4.3	Conclusions	83
5	Conclusion	84
6	Publications	86
6.1	Journals	86
6.2	Proceedings	86
7	Acknowledgements	88
8	Appendix A	89

1 Introduction

Powder Metallurgy is a net shape technology. In the conventional process, the powders are compacted in rigid dies to produce the so called green compact, which is then sintered to form the metallic bonding between the powder particles. Apart from some features, which cannot be realized in the uniaxial compaction (transversal holes, just as an example), the geometrical features are obtained during compaction and the dimensions of the green compact differ from the final one only by the dimensional change occurring during sintering. The proper management of all the production steps allows most of the dimensional and geometrical features required by the various applications to be obtained without the need of post-sintering machining. Any corrections of the dimensional and geometrical features prevents the cost effectiveness of the technology. Dimensional and geometrical precision of the sintered parts is very high. In many cases, even if some geometrical details and any strict tolerances required by the specific applications of the sintered parts cannot be obtained, a post-sintering machining or sizing is carried out without preventing the competitiveness of the technology.

The continuous development of the applications of Powder Metallurgy is supported by the availability of new powders (base powders, additives, lubricants) and by the innovation in compaction and in sintering promoted by powder, presses and furnaces manufacturers, and by the progress in design methodologies. This results in the continuous improvement of the performances, as well as in the continuous increase in the attainable geometrical complexity of the parts.

Despite of the importance of the dimensional and geometrical precision of sintered parts, the international literature is mostly focused on materials and processes. The knowledge of the influence of the materials and of the processing parameters on dimensional and geometrical precision belongs to the know-how of the part manufacturers, and it is mostly based on experience and on empirical relations. A systematic and comprehensive work on this subject has not been done even by the most important part manufacturers, and only a few information can be found in literature, without any practical reference to geometrical precision. However, such a work is of great importance to support the further development of Powder Metallurgy, in particular when the processing parameters are “forced” to further improve performances. As an example, sintering temperature of steel powders is nowadays limited to 1180-1250°C, due to the fear that the increased dimensional change induced by a higher temperature (which will further improve mechanical properties) may deteriorate the dimensional and geometrical precision. From this viewpoint, the approach of PM industry is still conservative.

Some years ago, the Mechanical Design and Metallurgy Group at Trento University started a research program in this field, by studying the effect of sintering temperature on the precision of parts produced with a novel Cr-Mo steel. On the basis of that experience, a systematic work was planned, which covers the whole of the process (from powders to secondary operations), with the aim of generating a solid knowledge on the influence of the processing parameters (materials and process) on dimensional and geometrical precision of the parts produced with the conventional PM process. The present PhD work is the first step of this project. Due to the very large amount of variables involved, the first step of the work was focused on some of them, just to build up a base to be progressively implemented through further investigation. The work considers two types of

powders, the Fe-Cu-C and the Fe-Cr-Mo-C systems; they represent the most widely used material for the mass production of structural parts and a highly performing material recently introduced into the market, respectively. The variables investigated are the composition, the lubricant, the type of copper powder for Fe-Cu-C parts and, in case of the Cr-Mo steel, the sintering temperature and the cooling rate; these variables represent the most important ones which are taken in consideration to adapt the properties to the requirements of the sintered products. Through a full factorial DoE approach, their effect on dimensional and geometrical precision of disks was investigated. The simplicity of the geometry of the specimens allows the inherent effect of the powder related variables on precision to be investigated, eliminating the effect of the part geometry. Then the study moves to the two processing steps: compaction and sintering.

In case of compaction, two case studies involving specific compaction strategies were investigated, studying the dimensional and geometrical precision of two different quite complex parts produced using the two powders mentioned above. In case of sintering, the study was aimed at investigating the effect of a very high sintering temperature on dimensional and geometrical precision of two parts made of the Cr-Mo steel and of a stainless steel.

As a last step, the sizing operation of a Cu-C steel part was investigated, by comparing the conventional displacement control approach and the innovative force control operation. Even in this case, attention was concentrated on dimensional and geometrical precision.

The work has several original contents. First, geometrical characteristics are considered in addition to dimensional precision. From this viewpoint, the work represents the first systematic investigation of geometrical precision of sintered parts. To this purpose, a measurement procedure was defined and implemented, which is described in detail in Chapter 3 and represents another original content of the work. The data collected by the coordinate measuring machine (CMM) were processed to calculate the surfaces of the parts and to describe their geometrical characteristics in order to interpret their changes during the processing steps. Even if the focus of the work is dimensional and geometrical precision, the material microstructures were investigated in order to interpret dimensional changes during sintering and the effect of the porosity distribution on geometrical features. This is very important since the peculiar characteristic of Powder Metallurgy is that the shape of the part is determined in the compaction step, while the chemical and physical transformations responsible for the formation of the material microstructure are related to the subsequent sintering step, and they may significantly influence the dimensional variations. The attempt to correlate the material evolution to the changes in dimensions and geometry is another original figure of the work.

The work was carried out in cooperation with some of the most important PM industries: Höganäs AB, (Sweden) world leader in the powder production; SACMI, a highly qualified Italian press manufacturer; TFM and Sinteris, highly qualified Italian part manufacturers. The author expresses the great gratitude to these companies for their support and in particular to SACMI, that financed the PhD grant.

2 Context and objective of the work

2.1 Dimensional and geometrical tolerances

2.1.1 Dimensional tolerances

The nominal dimensions of a mechanical part are defined by the designer according to the functional requirements. These dimensions are referred to ideal surfaces, so that, referring to the production processes, it is necessary to define how much the real dimension can differ from the nominal one always ensuring the functionality of the part.

In the following work the tolerances used refer to the ISO IT classes shown in Fig. 2.1.1. [1]

Dimensione nominale mm		GRADI DI TOLLERANZA NORMALIZZATI																	
		IT1	IT2	IT3	IT4	IT5	IT6	IT7	IT8	IT9	IT10	IT11	IT12	IT13	IT14	IT15	IT16	IT17	IT18
oltre	fino a	Tolleranze																	
		μm									mm								
-	3	0,8	1,2	2	3	4	6	10	14	25	40	60	0,1	0,14	0,25	0,4	0,60	1	1,4
3	6	1	1,5	2,5	4	5	8	12	18	30	48	75	0,12	0,18	0,3	0,48	0,75	1,2	1,8
6	10	1	1,5	2,5	4	6	9	15	22	36	58	90	0,15	0,22	0,36	0,58	0,9	1,5	2,2
10	18	1,2	2	3	5	8	11	18	27	43	70	110	0,18	0,27	0,43	0,7	1,1	1,8	2,7
18	30	1,5	2,5	4	6	9	13	21	33	52	84	130	0,21	0,33	0,52	0,84	1,3	2,1	3,3
30	50	1,5	2,5	4	7	11	16	25	39	62	100	160	0,25	0,39	0,62	1	1,6	2,5	3,9
50	80	2	3	5	8	13	19	30	46	74	120	190	0,3	0,46	0,74	1,2	1,9	3	4,6
80	120	2,5	4	6	10	15	22	35	54	87	140	220	0,35	0,54	0,87	1,4	2,2	3,5	5,4
120	180	3,5	5	8	12	18	25	40	63	100	160	250	0,4	0,63	1	1,6	2,5	4	6,3
180	250	4,5	7	10	14	20	29	46	72	115	185	290	0,46	0,72	1,15	1,85	2,9	4,6	7,2
250	315	6	8	12	16	23	32	52	81	130	210	320	0,52	0,81	1,3	2,1	3,2	5,2	8,1
315	400	7	9	13	18	25	36	57	89	140	230	360	0,57	0,89	1,4	2,3	3,6	5,7	8,9
400	500	8	10	15	20	27	40	63	97	155	250	400	0,63	0,97	1,55	2,5	4	6,3	9,7
500	630	9	11	16	22	32	44	70	110	175	280	440	0,7	1,1	1,75	2,8	4,4	7	11
630	800	10	13	18	25	36	50	80	125	200	320	500	0,8	1,25	2	3,2	5	8	12,5
800	1000	11	15	21	28	40	56	90	140	230	360	560	0,9	1,4	2,3	3,6	5,6	9	14
1000	1250	13	18	24	33	47	66	105	165	260	420	660	1,05	1,65	2,6	4,2	6,6	10,5	16,5
1250	1600	15	21	29	39	55	78	125	195	310	500	780	1,25	1,95	3,1	5	7,8	12,5	19,5
1600	2000	18	25	35	46	65	92	150	230	370	600	920	1,5	2,3	3,7	6	9,2	15	23
2000	2500	22	30	41	55	78	110	175	280	440	700	1100	1,75	2,8	4,4	7	11	17,5	28
2500	3150	26	36	50	68	96	135	210	330	540	860	1350	2,1	3,3	5,4	8,6	13,5	21	33

Fig. 2.1.1 ISO IT Tolerance Classes [1]

2.1.2 Geometrical tolerances

ASME 14.5Y – 2009 is used to control the geometry of the parts. Table 2.1.1 reports all the geometrical tolerances and the symbols to be used on drawings.

Application	Type of tolerance	characteristics	Symbol
Individual features	Form	Straightness	—
		Flatness	
		Circularity	
		Cylindricity	
Individual or related features	Profile	Profile of a line	
		Profile of a surface	
Related features	Orientation	Angularity	
		Perpendicularity	
		Parallelism	
	Location	Position	
		Concentricity	
		Symmetry	
	Runout	Circular runout	
Total runout			

Table 2.1.1 Geometrical characteristics [2]

The definition of the geometrical tolerances used in this work are following reported.

2.1.2.1 Tolerances controlling the intrinsic shape of the features defining the parts

2.1.2.1.1 Flatness

The flatness “is the condition of a surface or derived median plane having all elements in one plane. A flatness tolerance specifies a tolerance zone defined by two parallel planes within which the surface or derived median plane must lie”. [2]

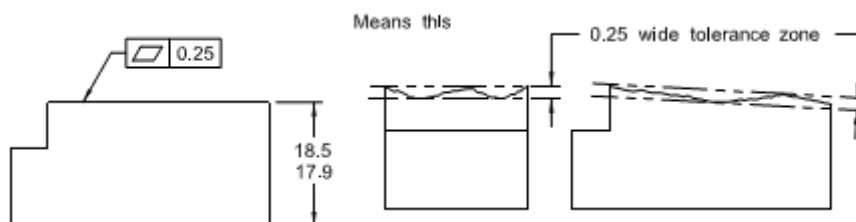


Fig. 2.1.2 Flatness condition [2]

2.1.2.1.2 Cylindricity

The cylindricity “is a condition of a surface of revolution in which all points of the surface are equidistant from a common axis. A cylindricity tolerance specifies a tolerance zone bounded by two concentric cylinders within which the surface must lie. [2]

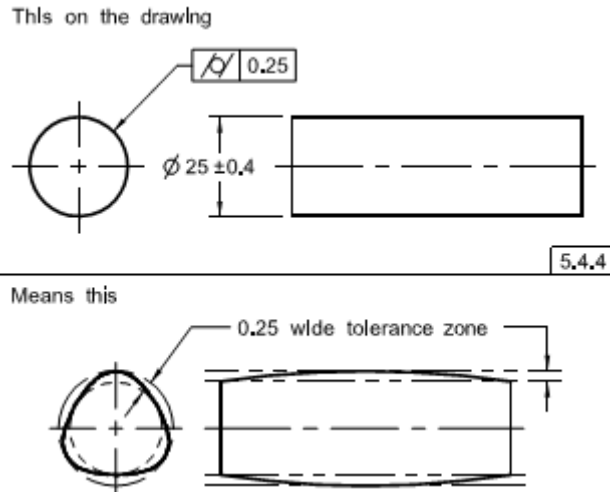


Fig. 2.1.3 Cylindricity condition

2.1.2.2 Orientation tolerance

“An orientation tolerance specifies a zone within which the considered feature, its line elements, its axis, or its center plane must be contained. An orientation tolerance specifies one of the following:

- (a) a tolerance zone defined by two parallel planes (...) parallel to, or perpendicular to one or more datum planes or a datum axis, within the surface or center plane of the considered feature must lie.(...)
- (c) a cylindrical tolerance zone (...) parallel to, or perpendicular to one or more datum planes or a datum axis, within which the axis of the consider feature must lie.”

2.1.2.2.1 Perpendicularity

The perpendicularity “is the condition of a surface, feature’s center plane, or feature’s axis at a right angle to a datum plane or a datum axis”

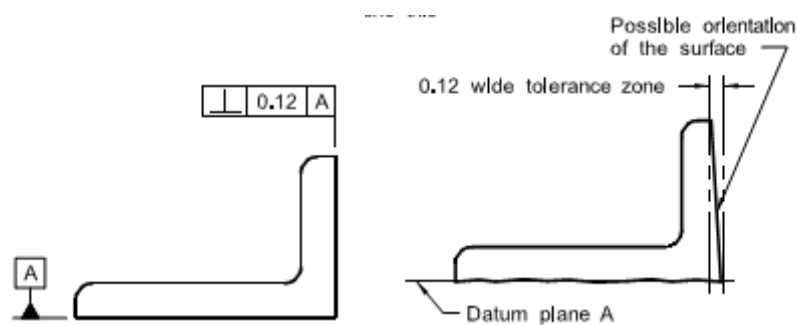


Fig. 2.1.4 Perpendicularity condition

2.1.2.2.2 Parallelism

The parallelism “is the condition of a surface, feature’s center plane, equidistant at all points from a datum plane”

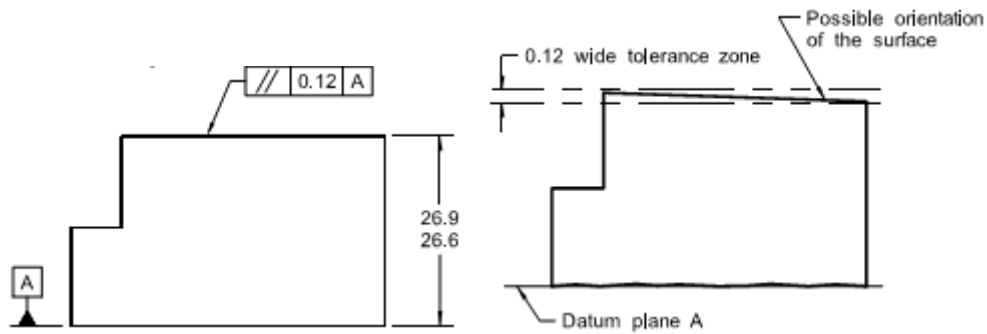


Fig. 2.1.5 Parallelism condition[2]

2.1.2.3 Location tolerance

2.1.2.3.1 Concentricity-coaxiality

The concentricity “is that condition where the median points of all diametrically opposed elements of a surface of revolution (...) are congruent with a datum axis. A concentricity tolerance is a cylindrical (...) tolerance zone whose axis (...) coincides with the axis (...) of the datum feature(s)”. [2]

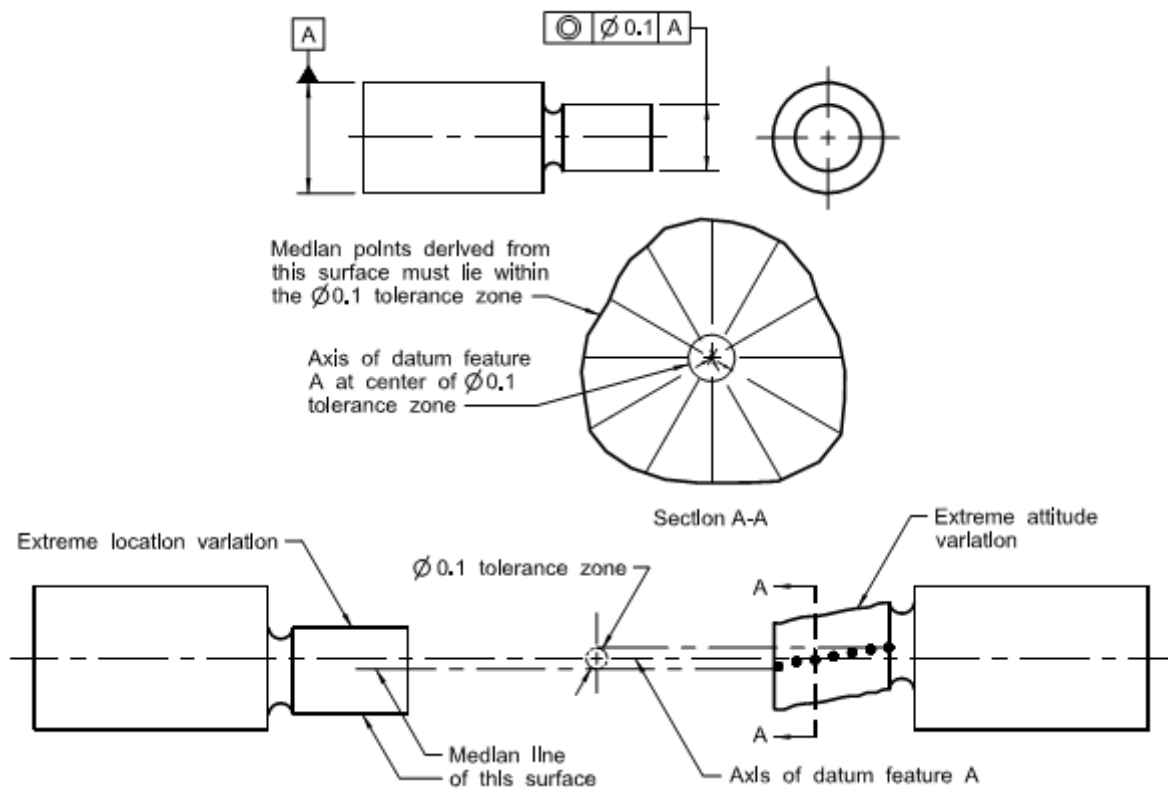


Fig. 2.1.6 Concentricity condition[2]

2.1.3 Typical tolerances for parts produced by PM conventional process

The dimensional precision of parts produced by the conventional PM process (cold compaction and sintering) is in general rather high. Due to the characteristics of the cold compaction process, dimensions parallel to the compaction direction are less precise than those perpendicular to it (in the compaction plane). With reference to the ISO IT classes, precision corresponds to IT11-12 for dimensions parallel to the compaction axis and IT9-10 for dimensions perpendicular to it [3]The

geometrical precision of parts produced by PM conventional process can be referred to the indication given by Assinter in its technical publication on design of the sintered parts [4]. In Table 2.1.2 are reported the typical attainable tolerances. To note that, in the Assinter technical publication, there is no reference for cylindricity, so the value for circularity (the corresponding 2-D tolerance) is taken as reference.

	Assinter indication
Dimension normal to compaction direction	IT8-9 (this value may be improved by sizing of 1 class tolerance)
Flatness	$\leq 0.001xD$ (where D is the maximum dimension of the flatness surface)
Cylindricity	(IT 8-10)/2
Parallelism	$\leq 0.002xD$ (where D is the maximum dimension of the flatness surface)
Perpendicularity	$\leq 0.002xD$

Table 2.1.2 Geometrical precision of PM technology, on the basis of reference data by Assinter

For the geometrical characteristics not in Table 2.1.2, the comparison is made with reference to the values measured in previous studies [5,6].

2.2 Parameter that affect the dimensions and the geometrical characteristics in PM technology

The standard powder metallurgy process is a net-shape, or near net-shape, technology that can be divided in four main steps: the production of powder, the shaping of powders to produce the green part, the sintering of the green parts and any secondary operations (the post-sintering treatment). The dimensional and geometrical precision of the final products depend on the processes involved in the four steps, and on the proper selection of the relevant parameters. With reference to the manufacturing process of a part, thus excluding the powder production, the chemical and physical characteristics of the powder mixture, the compaction parameters and strategy, the sintering parameters and all the variables of the different secondary operations not only influence the precision of the parts directly but even interact each other. For instance, the composition of the powder mixture influences the flowability and the filling homogeneity during compaction and the dimensional change during sintering. The whole of the effects is represented by Fig. 2.2.1.

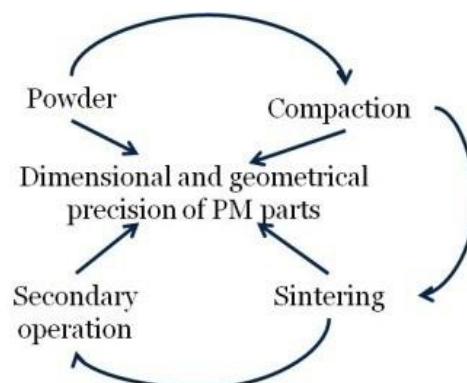


Fig. 2.2.1 The variables influencing the precision of parts in the PM process PM process

The influence of the different variables on the precision of parts in PM is scarcely reported in literature. There are a few papers [7-12], mainly focused on the Fe-Cu-C system, which however do not present any systematic study. The one systematic analysis on the effect of the process variables on dimensional precision was proposed by Bocchini [3], which does not consider geometrical characteristics. A short summary of the main variable affecting the dimensional precision of the parts is proposed in the following.

The powder influences the dimensional precision through the following factors:

1. any variation in the content of the smallest granulometric fraction, which mainly influences the apparent density, the powder flowability, its compressibility and the sintering dimensional change;
2. any variation in the distribution of the content of alloying elements, which mainly affect sintering dimensional change;
3. any variation in the content of lubricant, which affects flowability of the powder, its apparent density and its compressibility;
4. any variation in the content of additives, which influence the compressibility of the powder.

Since most of the part manufacturers buy the ready-to-press powder mixture, the quality of the powder is ensured by the powder producer.

The compaction of the powder to produce the green parts affects the precision through the following factors:

1. the dimensional tolerance of die and core rod;
2. the admissible wear of the die and core rod;
3. the scatter of the powder mass filled in the die cavity;
4. the homogeneity of the filling in the die cavity, which depends on the part geometry and dimensions;
5. any variation of the elastic compliance of the punches and, even less, of the machine;
6. any variation in the springback of the parts after ejection from the die cavity;
7. the precision of the tools design;
8. the quality of the press and the accuracy of the force and displacement controls;
9. the compaction strategy.

Some of these factors depend on the press and on the compaction strategy and control. The powder mixture influences springback of parts which depends on the green density. Any factors resulting from the forces applied to densify the powder have an increasing importance on increasing the green density of the parts.

Sintering affects the precision of parts since they are subject to dimensional changes. The sintering shrinkage or swelling depends on several parameters, all being critical in terms of effect on the precision of the sintered parts. The main parameters affecting dimensional changes are the composition of the powder, the sintering temperature and time, the sintering atmosphere, the green density and, in case of liquid phase sintering, the heating rate. In case of steels, the transformations of austenite on cooling contribute to dimensional change. As far as the effect on dimensional precision is concerned, the main factors are:

1. the homogeneity of the green density distribution within each part, which depends on the part dimensions and geometry, on the powder characteristics and on the compaction strategy;

2. the homogeneity of the temperature profile in the furnace, which depends on the quality of the plant and of the accuracy of its management and maintenance;
3. the size of the parts, which influences the heating rate and the actual temperature of the part along the sintering cycle.

In principle, the geometrical precision depends on the same factors, since it is mainly affected by the homogeneity of dimensional change within the single part. When sintering temperature is increased in order to improve the properties of the sintered parts, some part distortion may occur due to gravity [11]; however, this effect is relevant in some particular systems where a large amount of liquid phase forms during sintering.

Secondary operations contribute to dimensional and geometrical precision. In principle, there are two kinds of operations: those aiming at obtaining either specific properties (heat treatments for instance) or geometrical details which cannot be obtained by cold compaction (machining, joining) and those aimed at restoring the dimensional and geometrical precision lost during sintering (sizing, grinding). In the former case, and in particular in the case of heat treatments, precision is affected by dimensional variations associated to phase transformations. In the latter case, precision improves, but the efficiency of sizing strongly depends on the characteristics of the sintered parts, as well as on the sizing parameters and strategy. Even this last subject does not find any systematic analysis in the literature, a part from a paper by Bocchini [3].

2.3 The objective of the present work

The present work aims at investigating the influence of processing variables on the dimensional and geometrical precision of parts produced by Powder Metallurgy. With respect to Fig. 2.2.1, the doctorate project considers all the different steps of the technology: the type of powder, the compaction step, sintering and sizing as a secondary operation.

The selection of the powder was made with the aim of investigating one of the most common mixtures used in the industrial production (Fe-Cu-C) and the newest powder among those proposed by the powder manufacturers in the last fifteen years (Fe-Cr-Mo). The purpose is that of comparing the behavior of one well known base material in PM and of a new material which is not yet extensively utilized even if it may contribute to the attainment of excellent mechanical properties in the sintered parts. The study was made on ring shape parts, an easy geometry that allows the effect of the powder on dimensional and geometrical precision to be investigated, without any significant effect of the geometry of the parts.

For what concerns the processing, the study was focused on particular cases, characterized by some peculiarities.

In the case of compaction, the investigation was focused on two case studies proposed by a press manufacturer:

1. the effect of the compaction speed to produce a three-levels part using the Cr-Mo steel powder above mentioned, which is characterized by a “not-to-high” compressibility;
2. the influence of the lateral transfer of the powder in the production of a pulley with a stepped die; in this case, the powder utilized is the Cu-C steel above mentioned.

In case of sintering, the focus was on the effect of the sintering temperature. It was raised up to levels never used in the industrial production, since it is believed that a very high sintering temperature deteriorates the geometrical precision of the sintered parts. The effect of the sintering temperature was not investigated on Cu-C steel parts, since they do not take any significant benefit

from a very high temperature. The powder chosen in this part of the study was the Cr-Mo one investigated in the previous steps, and the AISI 316L. This latter powder was selected because of its low compressibility that reduces the green density and makes reasonable and of great interest the attempt to improve porosity by enhancing sintering by means of temperature.

The last subject investigated was sizing. In this case is not advisable to use a material as the Cr-Mo steel, since its high hardness makes it practically insensitive to sizing. The material was still the Fe-Cu-C steel, and sizing of a gear was investigated by comparing two sizing strategies and their parameters.

The work was carried out with the cooperation of Höganäs AB, Sacmi, Sinteris and TFM.

2.4 References

1. UNI EN 20286-1:1995: Sistema ISO di tolleranze ed accoppiamenti. Principi fondamentali per tolleranze, scostamenti ed accoppiamenti
2. ASME Y14.5-2009. Dimensioning and Tolerancing.
3. G. F. Bocchini, Powder Metallurgy, 28(3)(1985) 155-165
4. “Guida alla progettazione dei componenti sinterizzati”, ed. Assinter, Torino, 1995.
5. I. Cristofolini et al, Journal of Materials Processing Technology, 210 (2010) 1716-1725.
6. I. Cristofolini et al, Journal of Materials and Processing Technologies, 7(212)(2012) 1513-1519.
7. U. Engstrom et al, Advances in Powder Metallurgy and Particulate Materials 3(1992)317-328
8. S. Masuhara et al, Advances in Powder Metallurgy and Particulate Materials 3(1992)267-284
9. A. Griffo et al., Advances in Powder Metallurgy and Particulate Materials 3(1994)221-236
10. V. Arnhold et al., Advances in Powder Metallurgy and Particulate Materials 3(1994)237-249
11. E. A. Olevsky et al, Acta Materialia 48(2000b), 1167–1180.
12. A. Vo et al, Proc. Advances in Powder Metallurgy and Particulate Materials, Metal Powder Industries Federation, Princeton, NJ, 1(3)(1999) 123–138.
13. G.F. Bocchini, Modern Developments in Powder Metallurgy 18(1988) 507-532

3 Experimental procedure

3.1 Measurement of the dimensions and geometrical characteristics

3.1.1 Introduction

The coordinate measuring machine (CMM) shown in Fig. 3.1.1 was used to determine the points belonging to the surfaces of the parts, so to rebuilt the real surfaces, therefore deriving dimensions and geometrical characteristics.

The main characteristics of the CMM used are the following summarized, aiming at highlighting the items affecting the attainable precision:

- ✓ Dea global image 07-07-07 – Bridge configuration
- ✓ Measurement volume 700x700x700 mm³
- ✓ 3+2 degree of freedom – the scanning head moves along the x-y-z axes shown in Fig. 3.1.1 and two rotation are allowed to the tip stylus (angle α in the z-y plane, $0\div105^\circ$; angle β in the x-y plane, $-180\div180^\circ$)
- ✓ Point by point measurement precision 1.7 μm according to ISO 10360-2
- ✓ Scanning mode measurement precision 3.4/120 μm according to ISO 10360-4
- ✓ Software PC-DMIS 2011 MR1 CAD++. Allowing the direct comparison with the CAD model



Fig. 3.1.1 The CMM configuration

A reliable scanning measurement implies a continuous contact between the probe and the surface. This means that a slight force is applied to the surface, which is compensated from encoders so that the precision of the measurement is not affected. But this slight force might imply a movement of

the parts, which would affect the precision of the measurement particularly for thin parts, so that the gripping system has to be carefully designed. Examples are shown in Fig. 3.1.2

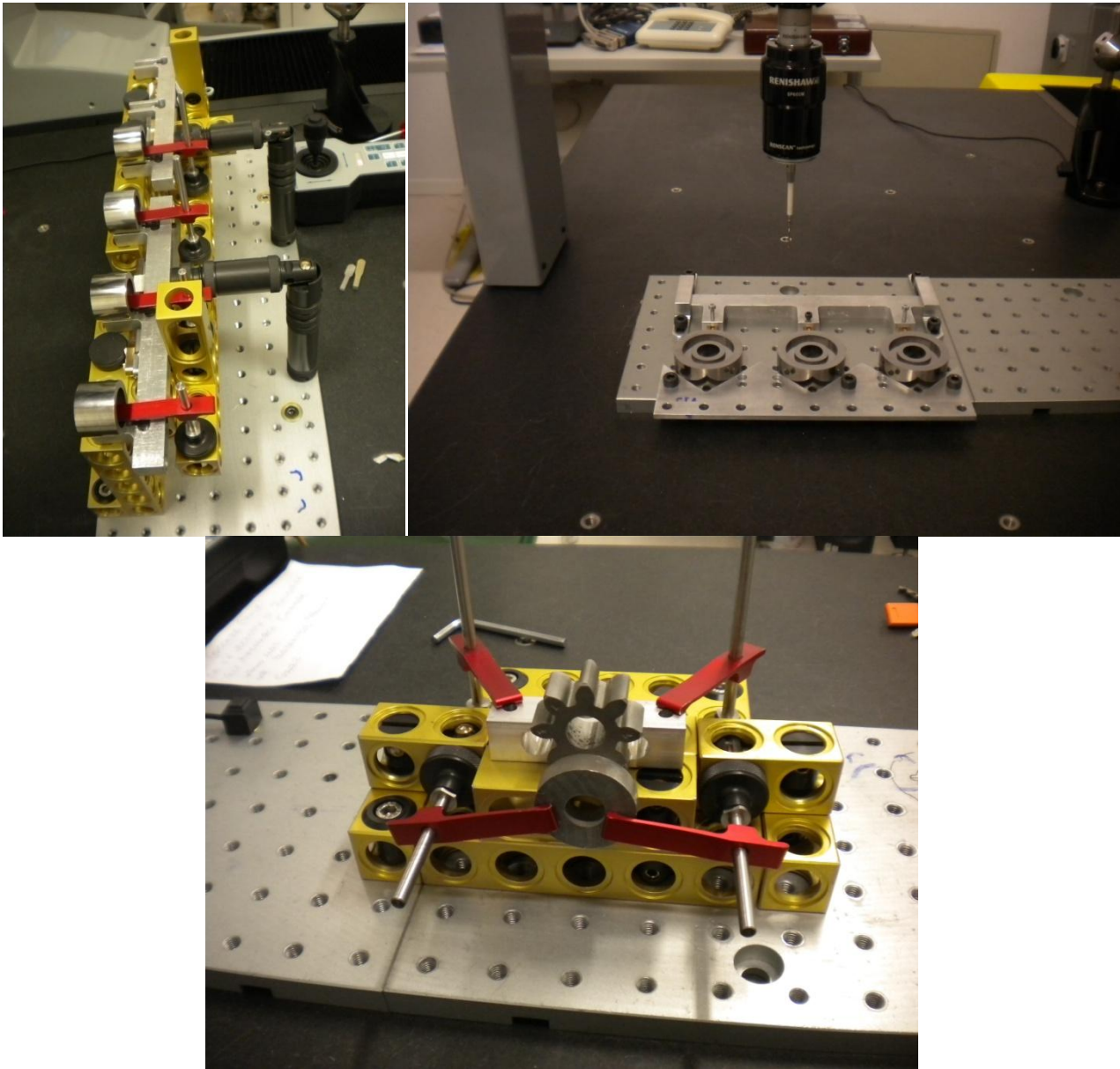


Fig. 3.1.2 Different gripping system

The choice of the probe is also an important step, aiming at guaranteeing the precision of measurement. In principle, long styli and very small probes should be preferably avoided, as well as frequent changes in the orientation of the stylus.

The alignment frame has then to be defined, in order to refer the measured points to the parts and not to the machine reference frame. According to the ASME Y14.5-M, the alignment frame should be defined on the basis of the Datum reference frame used for the geometric dimensioning of the part. In fact, the feature (surface/axis) defining the orientation of the part has to be identified first (surface/axis from which the z axis in the reference frame is derived). Then the feature defining the position of the part has to be identified (from which the x-y axes in the reference frame are derived) and finally the feature blocking the part has to be identified (from which the origin of the reference frame is derived).

If a plane is used to define the orientation (z axis) of the part, at least three not aligned points have to be acquired. If an axis is used to define the orientation, the points belonging to the relevant cylindrical surface have to be acquired, being the minimum number, in this case, three points on two sections. For this work a larger number of points has been acquired to obtain a more reliable reconstruction of the real plane/axis, as it will explain in a following section.

To define the position (x-y axes) a feature orthogonal to the previous one has to be identified, and at least two points belonging to that have to be acquired. Again, a larger number of points has been acquired in this work.

The last feature to be identified allow to define the origin of the reference frame, that means the point defined by the coordinates $O(0,0,0)$.

According to the alignment frame, one or more so called “clearance planes” have then to be defined. These planes allow to identify a safe volume around the part that the probe bumps against the parts of the gripping system during the measurement.

On the basis of this considerations above, it is now possible to define a program to automatically measure the part. feature will be measured both in point-by-point mode and in scanning mode, depending on the peculiar characteristics of the parts, as it will explained in the following.

3.1.2 Measurement procedure, a real part program

In the Appendix A is reported an example of a part program used to measure the real component shown in Fig. 3.1.3.

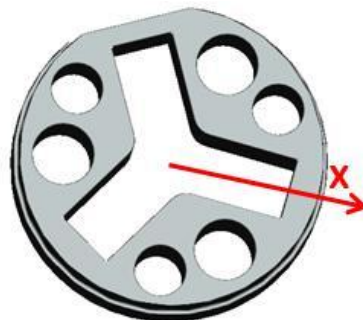


Fig. 3.1.3 Example of the part measured

The peculiar geometrical characteristics of this part adequately allow to explain the procedure used to make a part program for measurement. The part presents 3 holes of 5mm diameter and three holes of 4 mm diameter, and three rectangular grooves. All the different characteristics are placed at 120° one from the other. With respect to the median plane of the rectangular grooves, the plane passing through the axis of the large hole and the axis of the external cylinder forms an angle of 55° clockwise, while plane passing through the axis of the small hole and the axis of the external cylinder forms an angle of 45° counter clockwise.

Considering the dimensions of the part, a tip of 2 mm diameter was used to measure all the characteristics. The gripping system and the probe used to measure the part is shown in Fig. 3.1.4.



Fig. 3.1.4 Gripping system

According to the functional requirements, the alignment procedure is based on the acquisition of the feature which allow to define a datum reference frame, that means:

- ✓ the feature defining the orientation of the part (the upper surface, by the measurement of 9 points, from which x-y plane is derived),
- ✓ the feature used for positioning the part (the axis of the external cylindrical surface, by the measurement of continuous scans at different heights on the external cylinder, from which the origin is derived),
- ✓ the feature used to fix the part (the median plane of one rectangular groove, by the measurement of four continuous scans on the parallel planes defining the groove, from which the direction of x axis is derived). Point by point measurement is preferred to continuous scan when surfaces are small and/or irregular.

The features defining the part were then measured by continuous scan at different heights. By means of circles the cylindrical surfaces were derived (holes and external cylindrical surfaces) and by means of linear scans the plane surfaces were derived (planes defining the grooves). The geometrical characteristics of form of these features were controlled in terms of circularity-cylindricity and flatness, respectively. The related geometrical characteristics were controlled in terms of position of holes and grooves, concentricity of cylindrical surfaces and perpendicularity of the upper surface with respect to the axis of the external cylindrical surface.

It is important to underline that the dimensions were derived from the geometrical characteristics: linear dimensions from the distances between planes and diameters from the cylindrical surfaces [5, 6].

The main steps of the measurement procedure are summarized in Fig. 3.1.5

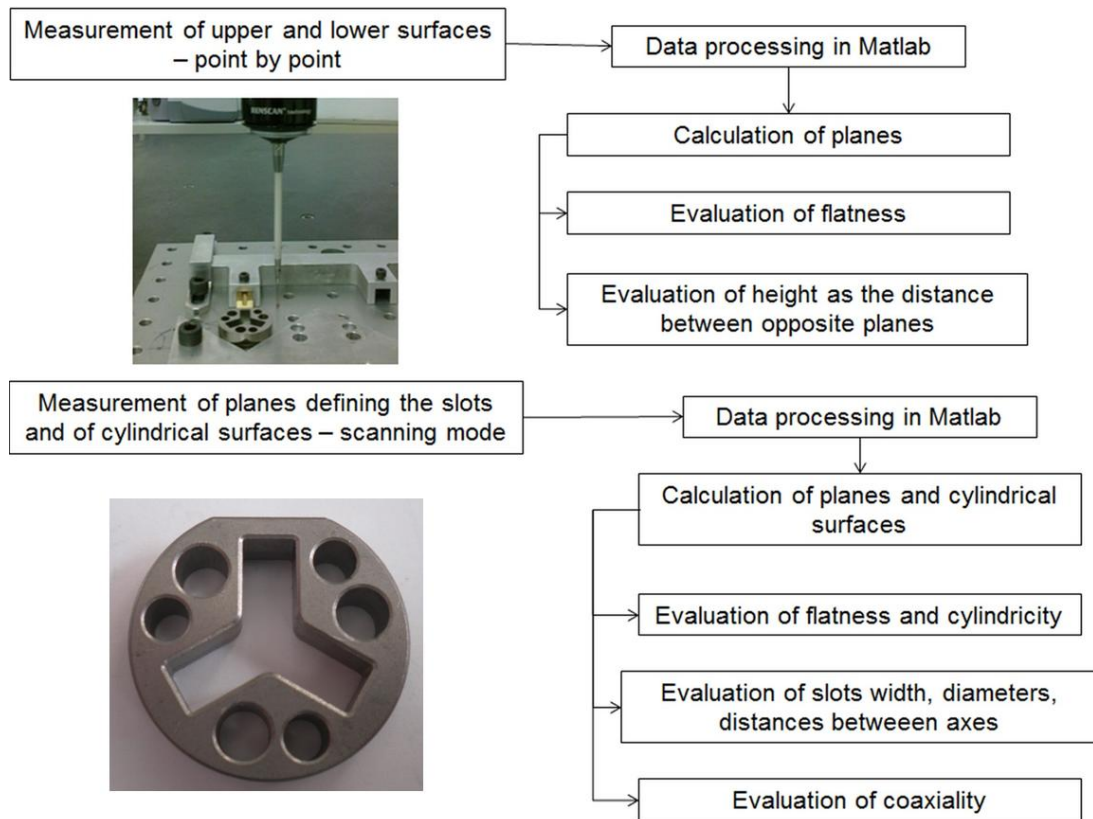


Fig. 3.1.5 the measurement procedure

3.1.3 Characterization

The microstructure and density of all the parts considered in the present work were analyzed. Density was measured by the water displacement method and, in some cases, the porosity distribution in the parts was investigated by Image Analysis of metallographic sections (six to nine Light Optical Microscope images at 100x). The microstructural characterization was made on etched metallographic sections, according to the standard procedure. Vickers hardness and microhardness was also measured.

3.2 References

1. M. M. Dowling et al., *Technometrics* 39 (1997) (1)3-17
2. K. Carr et al, *Precision Engineering* 17 (1995)131-143

4 Results

4.1 Powders

The analysis of the effect of the powder on the dimensional and geometrical characteristics has been done considering whether the parts shrink or swell on sintering. Two different chemical compositions have been considered, relevant to a “swelling system” and to a “shrinking system”. Fe-Cu-C powders determine the swelling system. Two different compositions have been considered, distinguished by the relative amount of Copper and Carbon. A different behaviour on sintering is expected with respect the two different compositions, being it well known that Cu-C combination influences the evolution of the transient liquid phase sintering [1-3] and, in turn, the dimensional and geometrical variations. Parts were compacted to 6.9 g/cm³ green density and sintered at 1120°C, as usual in industrial production.

Fe-Cr-Mo-C powders determine the shrinking system. Again two different compositions have been considered, distinguished by the carbon content. Different cooling rates have been also considered, given that the C content/cooling rate combination influences the phase transformation on cooling and, in turn, the dimensional and geometrical variations [4-6] . Parts were compacted to 6.9 g/cm³ green density and sintered at the two temperatures usually adopted in the industrial production: 1120°C and 1250°C.

Other parameters relevant to the powders and expectably affecting the dimensional-geometrical characteristics have been considered, that means the addition of copper in Fe-Cu-C as pure element or as diffusion bonded one. Moreover the effect of different lubricants has been investigated [7-8].

In this preliminary step of the project, the simple geometry shown in Fig. 4.1.1 Parts geometry has been defined. The simple ring-shaped parts allow to evaluate most of the geometrical characteristics, that means, flatness, circularity, parallelism, perpendicularity, concentricity.

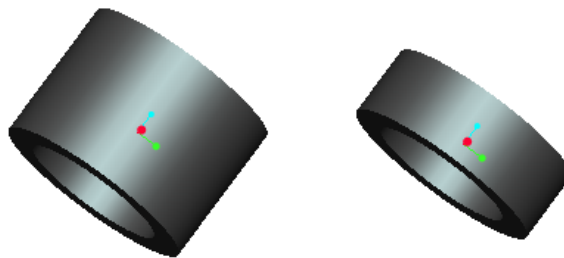


Fig. 4.1.1 Parts geometry

Sampling procedure: 10 parts have been measured for each experiment (in a sampling of 250 green parts, one part every 25 has been taken). The same part has been measured in the green and in the sintered condition.

Measurement procedure: the main steps of measurement procedure are summarized in the (§3.1.2, Fig. 3.1.5).

The influence of the parameters relevant of the powder on the dimensional and geometrical characteristics has been investigated by a DoE approach, as described in the following.

4.1.1 Swelling system

4.1.1.1 The DoE plan

This study was approached with a full factorial Design of Experiments analysis (DoE). This means 2⁴ experiments, given that four factors on two levels were considered:

- ✓ the chemical composition of the mixture: 2%Cu-0.8%C and 3%Cu-0.5%C; in this way two mixes characterized by a slight (the former) and a more pronounced (the latter) dimensional change were considered;
- ✓ the type of copper powder: Distaloy Cu and Cu 200; the former is a pure iron powder to which 10% of fine copper is diffusion bonded, the latter is a pure copper powder simply blended to the base iron powder;
- ✓ the type of mix: Premix and Bonded mix; the former is obtained by the addition of a conventional lubricant, amidewax, while the latest generation of lubricant binder is added to the latter, ensuring excellent filling and lubrication performances;
- ✓ the height of the ring: 12.5 mm and 25 mm; in this way different axial density gradients in the parts are expected (larger in the latter). The internal and the external diameter of the ring are fixed and the nominal values are: $\varnothing_{int} = 25 \text{ mm}$, $\varnothing_{ext} = 35 \text{ mm}$.

Table 4.1.1 summarizes the full factorial DoE plan.

factor	lower level (-)	upper level (+)
composition of the mixture	2%Cu-0.8%C	3%Cu-0.5%C
copper powder	Distaloy Cu	Cu 200
lubricant	Premix	Bonded mix
height	25 mm	12,5 mm

Table 4.1.1 The DoE plan

4.1.1.2 *Densification and microstructure*

The density of ten specimens from each experiment was calculated as the ratio between the mass (measured by a precision balance $\pm 0.001 \text{ g}$) and the volume of the parts. The mean values are reported in Table 4.1.2: the green density ρ_g , the sintered density ρ_s and the densification parameter defined as $(\rho_{sint} - \rho_g) / (\rho_{th} - \rho_g)$ (the negative value is indicative of a volume expansion).

Batch	Composition	Copper	Lubricant	Height	Green density [g/cm ³]	Sintered density [g/cm ³]	Densification Parameter
1	-	-	-	-	6.87	6.82	-0.05
2	-	-	-	+	6.89	6.85	-0.04
3	-	-	+	-	6.87	6.82	-0.06
4	-	-	+	+	6.89	6.85	-0.05
5	-	+	-	-	6.88	6.83	-0.05
6	-	+	-	+	6.89	6.85	-0.05
7	-	+	+	-	6.88	6.83	-0.05
8	-	+	+	+	6.91	6.88	-0.04
9	+	-	-	-	6.87	6.76	-0.13
10	+	-	-	+	6.88	6.76	-0.13
11	+	-	+	-	6.88	6.77	-0.13
12	+	-	+	+	6.87	6.76	-0.13
13	+	+	-	-	6.90	6.77	-0.14
14	+	+	-	+	6.89	6.76	-0.14
15	+	+	+	-	6.89	6.76	-0.15
16	+	+	+	+	6.89	6.76	-0.15

Table 4.1.2 Density and densification

As expected the expansion is higher in the powder with the higher content of copper, Fe-3%Cu-0.5%C. Density distribution in the axial direction has been also evaluated, highlighting the expected trend (higher close to the surfaces contacting the punches during compaction - 6.7-6.8 g/cm³ - and lower in the median section - 6.5-6.6 g/cm³). The difference in the distribution is less appreciable in the low batch than in the high batch.

The microstructural analysis shows, in the green part, the different type and dimensions of the copper particles Fig. 4.1.2, in the sintered parts is possible to show the secondary porosity.

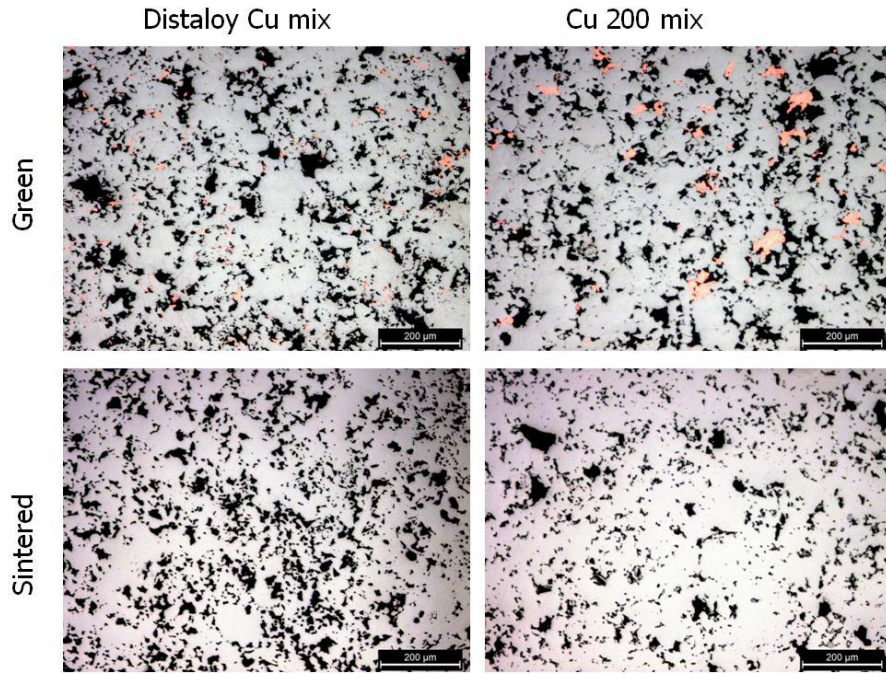


Fig. 4.1.2 Microstructure of Fe-Cu-C

4.1.1.3 Dimensions in green and sintered state

Fig. 4.1.3, Fig. 4.1.4 and Fig. 4.1.5 show the measured dimensions and their precision (in terms of scatter bands of the measured values) in the green and sintered state.

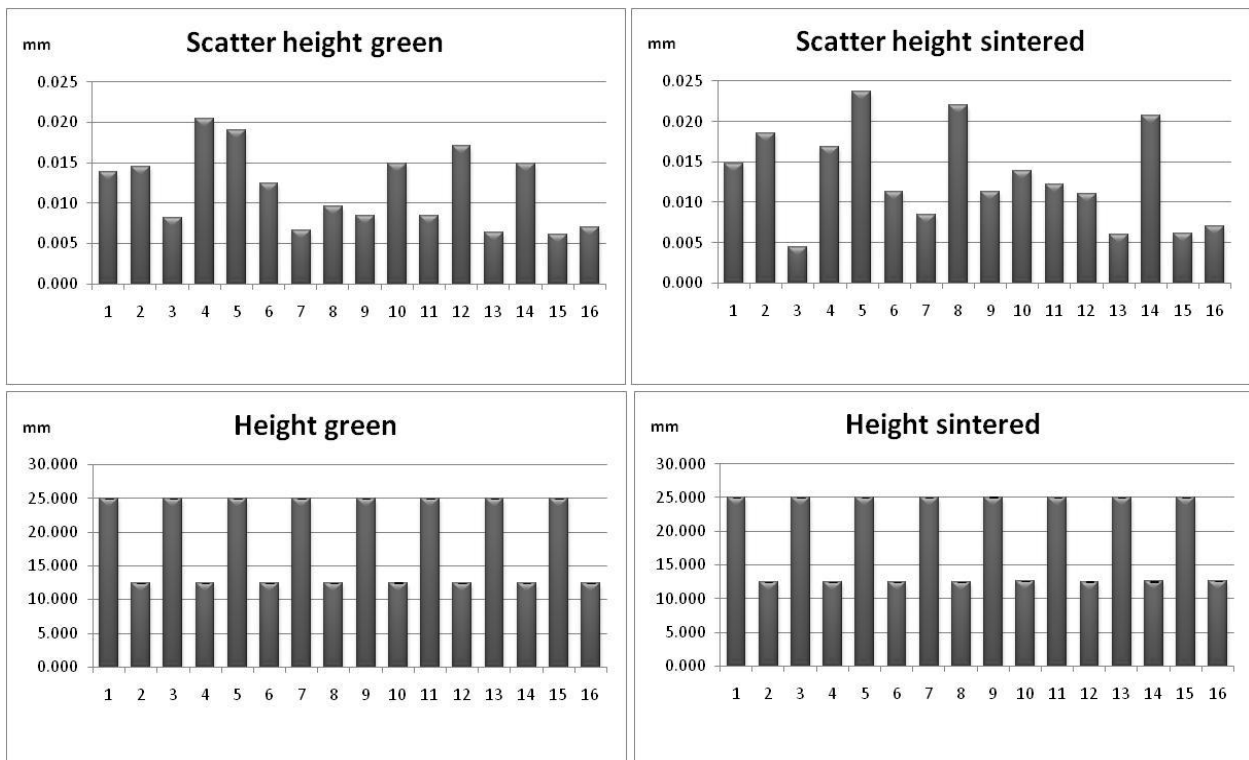


Fig. 4.1.3 height and scatter band in green and sintered state

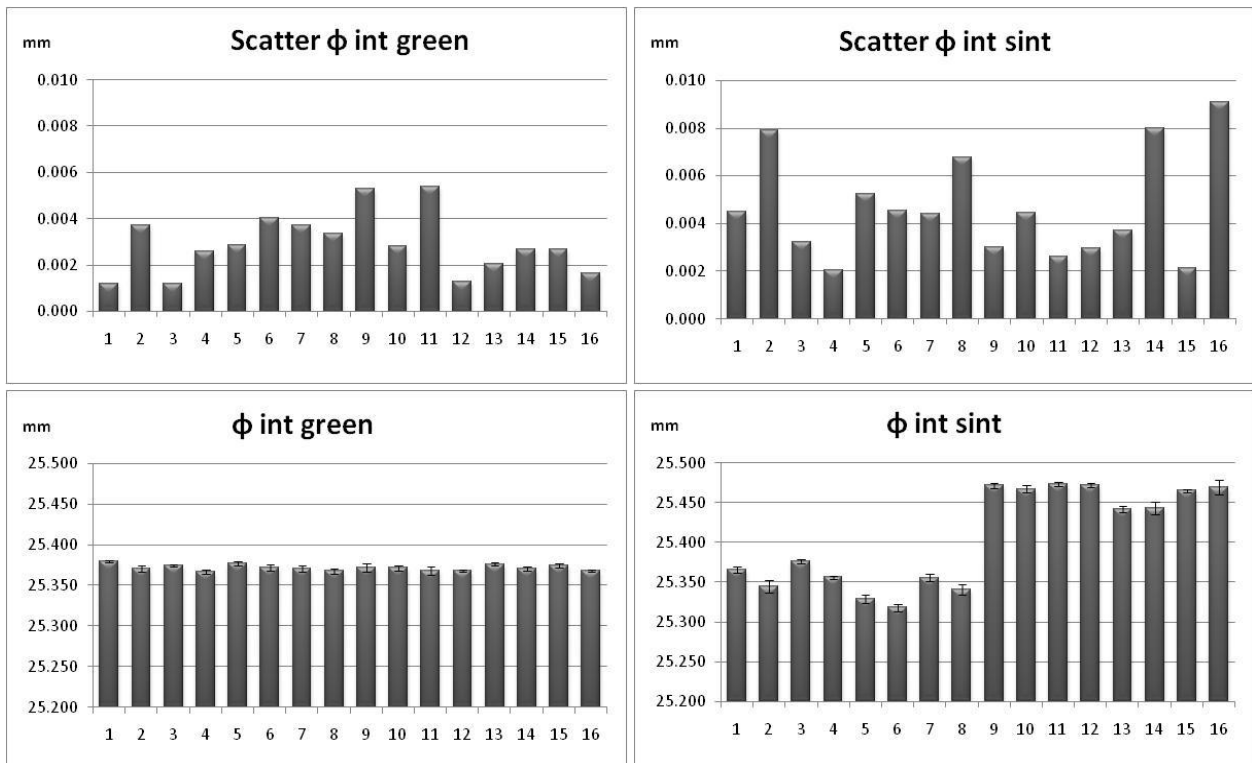


Fig. 4.1.4 Internal diameter and scatter band in green and sintered state

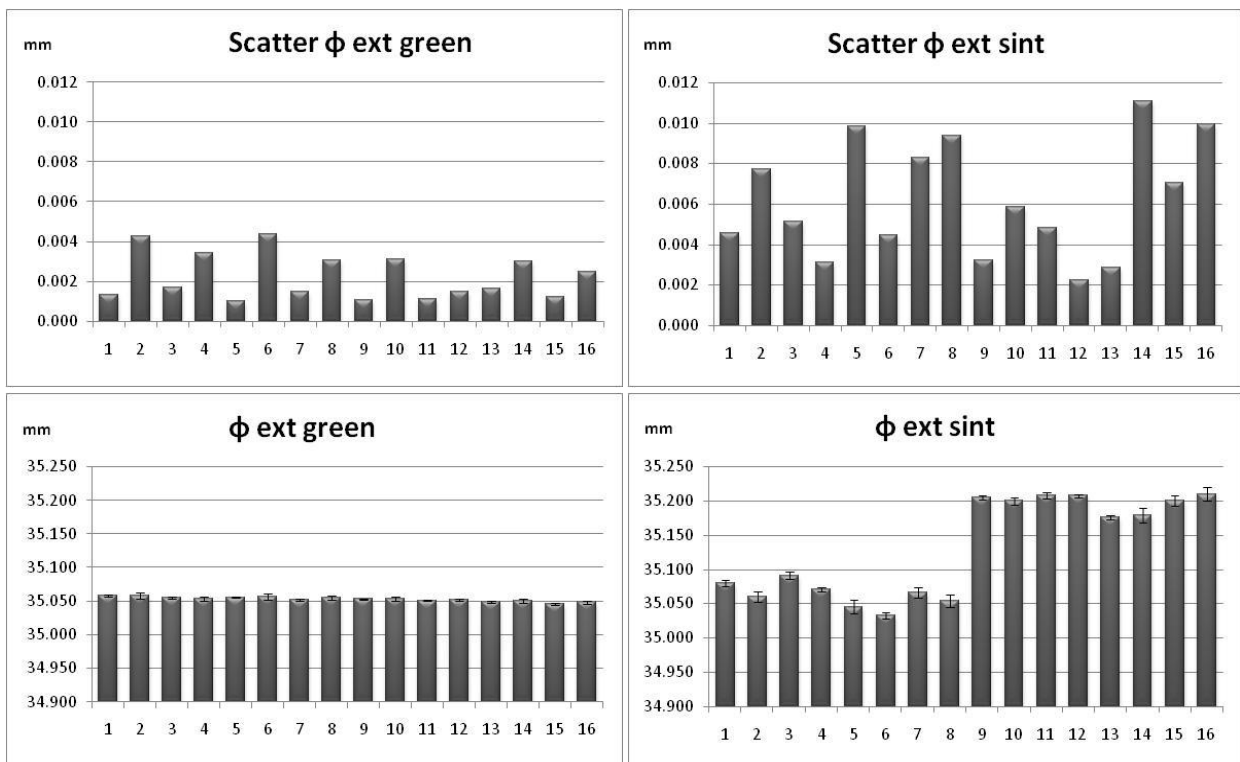


Fig. 4.1.5 External diameter and scatter band in green and sintered state

In the green state all the dimensions show good repeatability, the scatter value is very small, although it is larger in the axial dimensions than in the radial ones.

The range of the scatter in green parts is 0.006-0.025 mm with respect to the height, and 0.002-0.006 mm with respect to the diameters, in this last case it is slightly larger than the precision of the measurement. The scatter band, generally, tends to increase after sintering, but no significant trend

can be identified. The excellent dimensional precision of the green parts is anyway maintained after sintering.

4.1.1.4 Dimensional variation

Table 4.1.3 collects the dimensional variation of height and of the internal and external diameter and the wall thickness.

Batch	Composition	Copper	Lubricant	height	$\Delta h/h_0$	$\Delta\Phi_{int}/\Phi_{int0}$	$\Delta\Phi_{ext}/\Phi_{ext0}$	$\Delta t/t_0$
1	-	-	-	-	-0.144	-0.053	0.061	0.361
2	-	-	-	+	-0.189	-0.104	0.004	0.288
3	-	-	+	-	-0.118	0.007	0.101	0.347
4	-	-	+	+	-0.164	-0.041	0.048	0.279
5	-	+	-	-	-0.065	-0.192	-0.031	0.391
6	-	+	-	+	-0.066	-0.213	-0.070	0.303
7	-	+	+	-	-0.073	-0.059	0.041	0.303
8	-	+	+	+	-0.159	-0.105	-0.003	0.264
9	+	-	-	-	0.275	0.392	0.433	0.539
10	+	-	-	+	0.357	0.378	0.415	0.513
11	+	-	+	-	0.232	0.415	0.446	0.527
12	+	-	+	+	0.281	0.408	0.441	0.528
13	+	+	-	-	0.386	0.259	0.364	0.639
14	+	+	-	+	0.458	0.286	0.367	0.582
15	+	+	+	-	0.382	0.356	0.441	0.663
16	+	+	+	+	0.389	0.398	0.460	0.622

Table 4.1.3 Dimensional variation of height and diameters

The change of the three dimensions is higher in the material showing the larger swelling (batches 9÷16). It is possible however to note that the dimensional variations have a dual behavior:

- ✓ In the first 8 batches, with the composition 2%Cu-0.8C, the height and the internal diameter tends to shrink during sintering, while the external diameter does not change significantly, in some case shrink in other swells;
- ✓ In the other 8 batches, with the composition of 3%Cu-0.5%C, all the dimensions tends to swell after sintering. The external diameter increases, in the mean value, more than the internal diameter.

The dimensional variation of the disks is graphically shown in Fig. 4.1.6 to better highlight the different behavior of the two materials.

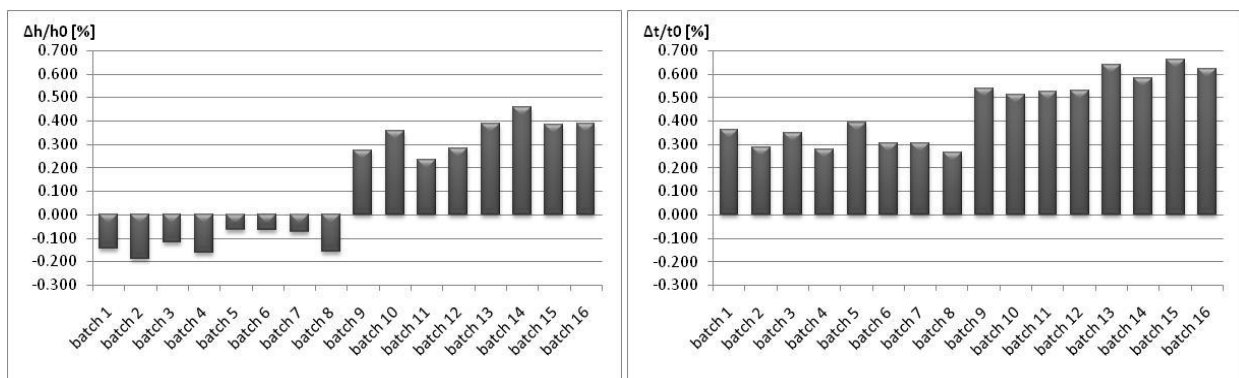


Fig. 4.1.6 Dimensional variation

In all the batches the total volume of the parts increases but while for the batches 9-16 all the dimensions increase after sintering for the batches 1÷8 height decreases. But the increase in the wall thickness is higher than the decrease of the height, which results in a volume increase.

Dimensional change is anisotropic, as common in Powder Metallurgy. This behavior has been investigated in detail in a specific work [9].

4.1.1.5 Analysis of variance

To investigate the most significant factors affecting the dimensional changes and their interactions, if any, an ANOVA analysis was performed for each dimension, considering the interaction between two parameters at time. The results are shown in the following tables (Table 4.1.4-Table 4.1.6) and figures (Fig. 4.1.7-Fig. 4.1.9). The highlighted rows in the tables indicate the most significant parameters.

ANOVA OF Height variation					
	DoF	Sum Sq	Mean Sq	F Value	Pr(>F)
Height	1	0.00007	0.00007	0.0918	0.774064
Lubricant	1	0.00363	0.00363	4.8978	0.077801
Copper	1	0.03249	0.03249	43.8366	0.001183
Composition	1	0.87282	0.87282	1177.6406	3.952*10⁻⁷
Height:Lubricant	1	0.00209	0.00209	2.8240	0.153696
Height: Copper	1	0.00015	0.00015	0.2025	0.671572
Height:Composition	1	0.00936	0.00936	12.6296	0.016321
Lubricant: Copper	1	0.00072	0.00072	0.9655	0.370939
Lubricant:Composition	1	0.00128	0.00128	1.7244	0.246160
Copper:Composition	1	0.00300	0.00300	4.0444	0.100509
Residuals	5	0.00371	0.00074		

Table 4.1.4 ANOVA of variation of height

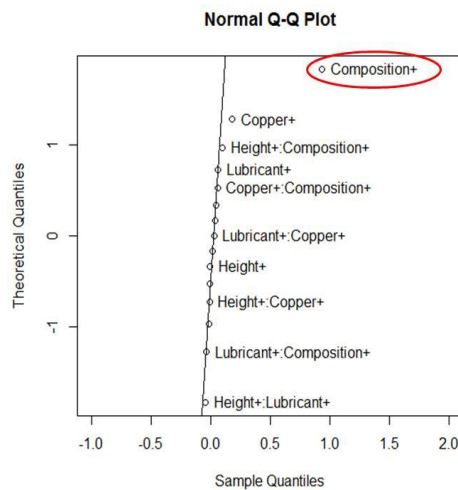


Fig. 4.1.7 ANOVA of variation of height

ANOVA OF variation of Internal Diameter					
	DoF	Sum Sq	Mean Sq	F Value	Pr(>F)
Height	1	0.00086	0.00086	8.5503	0.032857
Lubricant	1	0.02426	0.02426	242.4291	1.985*10 ⁻⁵
Copper	1	0.02814	0.02814	281.2249	1.378*10 ⁻⁵
Composition	1	0.83403	0.83403	8335.0462	2.989*10⁻⁹
Height:Lubricant	1	0.00000	0.00000	0.0056	0.943141
Height: Copper	1	0.00095	0.00095	9.4497	0.027656
Height:Composition	1	0.00289	0.00289	28.8726	0.003007
Lubricant: Copper	1	0.00459	0.00459	45.8720	0.001067
Lubricant:Composition	1	0.00069	0.00069	6.8863	0.046861
Copper:Composition	1	0.0045	0.0045	4.5128	0.087026
Residuals	5	0.00050	0.00010		

Table 4.1.5 ANOVA of variation of internal diameter

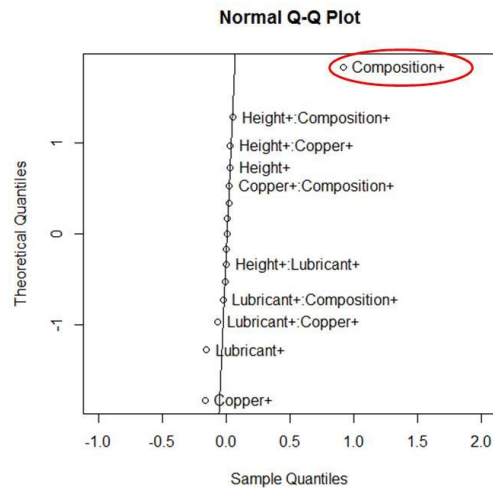


Fig. 4.1.8 ANOVA of variation of internal diameter

ANOVA OF External Diameter variation					
	DoF	Sum Sq	Mean Sq	F Value	Pr(>F)
Height	1	0.00233	0.00233	28.3004	0.0031406
Lubricant	1	0.01150	0.01150	139.8275	7.614*10 ⁻⁵
Copper	1	0.00898	0.00898	109.1331	0.0001386
Composition	1	0.64682	0.64682	7862.8544	3.457*10⁻⁹
Height:Lubricant	1	0.00004	0.00004	0.4749	0.5214294
Height: Copper	1	0.00033	0.00033	4.0488	0.1003696
Height:Composition	1	0.00233	0.00233	28.3004	0.0031406
Lubricant: Copper	1	0.00209	0.00209	25.4437	0.0039528
Lubricant:Composition	1	0.00002	0.00002	0.2196	0.6590848
Copper:Composition	1	0.00191	0.00191	23.2677	0.0047830
Residuals	5	0.00041	0.00008		

Table 4.1.6 ANOVA of variation of external diameter

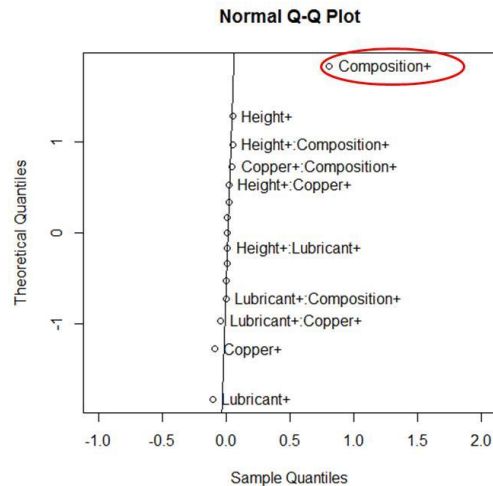


Fig. 4.1.9 ANOVA of variation of external diameter

As expected the main parameter affecting the dimensional variation is the composition of the powder. It is obvious since the two compositions have been designed with the aim of enhancing the differences in the dimensional behavior (less carbon and more copper versus more carbon and less copper). The other parameters, and their interaction, have a minor effect on the dimensional variation. In particular it does not observe any significant interaction between the parameters, but a lower effect of copper type and lubricant may be observed. Cu200 tends to either increase the growth or decrease the shrinkage of the diameter with respect to the Distaloy Cu mix. The effect of copper can be attributed to the particle size [10], which is smaller in Distaloy Cu than in Cu200. Moreover, diffusion bonded copper particles are more homogeneously distributed in the green parts which reduces the possibility of segregation during handling [11]. Concerning the effect of lubricant, Bonded mix tends to decrease swelling. In principle, Bonded mix ensures a better homogeneity of graphite distribution and a better contact between the graphite particles and the ferrous powder. This could prevent some of graphite from dusting off during compaction, as well as it could increase the extension of the graphite/iron interface. In both cases, the dissolved carbon content into the ferrous matrix when copper melts is increased, and grain boundary penetration by the liquid phase is limited, so swelling is reduced.

4.1.1.6 Geometrical characteristics in green and sintered state

The most significant geometrical characteristics for these parts are the concentricity between the axis of the external and the internal cylinders (that means between the external surface and the hole) and the perpendicularity between the plane surface and the axis of the internal cylinder (which is also affected by the flatness of the plane). For the different experiments these characteristics are shown in Fig. 4.1.10, Fig. 4.1.11 and Fig. 4.1.12.

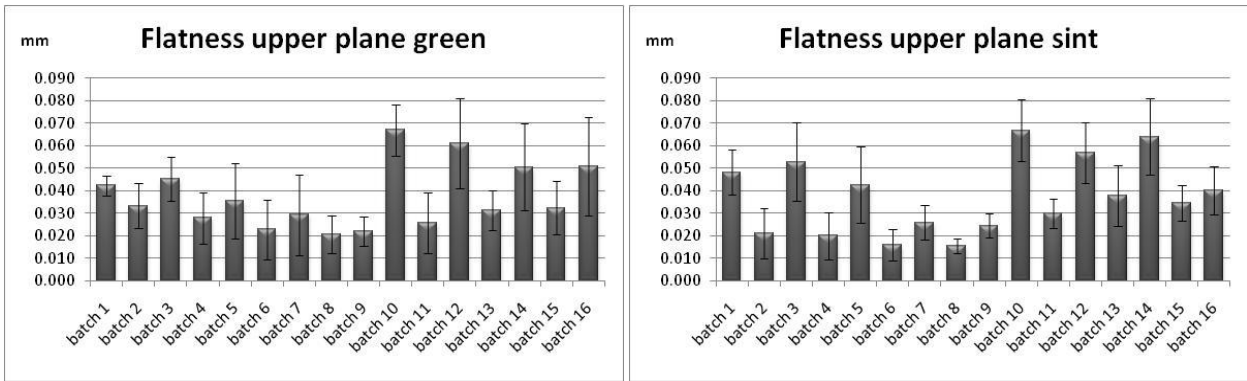


Fig. 4.1.10 Flatness in green and sintered state

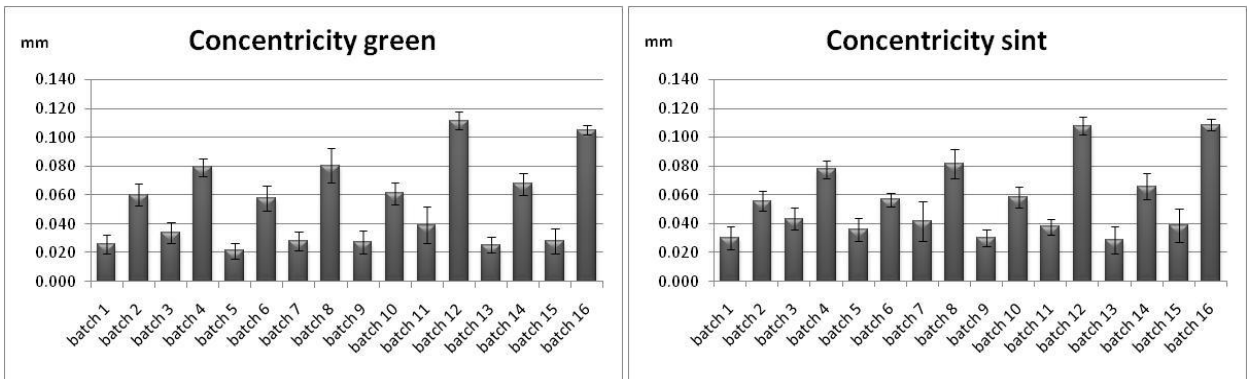


Fig. 4.1.11 Concentricity in green and sintered state

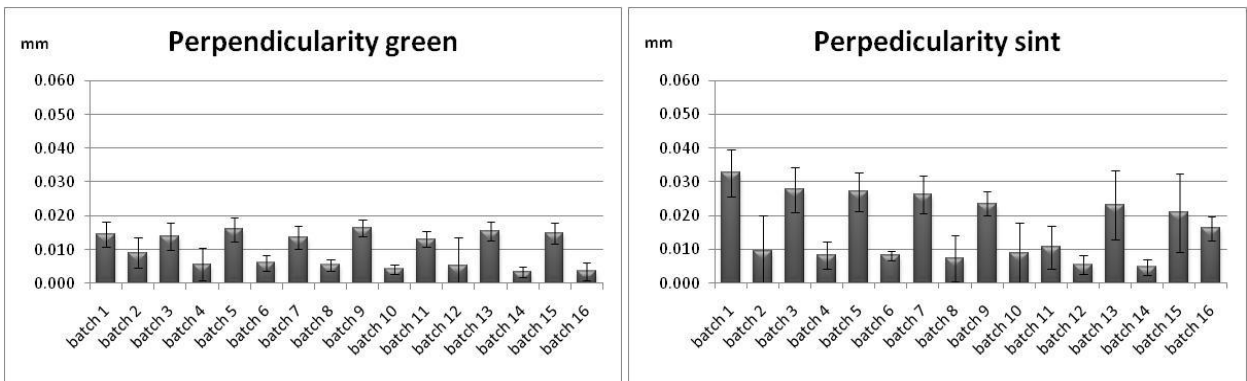


Fig. 4.1.12 Perpendicularity of plane with respect of the internal cylinder in green and sintered state

No significant worsening is observed after sintering in the geometrical characteristics, resulting values are coherent to those expectable in PM conventional process.

Flatness does not change after sintering significantly. The worst concentricity of the low specimens (even numbers batches) still in the green state may be attributed to the weaker constrain exerted by the powder columns surrounding the internal core during the tooling movements.

To investigate the most significant factors affecting concentricity, an ANOVA analysis was performed. Results relevant to the sintered parts are shown in Table 4.1.7 and Fig. 4.1.13, similar results have been obtained for green parts.

ANOVA OF Concentricity in sintered state					
	DoF	Sum Sq	Mean Sq	F Value	Pr(>F)
Height	1	0.006642	0.006642	194.7874	3.395*10 ⁻⁵
Lubricant	1	0.0019360	0.0019360	56.7742	0.000652
Copper	1	0.0000202	0.0000202	0.5938	0.475754
Composition	1	0.0001822	0.0001822	5.3446	0.068750
Height:Lubricant	1	0.0006503	0.0006503	19.0689	0.007244
Height: Copper	1	0.0000040	0.0000040	0.1173	0.745907
Height:Composition	1	0.0004410	0.0004410	12.9326	0.015606
Lubricant: Copper	1	0.0000062	0.0000062	0.1833	0.686380
Lubricant:Composition	1	0.0001322	0.0001322	3.8783	0.106014
Copper:Composition	1	0.0000000	0.0000000	0.0000	1.000000
Residuals	5	0.0001705	0.0000341		

Table 4.1.7 ANOVA of Concentricity

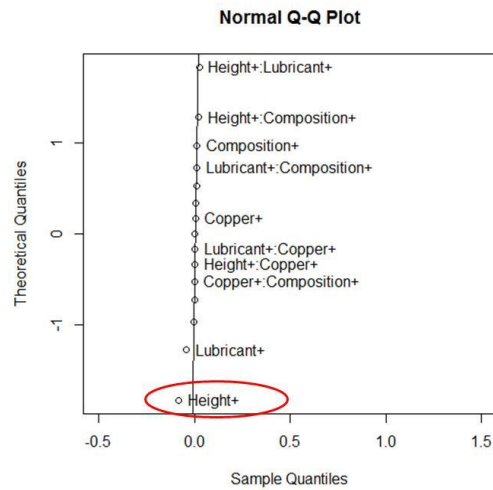


Fig. 4.1.13 ANOVA of Concentricity

The ANOVA analysis confirms that the main parameter affecting the concentricity is the height, while a less significant effect of the type of lubricant is observed. Flowability is much better in bonded mix and filling is faster; moreover, the apparent density and the filling height is lower, which could further influence the constrain of the powder during compaction movements.

For what concerns perpendicularity, a slight worsening on sintering is observed, with a significant effect of height. The other variables do not affect perpendicularity, as shown by ANOVA [12].

4.1.2 Shrinking system

This study of the shrinking system too was approached with a full factorial Design of Experiments analysis. This means 2^5 experiments, given that five factors on two levels were considered:

- the chemical composition of the mixture: the powder used is an atomized 3%Cr and 0.5% Mo iron alloy. Carbon was added as UF-4 Kröpfung graphite, in different amounts to obtain 0.2%C and 0.5%C in the sintered materials;
- the type of mix: Premix and Bonded mix; the former is obtained by the addition of a conventional lubricant, amidewax, while the latest generation of lubricant binder is added to the latter, ensuring excellent filling and lubrication performances;
- the height of the ring: 12.5 mm and 25 mm; in this way different axial density gradients in the parts are expected (larger in the latter). The internal and the external diameter of the ring are fixed and the nominal values are: $\phi_{int} = 25 \text{ mm}$, $\phi_{ext} = 35 \text{ mm}$;
- the sintering conditions: Sintering was carried out at 1120°C and 1250°C, 30 minutes, in a vacuum furnace, with 99.99% purity nitrogen backfilling at 900°C;
- the cooling rate: cooling was carried out in a nitrogen flux at different pressures to obtain two different cooling rates, namely 0.5°C/s and 2.5°C/s, measured by a thermocouple inserted in a dummy specimen.

Table 4.1.8 shows the full factorial DoE plan for the shrinking system.

Factor	lower level (-)	upper level (+)
Composition of the mixture	0.2%C	0.5%C
Lubricant	Premix	Bonded mix
Height	12.5 mm	25 mm
Sintering temperature	1120°C	1250°C
Cooling rate	0.5°C/s	2.5°C/s

Table 4.1.8 DoE plan of shrinking system

4.1.2.1 Analysis of density and microstructure

The density was derived as the ratio between mass and volume, as explained above (§4.1.1.2). Table 4.1.9 shows the density measured in the green and in the sintered state, and the densification parameter.

Composition	Sintering temperature [°C]	Cooling rate [°C/s]	Green density [g/cm ³]	Sintered density [g/cm ³]	Densification
0.2%C	1120	0.5	6.87	6.98	0.12
0.2%C	1120	2.5	6.87	6.94	0.08
0.2%C	1250	0.5	6.87	7.05	0.19
0.2%C	1250	2.5	6.87	7.00	0.14
0.5%C	1120	0.5	6.88	6.94	0.07
0.5%C	1120	2.5	6.88	6.92	0.04
0.5%C	1250	0.5	6.88	7.01	0.14
0.5%C	1250	2.5	6.88	6.98	0.11

Table 4.1.9 Density in green and sintered state

The density tends to increase on increasing the sintering temperature, and to decrease on increasing the cooling rate.

The microstructure of the sintered specimens with 0.2%C and 0.5%C, at the different sintering temperature and cooling rate is shown in the Fig. 4.1.14 and Fig. 4.1.15, the microhardness is also reported.

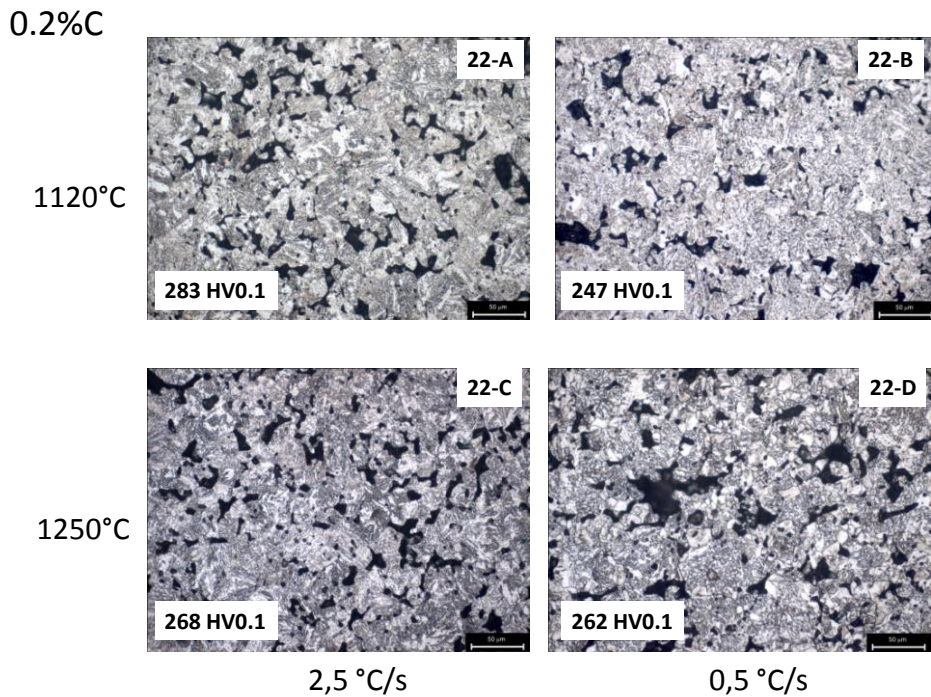


Fig. 4.1.14 Microstructure of Fe-Cr-Mo-0.2%C

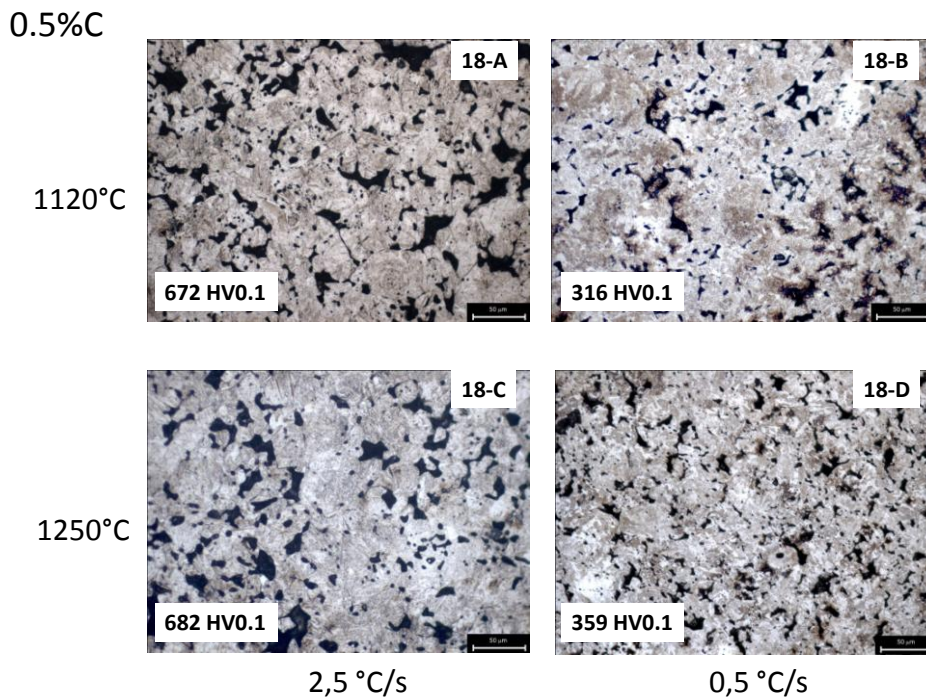


Fig. 4.1.15 Microstructure of Fe-Cr-Mo-0.5%C

The microstructure of the 0.2%C steel is a mixture of ferrite and upper bainite, the amount of upper bainite slightly increases on increasing the cooling rate. The microstructure of the 0.5%C steel is bainitic if resulting from the lower cooling rate and martensitic if resulting from the higher one. No effect of the sintering temperature on the microstructure is observed. In principle, sintering temperature should shift the CCT curves of the material towards the right due to the effect on austenite grain size. This effect is prevented by pores in sintered steels (grain boundary pinning effect), as it has been demonstrated by Santuliana et al. [13] and Dlapka et al. [14]. As a consequence, the sintering temperature does not influence the austenite transformations on cooling.

4.1.2.2 Dimensions in green and sintered state

Fig. 4.1.16, Fig. 4.1.17 and Fig. 4.1.18 show the measured dimensions and their precision (in terms of scatter bands of the measured values) in the green and sintered state. The three figures refer to height, internal and external diameter, respectively; the green and the sintered data are reported on the left and the right side, respectively; data for small (12,5 mm) and large (25 mm) height are reported in the upper and the lower side, respectively.

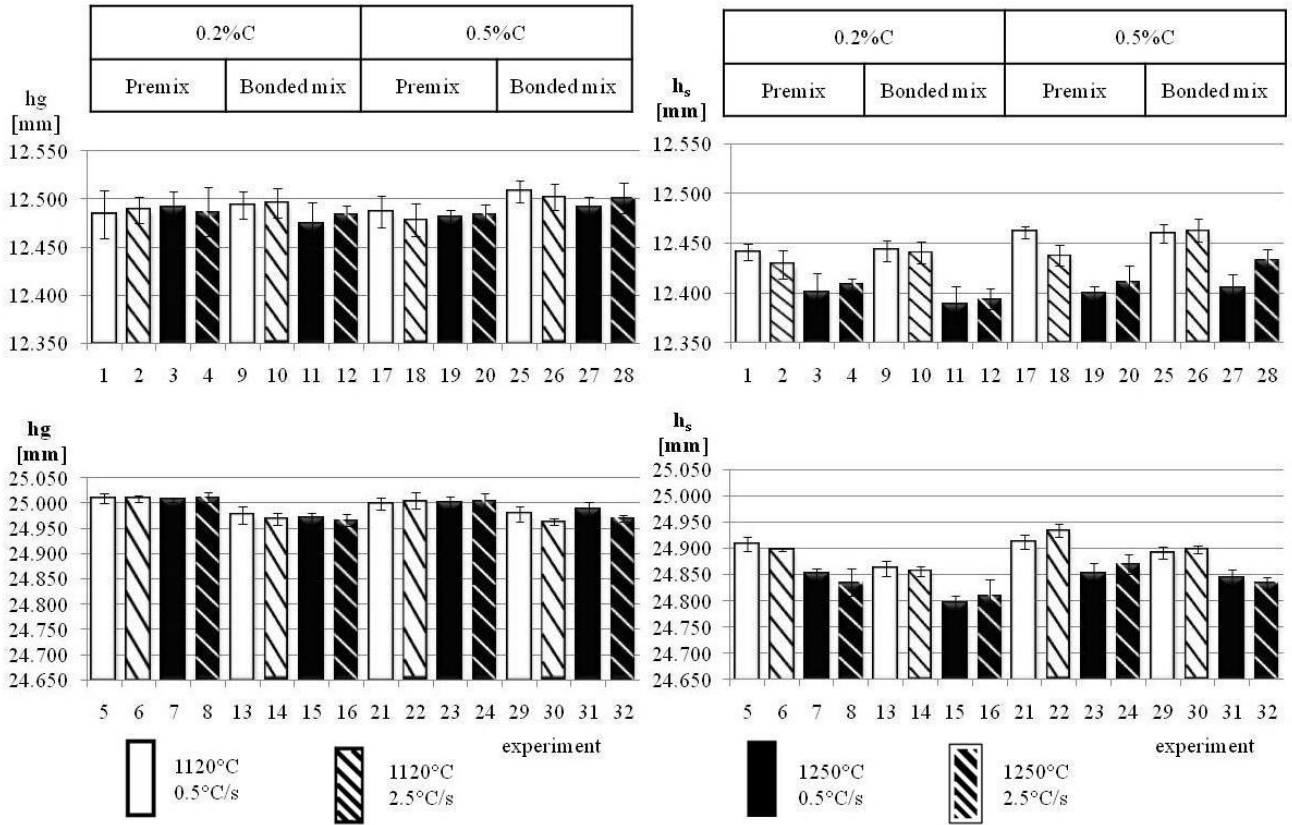


Fig. 4.1.16 Height of the green and sintered specimens

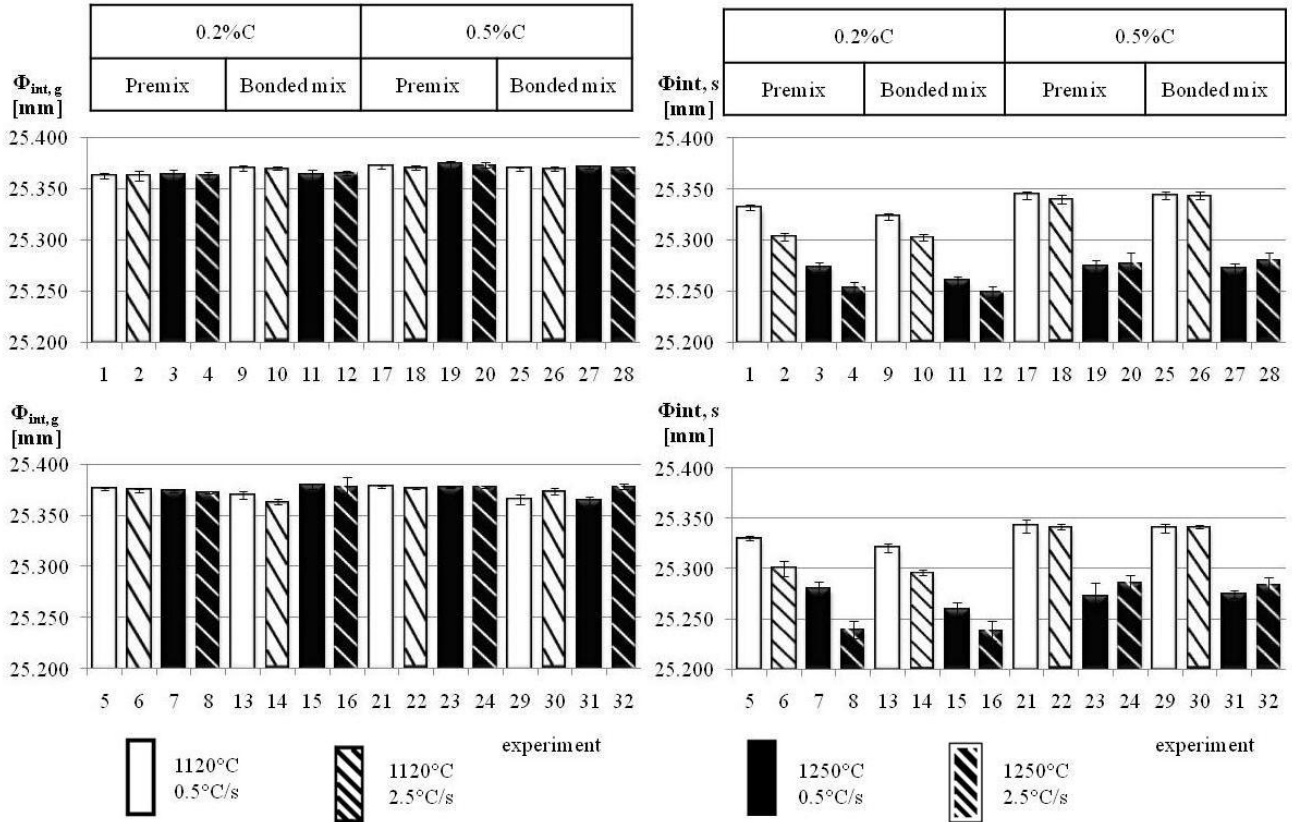


Fig. 4.1.17 Internal diameter of the green and sintered specimens

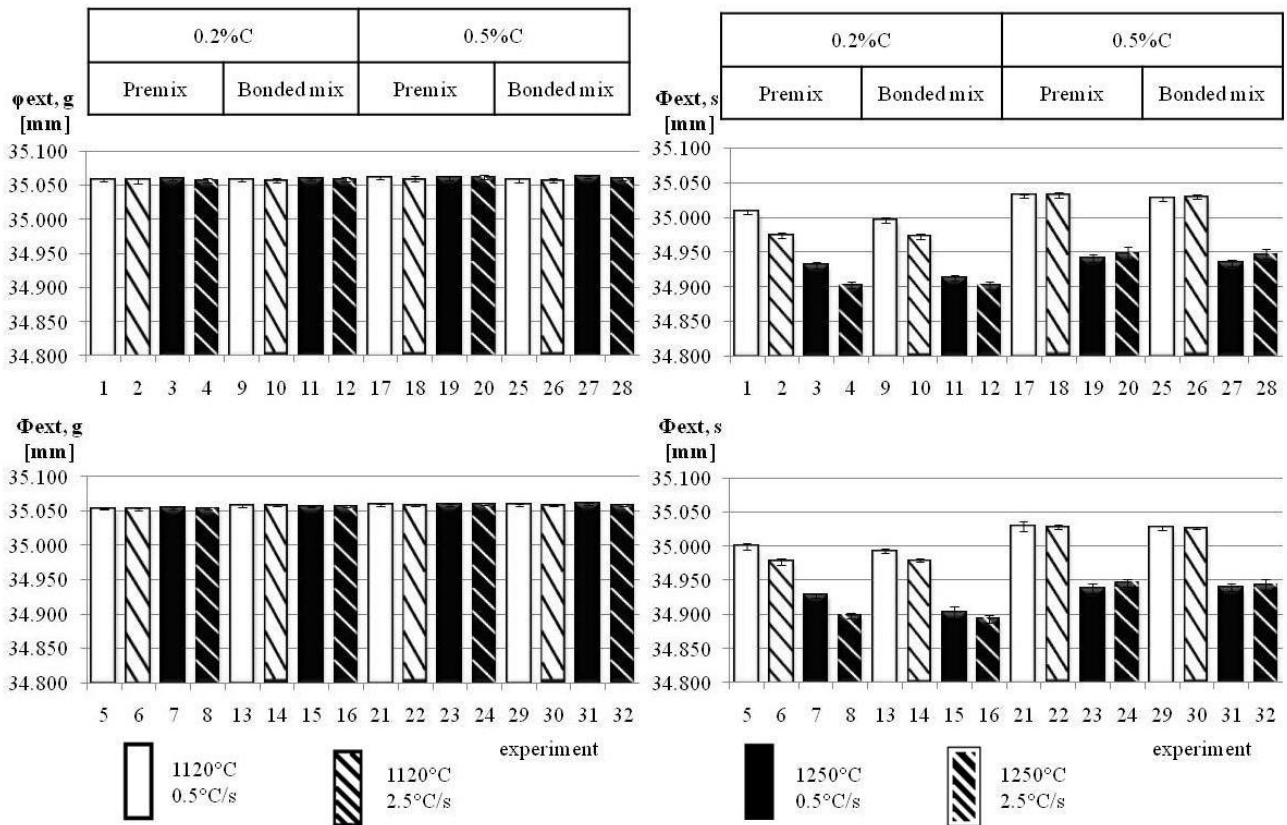


Fig. 4.1.18 External diameter of the green and sintered specimens

As it was expected, the dimensions in the green parts show a very good repeatability, as shown by the very small scatter. As usual in Powder Metallurgy, the scatter is higher in the dimension parallel to the compaction direction than in the dimensions in the compaction plane, and it ranges between 0.006 and 0.020 mm for height, and between 0.003 and 0.005 mm for diameters (comparable to the measurement accuracy). The excellent dimensional precision of the green parts is maintained after sintering; the scatter band either increases or decreases after sintering without any systematic trend.

4.1.2.3 Dimensional variation

Table 4.1.10 shows the dimensional variation of height and of the internal and external diameter.

Batch	Composition	Lubricant	height [mm]	Temperature [°C]	Cooling rate [°C/s]	$\Delta h/h_0$	$\Delta\Phi_i/\Phi_{i_0}$	$\Delta\Phi_e/\Phi_{e_0}$
1	0.2% C	Premix	12.5	1120	0.5	-0.346	-0.122	-0.143
2	0.2% C	Premix	12.5	1120	2.5	-0.482	-0.235	-0.236
3	0.2% C	Premix	12.5	1250	0.5	-0.730	-0.354	-0.365
4	0.2% C	Premix	12.5	1250	2.5	-0.628	-0.431	-0.439
5	0.2% C	Premix	25	1120	0.5	-0.408	-0.180	-0.150
6	0.2% C	Premix	25	1120	2.5	-0.445	-0.294	-0.214
7	0.2% C	Premix	25	1250	0.5	-0.622	-0.371	-0.360
8	0.2% C	Premix	25	1250	2.5	-0.706	-0.523	-0.443
9	0.2% C	Bonded mix	12.5	1120	0.5	-0.406	-0.185	-0.177
10	0.2% C	Bonded mix	12.5	1120	2.5	-0.445	-0.263	-0.242
11	0.2% C	Bonded mix	12.5	1250	0.5	-0.692	-0.408	-0.417
12	0.2% C	Bonded mix	12.5	1250	2.5	-0.721	-0.456	-0.443
13	0.2% C	Bonded mix	25	1120	0.5	-0.461	-0.193	-0.186
14	0.2% C	Bonded mix	25	1120	2.5	-0.449	-0.266	-0.224
15	0.2% C	Bonded mix	25	1250	0.5	-0.699	-0.469	-0.437
16	0.2% C	Bonded mix	25	1250	2.5	-0.627	-0.549	-0.468
17	0.5% C	Premix	12.5	1120	0.5	-0.204	-0.110	-0.085
18	0.5% C	Premix	12.5	1120	2.5	-0.327	-0.122	-0.076
19	0.5% C	Premix	12.5	1250	0.5	-0.647	-0.391	-0.341
20	0.5% C	Premix	12.5	1250	2.5	-0.585	-0.376	-0.327
21	0.5% C	Premix	25	1120	0.5	-0.347	-0.137	-0.082
22	0.5% C	Premix	25	1120	2.5	-0.284	-0.138	-0.086
23	0.5% C	Premix	25	1250	0.5	-0.602	-0.415	-0.344
24	0.5% C	Premix	25	1250	2.5	-0.540	-0.363	-0.324
25	0.5% C	Bonded mix	12.5	1120	0.5	-0.386	-0.101	-0.088
26	0.5% C	Bonded mix	12.5	1120	2.5	-0.312	-0.104	-0.081
27	0.5% C	Bonded mix	12.5	1250	0.5	-0.688	-0.392	-0.366
28	0.5% C	Bonded mix	12.5	1250	2.5	-0.539	-0.356	-0.322
29	0.5% C	Bonded mix	25	1120	0.5	-0.350	-0.101	-0.092
30	0.5% C	Bonded mix	25	1120	2.5	-0.261	-0.125	-0.089
31	0.5% C	Bonded mix	25	1250	0.5	-0.574	-0.351	-0.345
32	0.5% C	Bonded mix	25	1250	2.5	-0.545	-0.372	-0.327

Table 4.1.10 Dimensional variation of height and diameters

The dimensional variation in height is larger than the dimensional variation in the diameters, confirming anisotropy of dimensional change, which was investigated in depth in a specific work [15]. The effect of temperature and cooling rate revealed by densification is confirmed.

4.1.2.4 ANOVA analysis

To investigate the most significant factors affecting the dimensional changes and their interactions, if any, an ANOVA analysis was performed for each dimension, considering the interaction between two parameters at time. The results are shown in the following tables (Table 4.1.11-Table 4.1.13)

and figures (Fig. 4.1.19-Fig. 4.1.21). The highlighted rows in the tables indicate the most significant parameters.

ANOVA OF variation of height					
	DoF	Sum Sq	Mean Sq	F Value	Pr(>F)
Height	1	0.00149	0.00149	0.8662	0.365832
Lubricant	1	0.00198	0.00198	1.1575	0.297941
T_sint	1	0.55968	0.55968	326.4463	4.555*10⁻¹²
Composition	1	0.08778	0.08778	51.1998	2.285*10 ⁻⁶
Cooling rate	1	0.00819	0.00819	4.7782	0.044033
Height: Lubricant	1	0.00162	0.00162	0.9475	0.344838
Height: T_sint	1	0.00530	0.00530	3.0940	0.097690
Height: Composition	1	0.00072	0.00072	0.4211	0.525584
Height: Cooling rate	1	0.00031	0.00031	0.1823	0.675117
Lubricant: T_sint	1	0.00128	0.00128	0.7437	0.401206
Lubricant: Composition	1	0.00001	0.00001	0.0036	0.953078
Lubricant: Cooling rate	1	0.00128	0.00128	0.7437	0.401206
T_sint: Composition	1	0.00211	0.00211	1.2897	0.272832
T_sint: Cooling rate	1	0.00143	0.00143	0.8347	0.374470
Composition: Cooling rate	1	0.01950	0.01950	11.3756	0.003877
Residuals	16	0.02743	0.00171		

Table 4.1.11 ANOVA analysis of variation of height

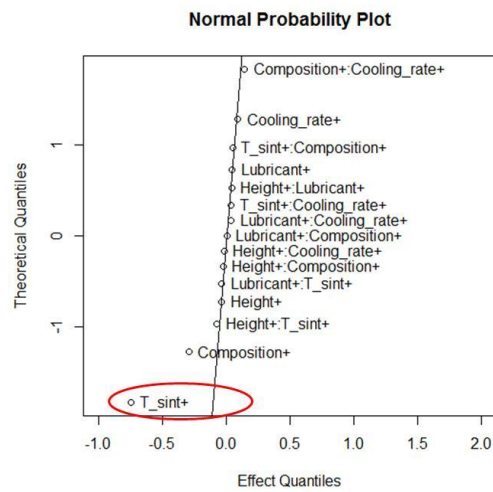


Fig. 4.1.19 ANOVA analysis of variation of height

ANOVA OF variation of external diameter					
	DoF	Sum Sq	Mean Sq	F Value	Pr(>F)
Height	1	0.00002	0.00002	0.1299	0.7232054
Lubricant	1	0.00261	0.00261	20.5161	0.0003421
T_sint	1	0.45530	0.45530	3578.8477	<2.2*10⁻¹⁶
Composition	1	0.07693	0.07693	604.7067	3.873*10 ⁻¹⁴
Cooling rate	1	0.00412	0.00412	32.3677	3.354*10 ⁻⁵
Height: Lubricant	1	0.00005	0.00005	0.4129	0.5295920
Height: T_sint	1	0.00003	0.00003	0.2675	0.6120885
Height: Composition	1	0.00000	0.00000	0.0710	0.7933041
Height: Cooling rate	1	0.00018	0.00018	0.0061	0.9385098
Lubricant: T_sint	1	0.00124	0.00124	1.3817	0.2570036
Lubricant: Composition	1	0.00124	0.00124	9.7276	0.0066126
Lubricant: Cooling rate	1	0.00109	0.00109	8.5898	0.0097933
T_sint: Composition	1	0.00147	0.00147	11.5669	0.0036523
T_sint: Cooling rate	1	0.00050	0.00050	3.9619	0.0639058
Composition: Cooling rate	1	0.01069	0.01069	84.0641	9.061*10 ⁻⁸
Residuals	16	0.00204	0.00013		

Table 4.1.12 ANOVA analysis of variation of external diameter

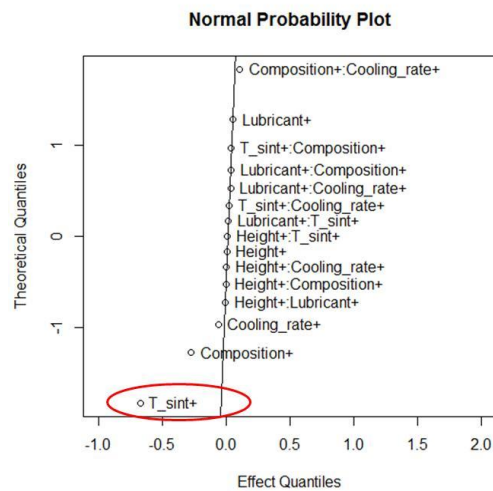


Fig. 4.1.20 ANOVA analysis of variation of external diameter

ANOVA OF variation of internal diameter					
	DoF	Sum Sq	Mean Sq	F Value	Pr(>F)
Height	1	0.00608	0.00608	12.0826	0.003118
Lubricant	1	0.00052	0.00052	1.0339	0.324384
T_sint	1	0.47556	0.47556	945.4399	1.164*10⁻¹⁵
Composition	1	0.05623	0.05623	112.3894	1.212*10 ⁻⁸
Cooling rate	1	0.01501	0.01501	29.8365	5.217*10 ⁻⁵
Height: Lubricant	1	0.00044	0.00044	0.8798	0.362205
Height: T_sint	1	0.00010	0.00010	0.2019	0.659257
Height: Composition	1	0.00363	0.00363	7.2252	0.016171
Height: Cooling rate	1	0.00055	0.00055	1.0990	0.310071
Lubricant: T_sint	1	0.00052	0.00052	1.0339	0.324384
Lubricant: Composition	1	0.00575	0.00575	11.4340	0.003807
Lubricant: Cooling rate	1	0.00039	0.00039	0.7655	0.394566
T_sint: Composition	1	0.00203	0.00203	4.0398	0.061611
T_sint: Cooling rate	1	0.00064	0.00064	1.2704	0.276305
Composition: Cooling rate	1	0.01887	0.01887	37.5080	1.466*10 ⁻⁵
Residuals	16	0.00805	0.00050		

Table 4.1.13 ANOVA analysis of variation of internal diameter

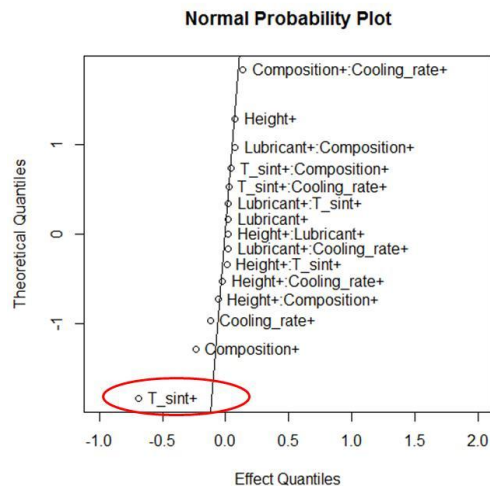


Fig. 4.1.21 ANOVA analysis of variation of internal diameter

ANOVA shows that the effect of the sintering temperature is much more significant than that of carbon content, while the interaction between carbon content and cooling rate is almost negligible. Two phenomena govern dimensional variations of sintered steels: sintering shrinkage and dimensional change associated with austenite transformations on cooling. As previously discussed, the sintering temperature does not influence the austenite transformations on cooling, so that sintering temperature does not have an effect on dimensional change through the austenite transformations. The effect of temperature is therefore due to its well known effect on sintering shrinkage. Carbon content could influence dimensional change since it promotes the carbothermal reduction of chromium oxide, it increases the iron self diffusion coefficient in austenite and it influences the austenite transformations moving the CCT curves to the right, thus favoring the formation of martensite; the volume expansion due to the martensite formation is larger than that due to the bainite and pearlite formations. The increase in shrinkage on decreasing carbon content

from 0.5% to 0.2% demonstrates that the third phenomenon prevails over the other two, indicating the importance of the austenite transformations on the dimensional change.

4.1.2.5 Geometrical characteristics:

The most significant geometrical characteristics for these parts (see §4.1.1.6) are shown for the different experiments in Fig. 4.1.22, Fig. 4.1.23 and Fig. 4.1.24.

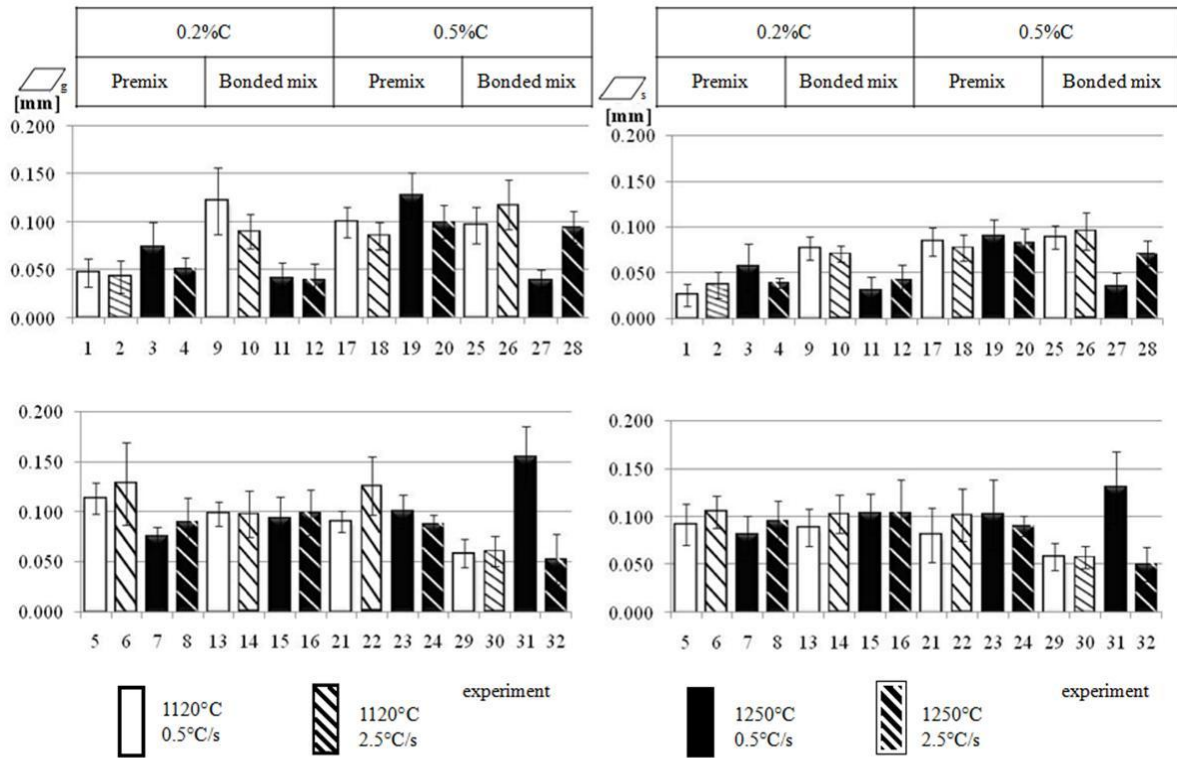


Fig. 4.1.22 Flatness in green and sintered state

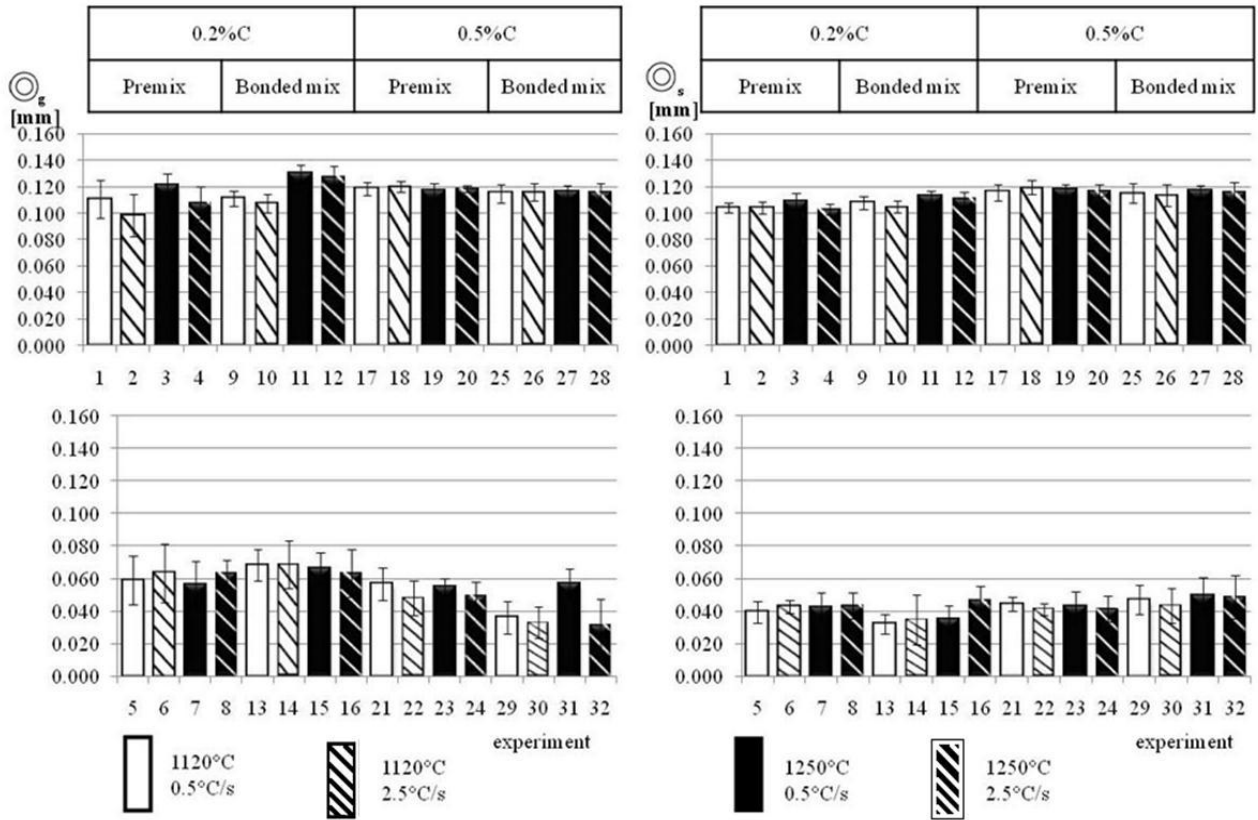


Fig. 4.1.23 Concentricity in green and sintered state

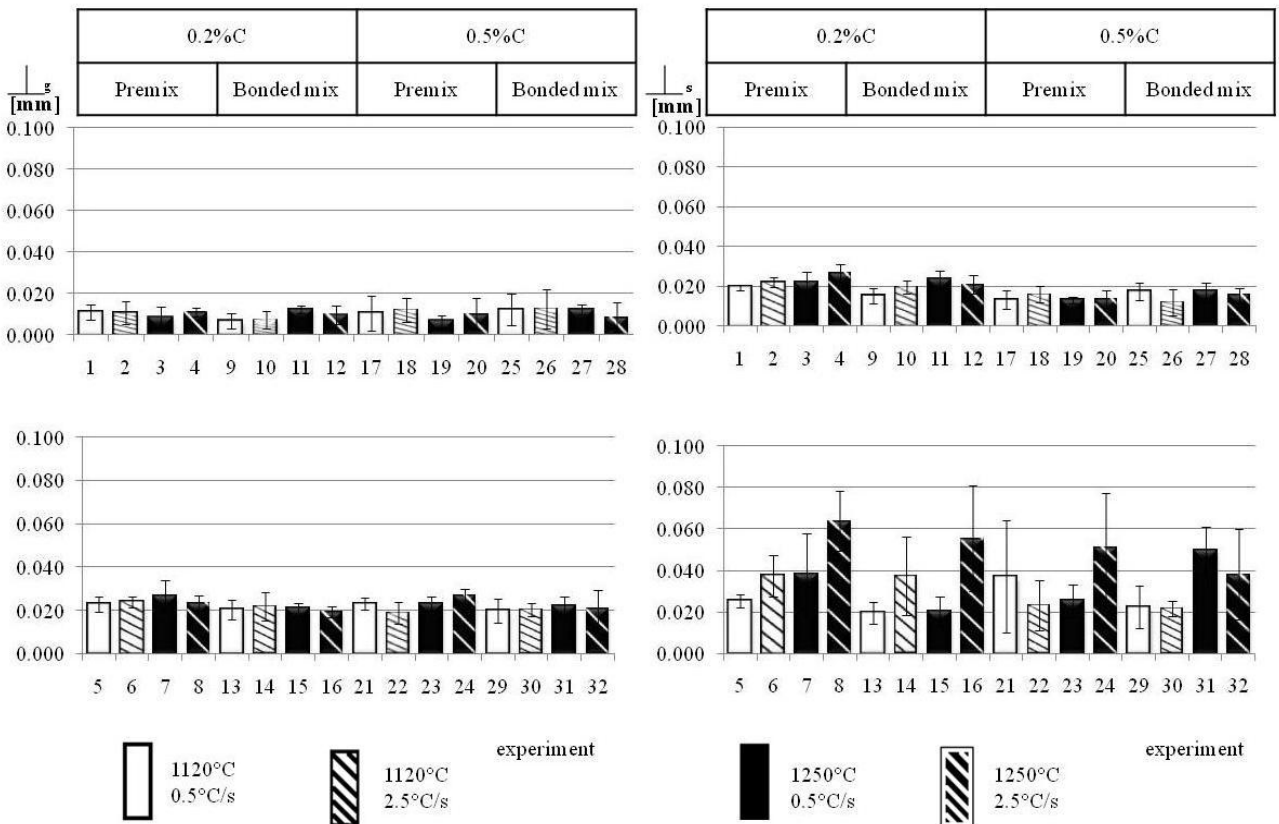


Fig. 4.1.24 Perpendicularity of the upper plane with respect the internal diameter in green and sintered state

Flatness of the upper plane (as representative of the lower one, too) does not worsen after sintering and the precision of the green parts is maintained. A slight effect of composition is observed in the

green parts, which may be due to the effect of graphite particles on flowability of the powder mixture during filling.

Concentricity does not apparently change after sintering, while a clear influence of the height is observed still in the green parts: concentricity is better in the high rings than in the small ones in the green specimens and the difference is maintained after sintering. As in the previous material, this effect may be attributed to the weaker constraint exerted on the low parts by the column of powder during the movement of the compaction tools. Perpendicularity is the one characteristic which worsens after sintering, specifically in the tall parts, but it remains within the ranges typical of the PM process.

4.1.3 Conclusions

In the Fe-Cu-C steel, dimensional change is influenced by the chemical composition, while the copper powder and the lubricant have a minor effect. The use of diffusion bonded copper and of the Bonded mix as a lubricant may contribute to a better control of dimensional change, even if their effect resulted quite slight.

In the Fe-Cr-Mo-C steel, dimensional change is influenced by sintering temperature and, less, by carbon content. The effect of temperature is simply due to its influence on the mass transport mechanisms responsible for the sintering shrinkage, whilst that of carbon content is effectively due to its influence on the products of the austenite transformations on cooling. The use of Bonded mix as a lubricant does not affect dimensional change significantly.

The excellent precision of the green parts is maintained after sintering in both the swelling Fe-Cu-C and the shrinking Fe-Cr-Mo-C steels. The precision of sintered parts may be related to the IT7-IT8 and IT5-IT6 ISO classes for the dimensional tolerances of height and diameters, respectively. This result has to be attributed to the excellent distribution of density in the green compacts, which is favored by the simple geometry considered in the present study. The two systems investigated allow an excellent dimensional control in sintering, provided that a highly homogeneous distribution of green density is ensured.

The excellent geometric precision of the green rings is maintained after sintering, with the exception of perpendicularity, which however remains within the ranges typical of the technology. Geometrical precision is therefore defined by compaction. The proper design of the compaction tools and of the compaction movements and strategy leads to a strict control of the geometrical features of the green parts, as well as to a homogeneous distribution of green density which not only ensures an optimum dimensional control, but even a homogeneous shrinkage/swelling which does not impair geometrical precision.

4.1.4 References

1. Y. Wanibe et al., *Powder Metallurgy*, 33(1)(1990)65-69.
2. A. Griffo et al, *Advances in Powder Metallurgy and Particulate Materials*, 3(1994) 221-236.
3. S. J. Jamil et al, *Powder Metallurgy*, 28(2)(1985) 65-71.
4. R.L. Lawcock et al, *Powder Metallurgy*, vol. 33(2)(1990) 147-150
5. H. Danninger et al, *Materials Science Forum*, 534–536(2007) 577
6. H. Danninger et al, *Science of Sintering*, 40(1)(2008), p. 33-46

7. M. Larsson et al, Proceedings Euro PM2008, Mannheim (Germany), 29th September- 1st October 2008, ed. EPMA Shrewsbury (UK), 3(2008) 211-216.
8. M. Larsson et al, Advances in Powder Metallurgy & Particulate Materials, 3(2008) 165-175
9. I. Cristofolini et al, International Journal of Powder Metallurgy, 48(4)(2012)37-43
10. M. Marucci, Advances in Powder Metallurgy and Particulate Materials, 7(2010) 11-21.
11. U. Engstrom, Advances in Powder Metallurgy and Particulate Materials, 3(1992) 317-328.
12. I. Cristofolini et al, Proceedings EUROPM2011, Barcellona, 9-12 October 2011, ed. EPMA, Shrewsbury (UK), 3(2011) 405-410
13. E. Santuliana et al, Powder Metallurgy,54(3)(2011) 331-337
14. M. Dlapka, Praktische Metallographie, 47(12)(2010) 686-699
15. I. Cristofolini, et al, Powder Metallurgy Progress 3(12)(2012)127-143

4.2 Compaction

The study of the compaction step was focused on two case studies related to the multilevel parts shown in Fig. 4.2.1.

The pulley (left side) is compacted in a stepped die, which represents a compaction solution frequently adopted to realize flanges. When the thickness of the flange is small, a specific compaction strategy has to be implemented, which will be described in the following, which may influence the homogeneous distribution of green density and, in turn, the precision of the sintered parts.

The part shown in the right side of the figure is a simplified model of a three-level gear. In this case the compaction strategy involves the coordinated movement of six punches, of the die and of the core rod. One of the most important parameter is the compaction speed, i.e. the speed of the punches and of the die during the compaction step. Due to the criticism of the part, compaction speed is tendentially and sometimes conservatively low. An increase in the compaction speed results in an increase in the production speed, with significant economical advantages. The focus of the investigation was therefore on the influence of the compaction speed on dimensional and geometrical precision.

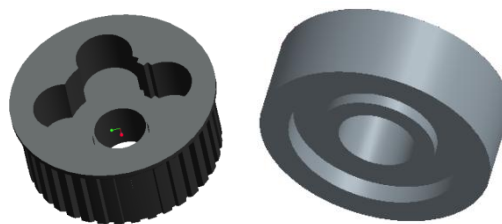


Fig. 4.2.1 Multilevel steel parts

4.2.1 The pulley

The pulley was produced using a Fe-2%Cu-0.5%C powder, compacted to 6.4-6.5 g/cm³ green density.

4.2.1.1 The steps of compaction

The powder were compacted with a hydraulic press with 9 completely independent and closed-loop controlled hydraulic axes. The part is compacted in a stepped die, as shown in Fig. 4.2.2. For this reason, only two upper and two lower auxiliary axes were employed (for the upper punch namely X2-X3 and for the lower part Y2-Y3).

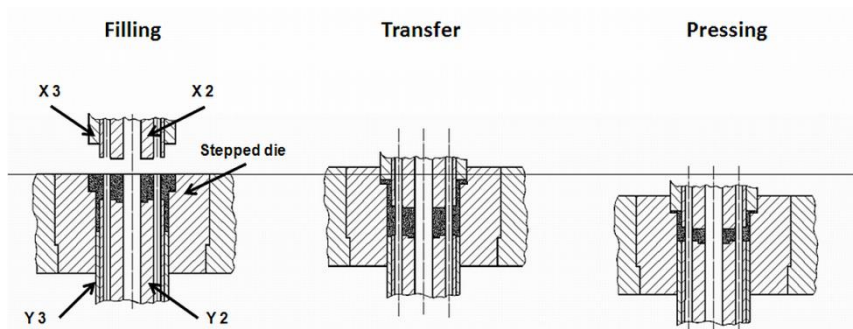


Fig. 4.2.2 Compaction step

A specific compaction strategy is implemented to produce the pulley, due to the thin thickness of the flange which is obtained in the stepped die [1]. Because of the small height of the flange in comparison to that of the other columns, the filling height in the stepped die is 12mm, much higher than that required by the compaction ratio to balance the movement of the punches. Therefore, the compaction strategy involves a preliminary lateral transfer from the die step towards column 2 and 3, to avoid the overstressing of the tools in the flange region. The lateral transfer of the powder from the stepped die is obtained by the upwards movement of the die and the concurrent downwards movement of the punch Y3. In the whole compaction process, only the displacement of the die (stroke) and its speed were changed, both of them are supposed to affect the lateral flow.

Three different compaction cycles were studied, the movement of the Y3 axis was kept constant, while the stroke and the speed of the matrix varied as reported in Table 4.2.1.

	Stroke (mm)	Speed (mm/s)
Batch 1	7	35
Batch 2	7	50
Batch 3	5	50

Table 4.2.1 Compaction condition

4.2.1.2 Dimensions in the green state

The dimensions measured for all the batches are shown in Fig. 4.2.3.

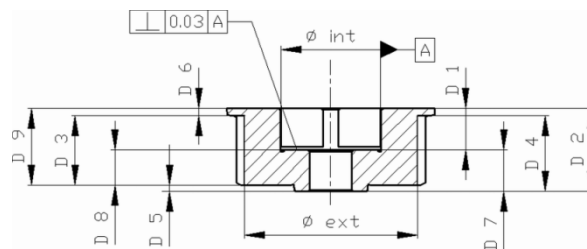


Fig. 4.2.3 Measured dimensions

Some of the most significant dimensions are shown for the different batches in Fig. 4.2.4, Fig. 4.2.5 and Fig. 4.2.6, that means the height of the flange (the most critical dimension relevant to the lateral flow), the height relevant to column 2 and the diameter of the hole taken as Datum.

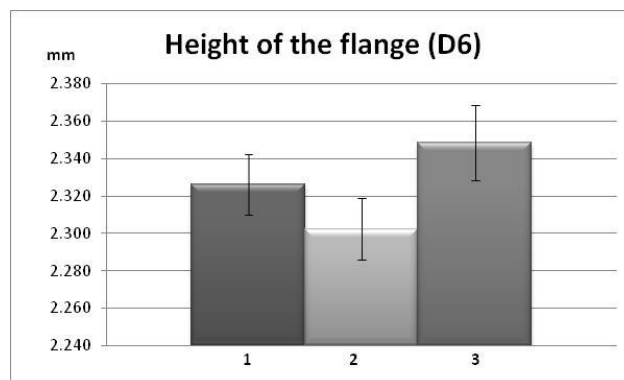


Fig. 4.2.4 Height of the flange

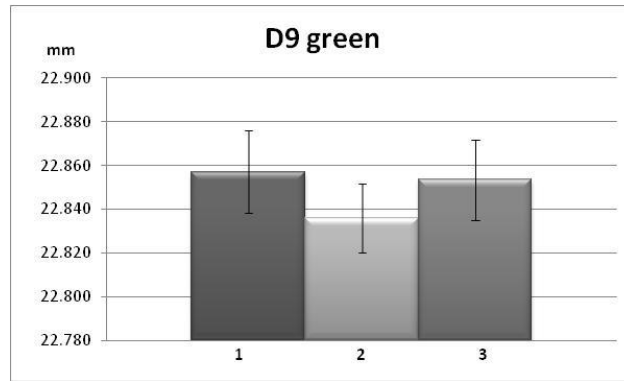


Fig. 4.2.5 Height of D9

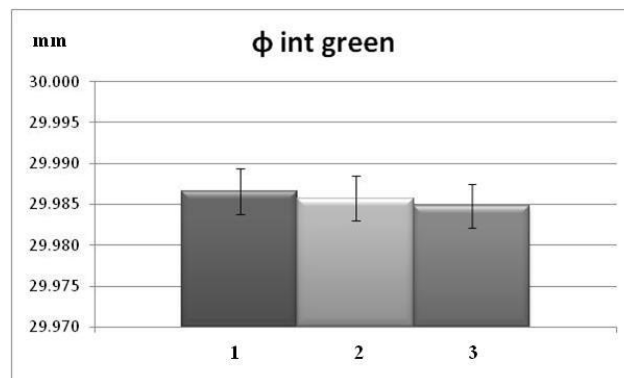


Fig. 4.2.6 Internal diameter

The dimension of the flange shows significant differences in the mean values for the three batches. The scatter is also quite large, it can be related to a tolerance class IT10-IT11. On the other hand, the mean values of the height relevant to column 2 (D9) are comparable in the three batches, analogously scattered, and they can be related to a tolerance class IT9. The dimension in the compaction plane is about the same for all the batches, and the dimensional precision is very good (ISO IT class 5-6). The significant difference highlighted by the flange lead to the analysis of density distribution.

4.2.1.3 Density distribution

The density distribution in the flange was derived from the measurement of porosity obtained by Image Analysis. The mean density and the scatter band are shown in Table 4.2.2; the minimum density is also reported, corresponding to the inner upper part region, due to the movement of the powder during the lateral transfer step (see Fig. 4.2.7); here the powder particles can flow from more freely than in other regions, where friction against the die step walls during the upwards movement of the die exerts some resistance.

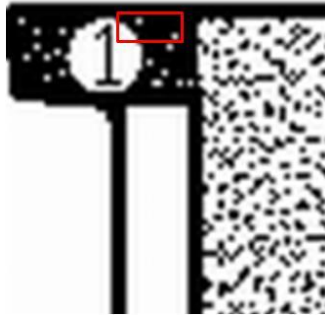


Fig. 4.2.7 The Minimum density zone in the flange

	ρ [g/cm ³]	σ	ρ_{\min} [g/cm ³]	$\rho - \rho_{\min}$
Batch 1	6.86	0.15	6.58	0.28
Batch 2	6.60	0.17	6.40	0.20
Batch 3	6.53	0.19	6.32	0.19

Table 4.2.2 Density in the Flange

The density values in the flange are different and quite scattered, as shown in Fig. 4.2.8.

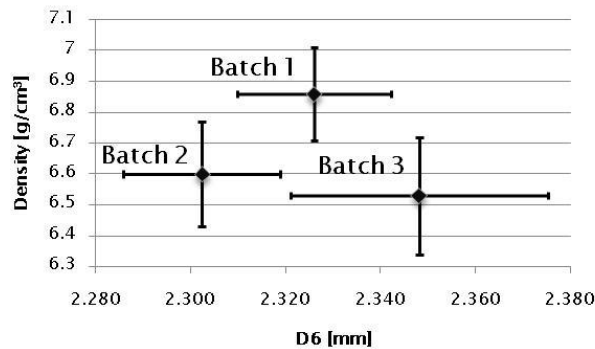


Fig. 4.2.8 Density of the flange with respect to its height

Even in presence of a large scatter of dimensions and densities, it may be observed that in batch 2 both the height and the density of the flange are lower than in batch 1, which means that the column contains a smaller amount of powder. Multiplying the mean height by the mean density, an indication is given of the mass of powder per unit of compaction area; the resulting value is about 7% less in batch 2 than in batch 1. This result indicates that, on increasing the die speed from 35 mm/s up to 50 mm/s at constant stroke (batch 1 vs. batch 2), the lateral transfer increases. On the other side, in batch 3 the flange has a lower density but a larger height than in batch 1 and, again considering the mean values for height and density, it may be estimated that it contains around 4% less powder than flange of batch 1. This means that, on decreasing the stroke from 7 mm to 5 mm at constant speed (batch 2 vs. batch 3), the lateral flow decreases, anyway remaining higher than in batch 1.

The distribution of the density in the central column, for all the three batches is shown in Fig. 4.2.9.

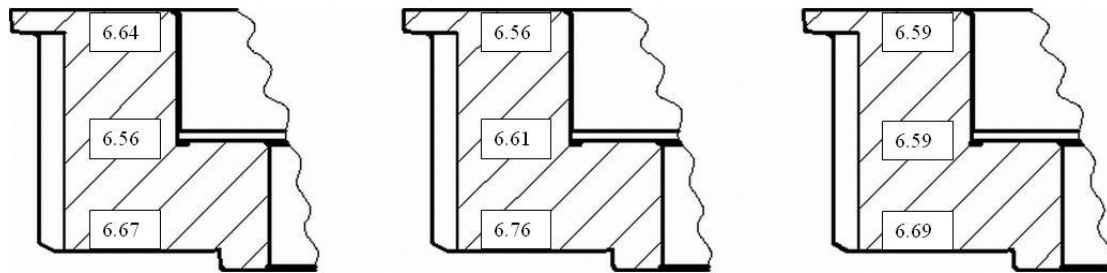


Fig. 4.2.9 Density distribution of the sample

Being the precision in the evaluation of the density $\pm 0.1\text{g/cm}^3$, the mean density shows very slight differences in the three batches. There is a trend in the change of gradient, which could be related to the different lateral transfer. In batch 1 the minimum density is measured in the median section, which confirms the effectiveness of the double action [2] whilst in batches 2 and 3 the lowest density is on the upper section, and in particular in the outer layer analyzed. The standard deviation of the local densities is 0.05%- 0.10%, then differences in the mean values are again very small. However, the lower density in the upper region might be attributed to a less packing of the powder particles after the lateral flow, because of the frictional effect exerted by the upper punch X3. It has to be considered that the whole tools movement was set-up for batch 1, and only the matrix movement was varied in batches 2 and 3. The results indicate that the whole of the compaction strategy has to be adapted in order to obtain the right axial gradient, when the lateral transfer of the powder is modified by changing the movement of the matrix and of the upper punch relevant to the flange.

4.2.1.4 Geometric characteristics

As shown in Fig. 4.2.3, a specific geometrical tolerance is required, the perpendicularity of the plane with respect the axis of the hole taken as Datum.

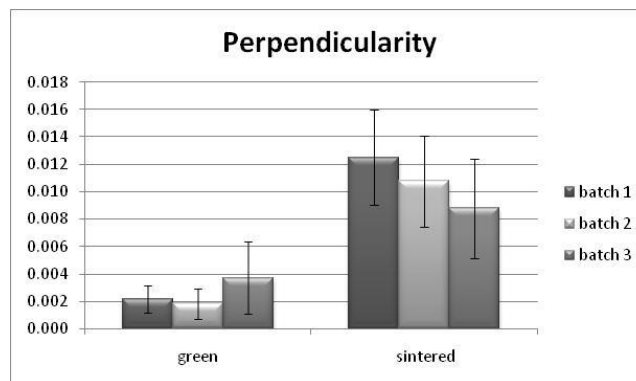


Fig. 4.2.10 Perpendicularity of the plane with respect the internal cylinder

Perpendicularity value is very small in the three batches after compaction and increases on sintering. The three mean values are different, but within the scatter band.

Perpendicularity value may be affected both by the flatness of the plane and by the straightness of the axis of the cylindrical surface. The planes have been calculated, and Fig. 4.2.11 shows an example relevant to the same plane before and after sintering, which is representative of all the parts measured.

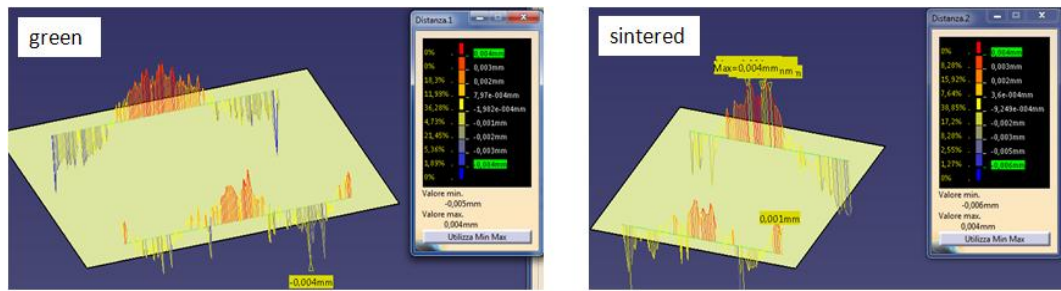


Fig. 4.2.11 Flatness in green and sintered parts

It may be seen that flatness worsens very slightly in sintering, then the increase in perpendicularity can be attributed to the orientation and/or position of the datum axis, which in turn may be related to the trend of the internal cylindrical surfaces. Fig. 4.2.12 shows the internal diameter of the three batches.

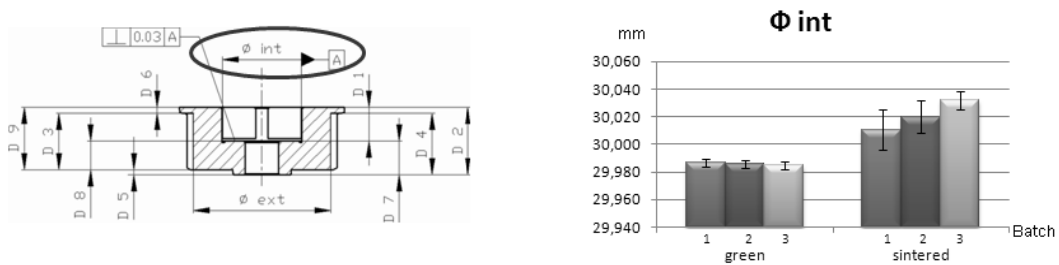


Fig. 4.2.12 Internal diameter for both green and sintered parts

In the green state the values are the same for the three batches and the scatter is extremely low. Diameter grows slightly on sintering (0.1-0.2%), with a slight increase from batches 1 to 2 and further to 3. The as-sintered scatter can be related to a tolerance class IT7-IT8. Data reported in Fig. 4.2.12 are the mean values of measurements carried out at three different heights in the internal hole, whose results are shown in Fig. 4.2.13.

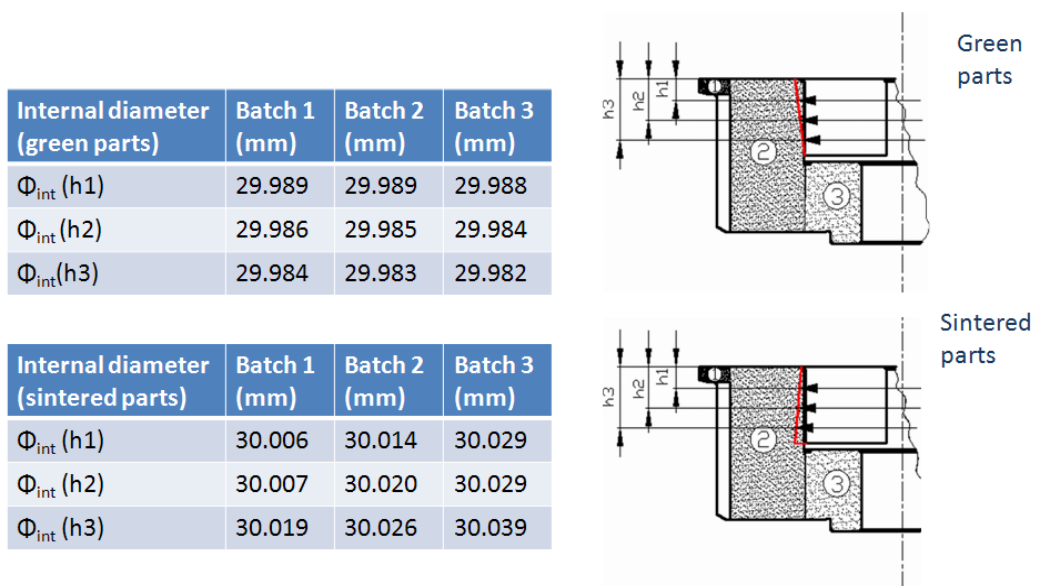


Fig. 4.2.13 Internal diameter measured on different heights

In the green parts the surface derived from the internal diameter measured at different heights is that expected, due to the need of extracting the part. On sintering there is a slight increase in conicity but the most interesting result is the change in the span, which is inverted after sintering. The same trend is observed for the external diameter (Fig. 4.2.14): the part swells on sintering (around 3%), and the growth is larger on increasing the distance from the upper surface. This is due to the greater wall thickness of the pulley in the lower part, which enhances the swelling, but also to the friction with the tray, since during sintering the upper surface is in contact with the tray. Friction between parts and sintering trays has been reported as the main factor influencing the distortion of parts by Vo and Guillot [5]. The same effect may be claimed to justify the change in the span of the internal hole.

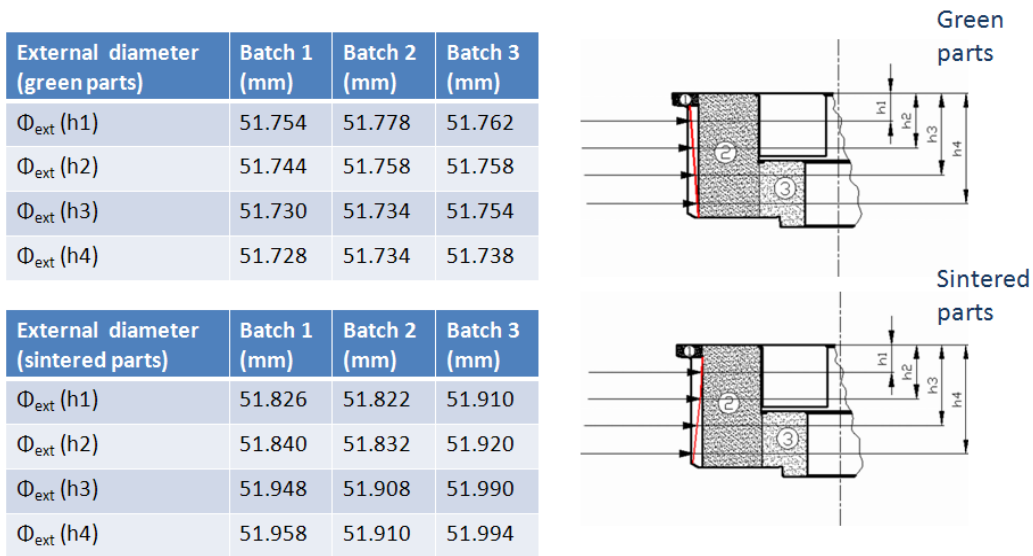


Fig. 4.2.14 External diameter measured on different heights

In conclusion, the lateral transfer of the powder from the die step is influenced by the stroke and the speed of the upwards movement of the matrix. As a consequence, the green density in the column related to the step changes, but the effect on the compaction of the other columns is nearly negligible, a part from a slight difference in the axial density gradient in the nearest column was observed. The dimension of the column produced in the step of the die is significantly influenced by the lateral transfer of the powder, whilst all the other dimensions, both parallel and orthogonal to the pressing direction, are slightly affected. The geometrical characteristics of the green parts are very similar even after sintering, irrespective to the powder transfer. Only perpendicularity worsens after sintering, but this result is not correlated to the lateral powder transfer.

4.2.2 The ring-shaped part

The part was produced using a Fe-3%Cr-0.5%Mo-C powder compacted to 6.8-6.9 g/cm³ green density.

4.2.2.1 The steps of compaction

As in the previous case the parts were compacted with a hydraulic press equipped with 9 completely independent and closed-loop controlled hydraulic axes. Three upper and three lower auxiliary axes were employed (for the upper part namely X1-X2-X3 and for the lower part Y1-Y2-Y3). During the

compaction step the displacement of all the axes of the system and the force acting on the upper punch were continuously recorded. Six steps were identified in the compaction cycle: the end of filling, the powder transfer, the compaction and three different steps of ejection, due to the differences observed in the movement of the axes during ejection. Fig. 4.2.15 shows the different step of the compaction.

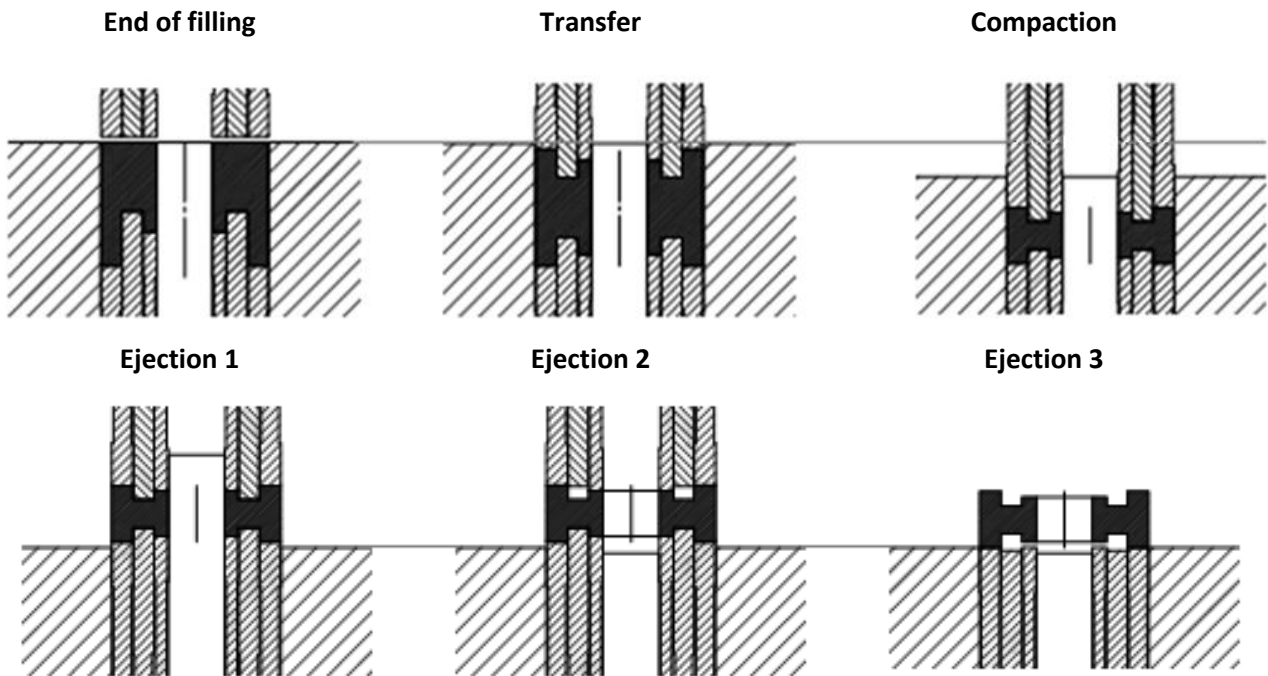


Fig. 4.2.15 The compaction cycle

After filling, the relative movements of upper and lower axes during transfer determine a rearrangement of the powder particles. The dimensions of the part are determined by the relative movements of the punches, the core rod and the die, neglecting the spring-back. In the first step of ejection the core rod does not move moves up, while the die moves down, so that the part is only constrained by the punches. In the second step the X2 upper punch moves up and core rod moves down and in the third steps the remaining upper punches and lower punches move, until the part is completely free.

Fig. 4.2.16 shows an example of the curve plotting the recorded data - force and displacement of the upper transom - during the whole compaction cycle. The different steps are also highlighted.

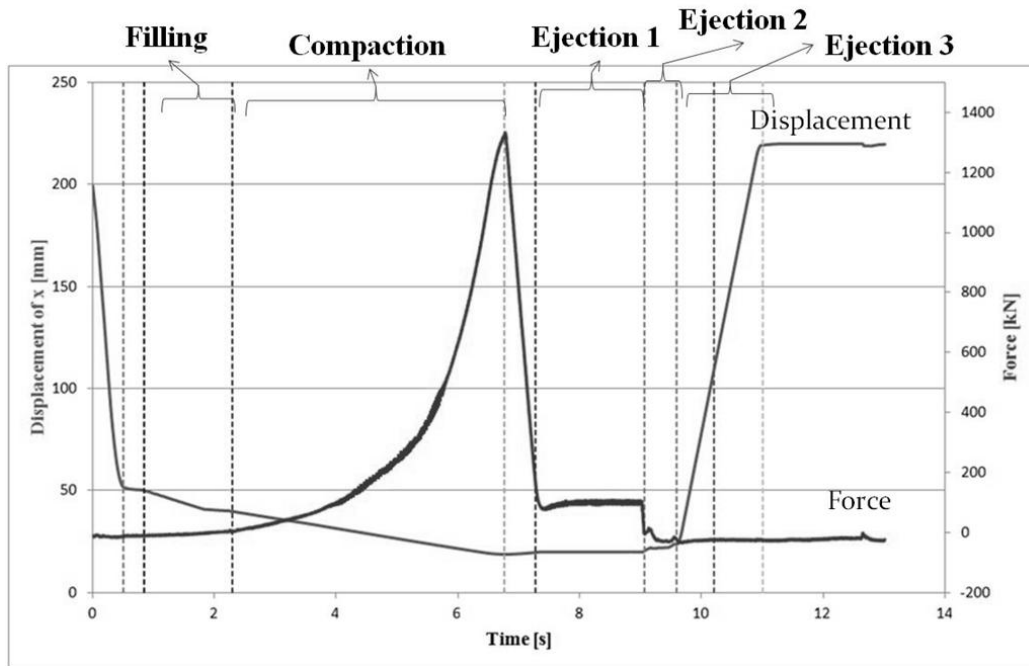


Fig. 4.2.16 Motion of upper punch and force applied during the compaction step

The applied force reaches its maximum when the position of the upper punch is at the lower height. At the end of the compaction the force acting on the transom starts to decrease rapidly, while the transom does not move significantly. A small force is applied during the first ejection step, which may lead to a sort of post compaction.

4.2.2.2 Dimensions in green state

The dimensions shown in Fig. 4.2.17 relevant to the different columns, measured on the green parts, are reported in Fig. 4.2.18 with respect to the compaction speed.

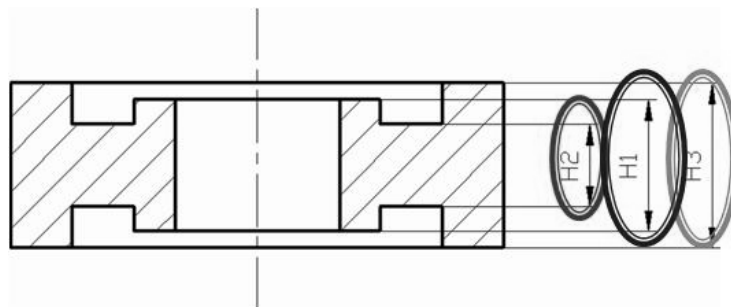


Fig. 4.2.17 Dimensions corresponding to the different columns

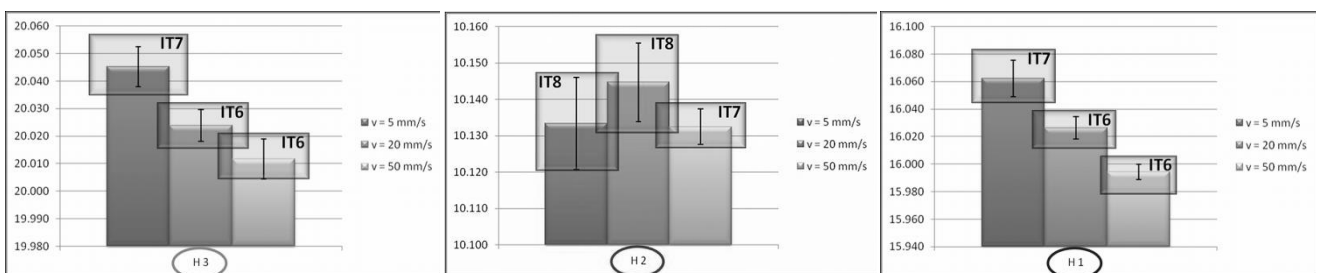


Fig. 4.2.18 Dimensions corresponding to the different columns in function of the compaction speed

On increasing the compaction speed, the height of the columns in contact to the die (H3) and to the core rod (H1) decreases, whilst the height of H2 does not show a significant trend, since the

increase measured at the intermediate speed is comparable to the scatter band. The scatter band corresponds to the ISO IT8 class, while the differences between the mean values correspond to the ISO IT10, thus confirming the excellent precision of the green parts; however the trend of H3 and H1 is significant and has been investigated in depth, as following explained.

It has to be considered that the only direct measure is the total height of the part H3, the other two dimensions are derived subtracting from the total height the dimensions named upper and lower step highlighted in Fig. 4.2.19 and directly related to the columns in the compaction step. Fig. 4.2.20 shows these dimensions in function of the compaction speed.

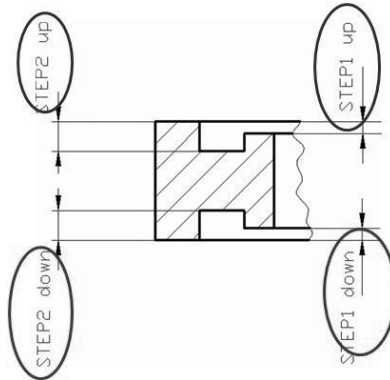


Fig. 4.2.19 Dimensions directly related to the columns

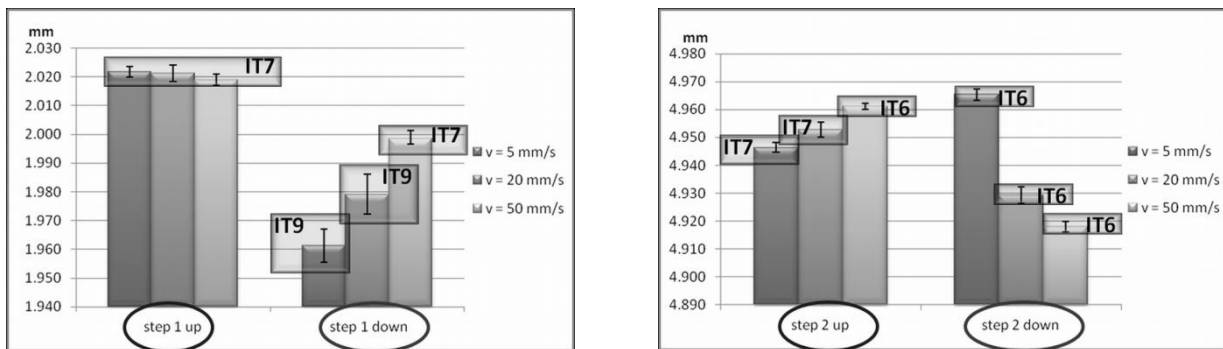


Fig. 4.2.20 Dimensions directly related to the columns in function of the compaction speed

Again the differences are much smaller than the ranges corresponding to the tolerance required, but the trend is significant and depicts a downwards shift of the intermediate column (H2) and an upwards movement of the internal column (H1) on increasing the compaction speed. A schematic representation of the trend of the step dimensions at the different compaction speeds is shown in Fig. 4.2.21 (not to scale).

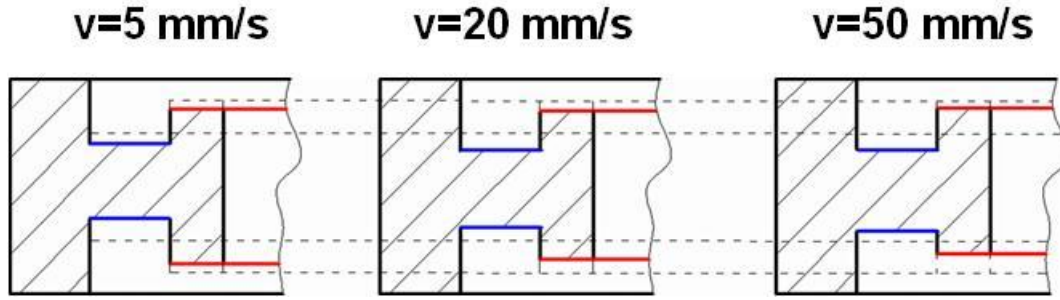


Fig. 4.2.21 Motion of the step on the compaction cycle with respect the compaction rate

4.2.2.3 Geometrical characteristics

In Fig. 4.2.22 the main geometrical characteristics required are reported.

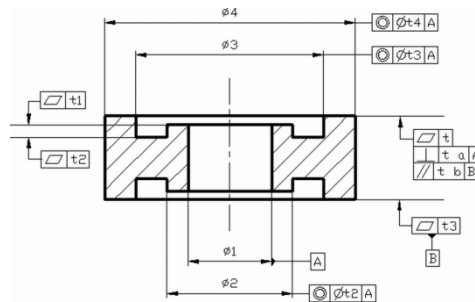


Fig. 4.2.22 Geometrical characteristics

Concentricity of the external cylinder ($\Phi 4$) and of the upper and lower circumferences $\Phi 3$ and $\Phi 2$ with respect to the internal one ($\Phi 1$), and flatness are shown in Fig. 4.2.23.

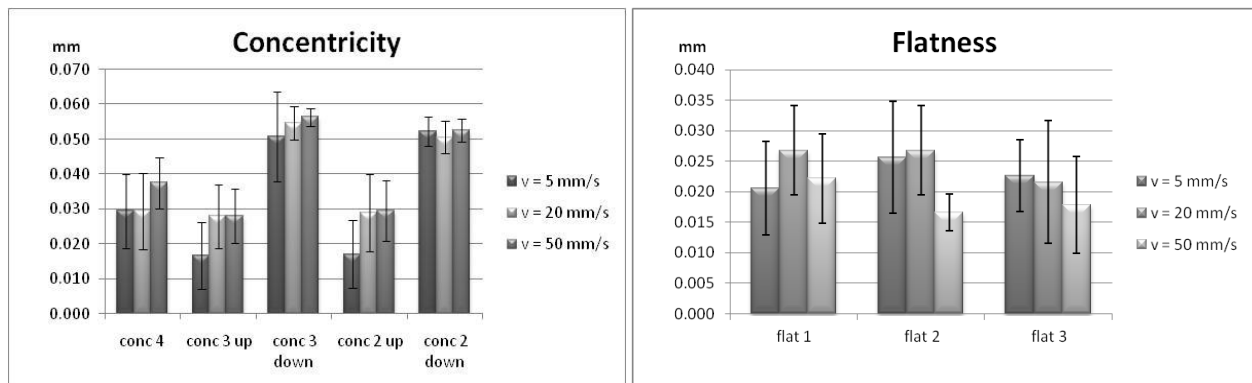


Fig. 4.2.23 Concentricity and flatness

Considering the scatter bands, there is no significant effect of the compaction speed on concentricity. It's interesting to observe that concentricity of the upper circumferences is lower than that of the lower ones, whilst that measured considering the whole surface of the external cylinder is constant (the mean value is reported in the figure). Concentricity is similar to that measured on one-level parts of the same dimensions [3]. The flatness of the compaction surfaces is around 0.03 mm, with a scatter band of 0.02 mm, irrespective to the compaction speed. Considering that the flatness requirement for the upper surface of the die is 0.03 mm, the values of flatness for the measured surfaces may be considered as good ones.

4.2.2.4 Density distribution

The density distribution was evaluated by water displacement method cutting in 9 section the parts. The values obtained are shown in Fig. 4.2.24.

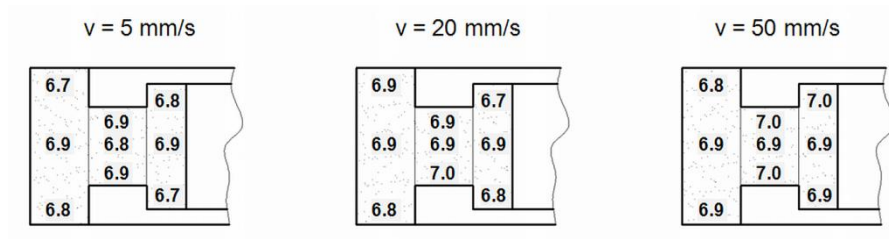


Fig. 4.2.24 Density distribution

The precision of the measure of density is $\pm 0.1 \text{ g/cm}^3$, then density is homogeneous along the axial direction, as well as among the three columns, and it does not change on increasing the compaction speed. Since the increase in the compaction speed does not affect the powder mass in the columns (die filling and powder transfer were kept constant), density cannot be significantly influenced by the change in height of the columns. The corresponding differences in height, indeed, may be related to $\pm 0.02 \text{ g/cm}^3$, much lower than the precision of the measure.

The increase of the compaction speed has a positive effect on the morphology of the cylindrical surfaces (in contact with the die during compaction). Fig. 4.2.25 show the SEM images representative of the compaction speed of 5 mm/s and 50 mm/s of the upper, median and lower part of the external surface of the green part.

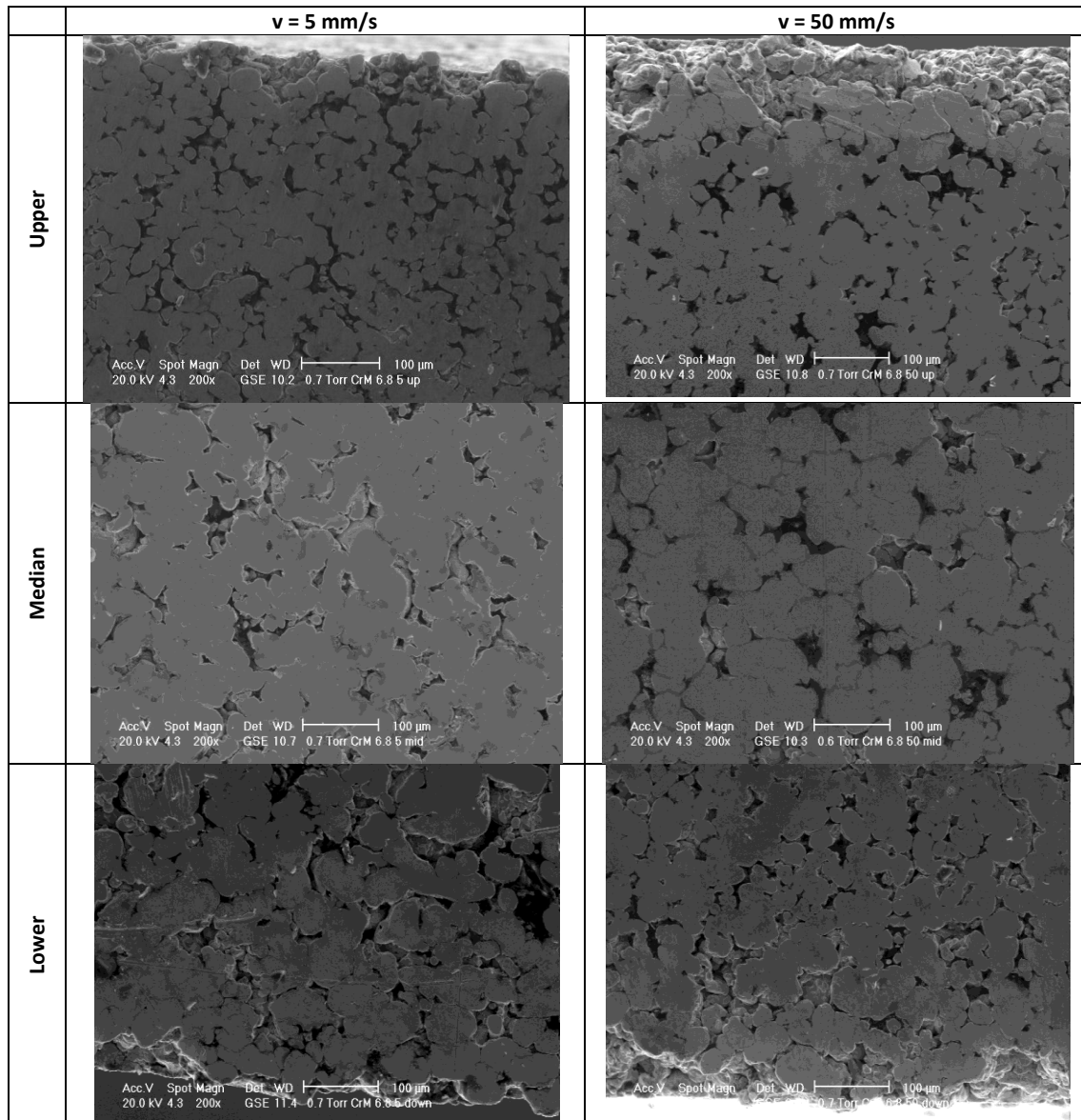


Fig. 4.2.25 Surface morphology of the 5 mm/s and 50 mm/s specimens

The surface porosity is more homogeneous along the axial direction in the parts compacted at the highest speed. Moreover, there is an evidence of a different distribution of the lubricant, which fills pores more homogeneously on increasing the compaction speed. This improvement may be due to the effect of compaction speed on the fluidity of the lubricant, as a result of the enhanced temperature reached in contact with the die surface, due to friction.

4.2.2.5 Compaction cycle

Even if within the precision defined by the dimensional tolerances required, a trend in the change of some dimensions is observed on increasing the compaction speed. In order to interpret such a trend, a deeper analysis of the data collected during compaction was performed. Considering the movement of the different axes (upper and lower punches), and the force applied during all the process, the force applied on the different axes was derived, under these assumptions

- ✓ Only normal stresses are applied (no tangential one);
- ✓ No friction on the contacting surfaces is considered;

- ✓ The pressure applied on the three axes is the same, with the exception of the first part of the compaction step, when the motion of the axes is in force control.

Fig. 4.2.26 shows how the force diagrams are transformed in pressure diagrams in the case of the lowest compaction speed. During the first part of the cycle, not all the punches are in contact with the powder columns, and the force is not homogeneously distributed on the three columns. After about 4.8 s, compaction is exerted by all the punches, and the compaction pressure is the same on the three columns.

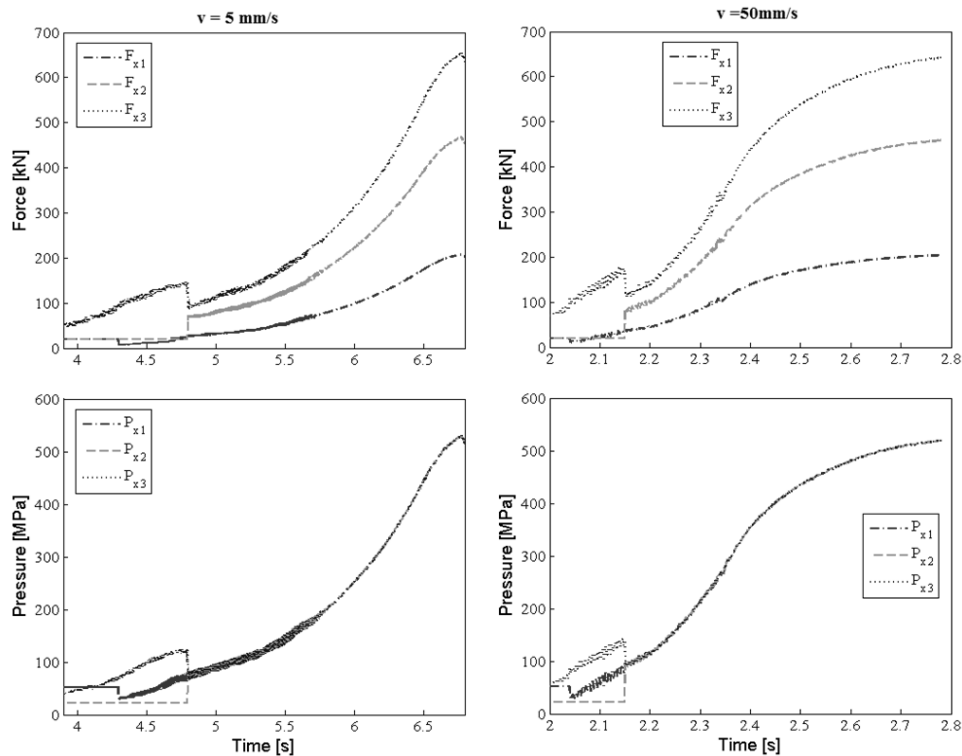


Fig. 4.2.26 Force and pressure act on the axes during the compaction

The maximum force applied on the different axes slightly changes with the compaction speed. For instance it is:

- ✓ $v = 5 \text{ mm/s}$: $F_{x1} = 208 \text{ kN}$, $F_{x2} = 470 \text{ kN}$, $F_{x3} = 657 \text{ kN}$;
- ✓ $v = 50 \text{ mm/s}$ $F_{x1} = 204 \text{ kN}$, $F_{x2} = 460 \text{ kN}$, $F_{x3} = 643 \text{ kN}$.
- ✓ The slight decrease on increasing the compaction speed may be correlated to the better efficiency of the lubricant above mentioned. The maximum pressure applied is in the range of 515-535 MPa. That is comparable with the compacting pressure needed to obtain a green density of 6.8-6.9 g/cm^3 .

Fig. 4.2.27 plots the movement of the X axes during the compaction step for the different compaction speed.

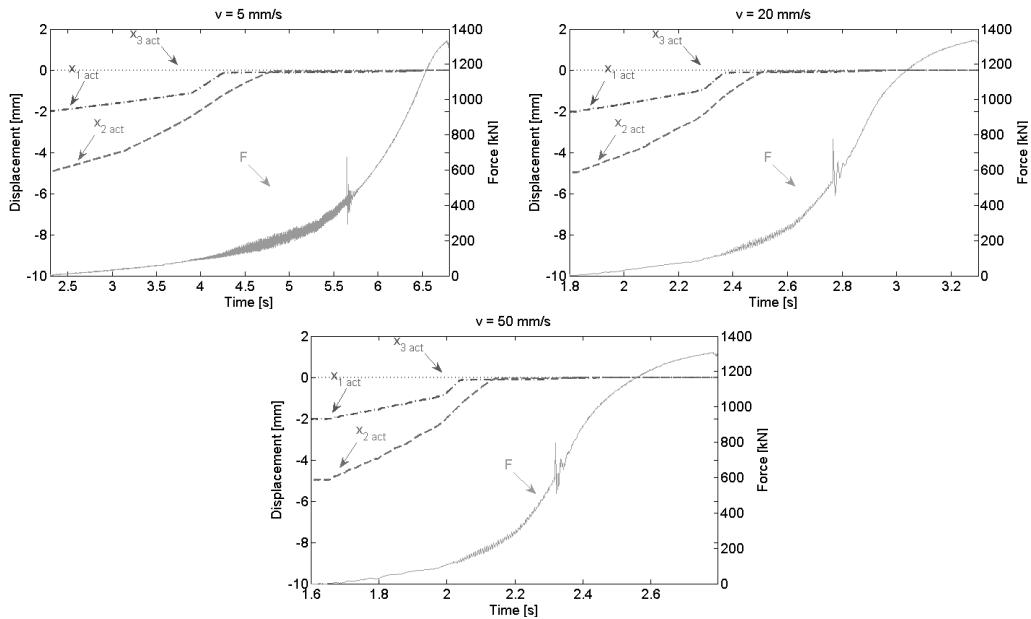


Fig. 4.2.27 Motion of the x axes during the compaction step

The movement of the three axes is different in the first part of the compaction cycle, when the applied force is still low; therefore, no effect on the compaction and on the final position of the columns which might be correlated to the different dimensions of the steps may be hypothesized. Significant differences were instead observed during the first step of the ejection of the green parts. Fig. 4.2.28 shows the record of the force F , of the Z axis (z_{act} representing the downwards displacement of the die), of the Z1 axis ($z1_{act}$ representing the upwards movement of the core rod) and of the X transom in the upper part (x_{act}). The Y1, Y2 and Y3 axes displacement is also shown. The three upper axes (X1, X2 and X3) are kept fixed during this step, as it is shown by X. The different displacements of the Y axes on increasing the compaction speed were imposed to adapt the compaction strategy to the increased speed, to prevent green cracks.

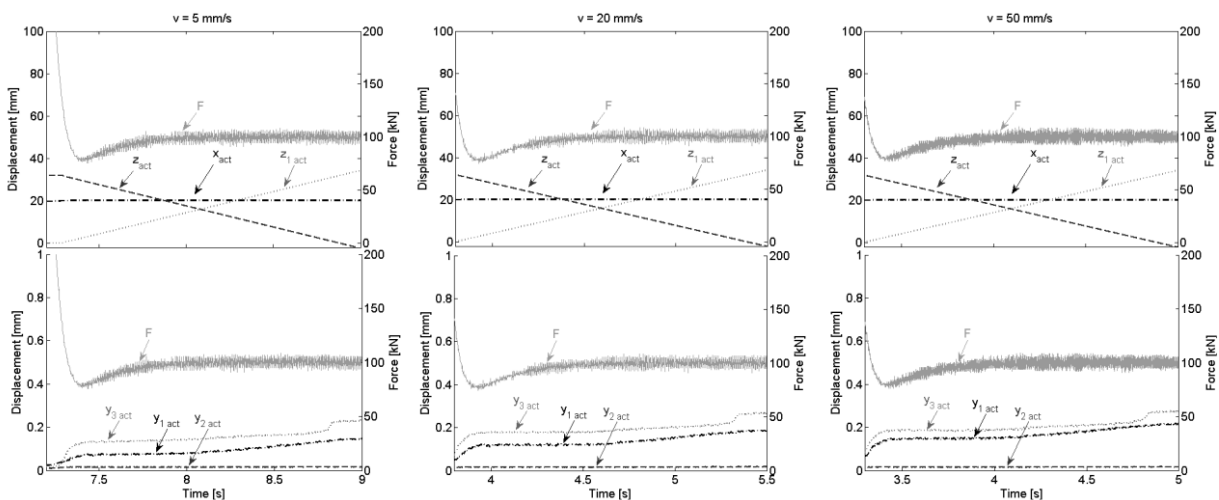


Fig. 4.2.28 Force and motion of lower axes, punch, die and core rod during the ejection 1

The figure shows that, whilst the force decreases to 100 kN (hold-down force) and the die moves downwards to eject the green part, the Y1 and Y3 punches move upwards primarily to compensate for spring-back effects, and in such a way applying a slight post-compaction [4] on the relevant columns. The displacements are different in the three experiments, as shown by Table 4.2.3 where the maximum values at the end of the first ejection step are reported.

	v = 5 mm/s	v = 20 mm/s	v = 50 mm/s
Y1	0.14 mm	0.18 mm	0.22 mm
Y2	0.01 mm	0.01 mm	0.01 mm
Y3	0.23 mm	0.26 mm	0.28 mm

Table 4.2.3 Displacement of the y axes during ejection 1

In particular, the set-up of the compaction strategy results in an increasing displacement of the two punches Y1 and Y3 with the compaction speed, whilst the displacement of Y2 is constant other than much lower. The motion of the Y axes, with except of the intermediate one, increases with the increasing of the compaction speed, and the value of the motion of the Y1 and Y3 axes are comparable with the motion of the different step. The post compaction may be reasonably responsible of the decrease of the height of the external and the internal column.

In conclusion, increasing the compaction speed the efficiency of the lubricant is enhanced, and an improvement in the homogeneity of the porosity on the surfaces contacting the die and the core rod is observed. The adjustment in the compaction strategy due to the increase in the compaction speed also implies a post-compaction effect which affects the height of the columns.

4.2.3 Conclusions

The study of the effect of the compaction parameters on dimensional and geometrical precision of multilevel parts highlights some important issues related to the compaction strategy which is implemented in different cases.

The production of a green part with a stepped die which requires a lateral powder transfer may result critical since the lateral transfer of the powder may influence the dimension of the column produced in the step and the axial density gradient in the adjoining column. Any strategy aimed at modifying the lateral transfer of the powder has to be verified.

The change of compaction speed during compaction of a three-level parts may also be critical if the compaction strategy, in particular during the ejection step, is not adapted to the increasing compaction speed. The different post-compaction exerted by the lower punches may have an important influence on the dimensional precision of the parts.

The two effects highlighted do not depend on the powder utilized; they are directly correlated to the compaction strategy. In both cases the dimensional and geometrical precision of the parts did not worsen significantly, but the results show that even secondary parameters of the compaction cycles may influence the characteristics of the green parts.

4.2.4 References

1. R.M. German, Powder metallurgy of iron and steel, ed. John Wiley and sons, 1998
2. M. Rajab et al: Powder Metallurgy, 28(4)(1985) 207-216
3. I. Cristofolini et al., Proceedings EUROP2011, Barcellona, 9-12 October 2011, ed. EPMA, Shrewsbury (UK), vol. 3, pp. 405-410
4. E. Ernst et al., Powder Metallurgy International, 23(2)(1991)77-83
5. A. Vo et al, Advances in Powder Metallurgy and Particulate Materials, 1(3)(1999) 123–138.

4.3 Sintering

In this chapter the effect of a very high sintering temperature on dimensional and geometrical characteristics of two real parts was investigated. The increase in the sintering temperature is expected to increase densification and to improve the pore morphology, thus improving mechanical properties [1-5]. In the case of Cr containing steels, the increase in sintering temperature enhances the reduction of chromium oxides, improving the quality of the microstructure [6-7]. A Cr-Mo low alloy steel and an austenitic stainless steel were considered, and sintered up to 1350°C to verify how the enhanced shrinkage affects precision of the parts. The low Cr-Mo steel was both sintered and sinterhardened [8, 9]. The parts investigated are shown in Fig. 4.3.1; they have quite a complex geometry and they can therefore represent critical practical examples of the products of Powder Metallurgy.

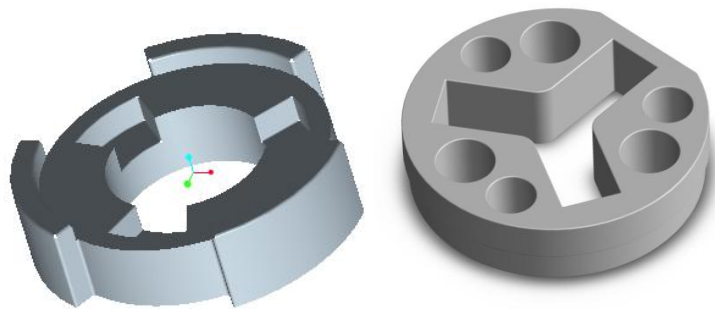


Fig. 4.3.1 Parts studied

Main parameters relevant to the part represented in Fig. 4.3.1 on the left are:

Composition: Fe-3%Cr-0.5%Mo-0.5%C

Green density: 6,8 g/cm³

Sintering temperature: 1250-1300-1350 °C.

Cooling rate: 0.1 C/s (sintering) -2°C/s (sinterhardening)

Main parameters relevant to the part represented in Fig. 4.3.1 on the right are:

Composition: prealloyed AISI 316 L

Green density: 6.4-6.6-6.8 g/cm³.

Sintering temperature: 1250-1300-1350 °C.

4.3.1 Fe-3%Cr-0.5%Mo-0.5%C

4.3.1.1 Density and microstructure

The green and sintered density were measured by the water displacement method. Green density is 6.9 g/cm³; Table 4.3.1 shows the density after sintering and sinterhardening.

	2°C/s (sinterhardening)			0.1°C/s (sintering)		
Sintering temperature [°C]	1250	1300	1350	1250	1300	1350
Sintered density [g/cm³]	6.93	6.97	7.04	6.97	7.02	7.07

Table 4.3.1 Density in sintered state

Density slightly increases with sintering temperature and it is slightly higher in sintered parts than in the sinterhardened ones at the same temperature.

Fig. 4.3.2 shows the microstructure, and the relevant microhardness, of the sinterhardened parts, and Fig. 4.3.3 shows the microstructure of the sintered parts.

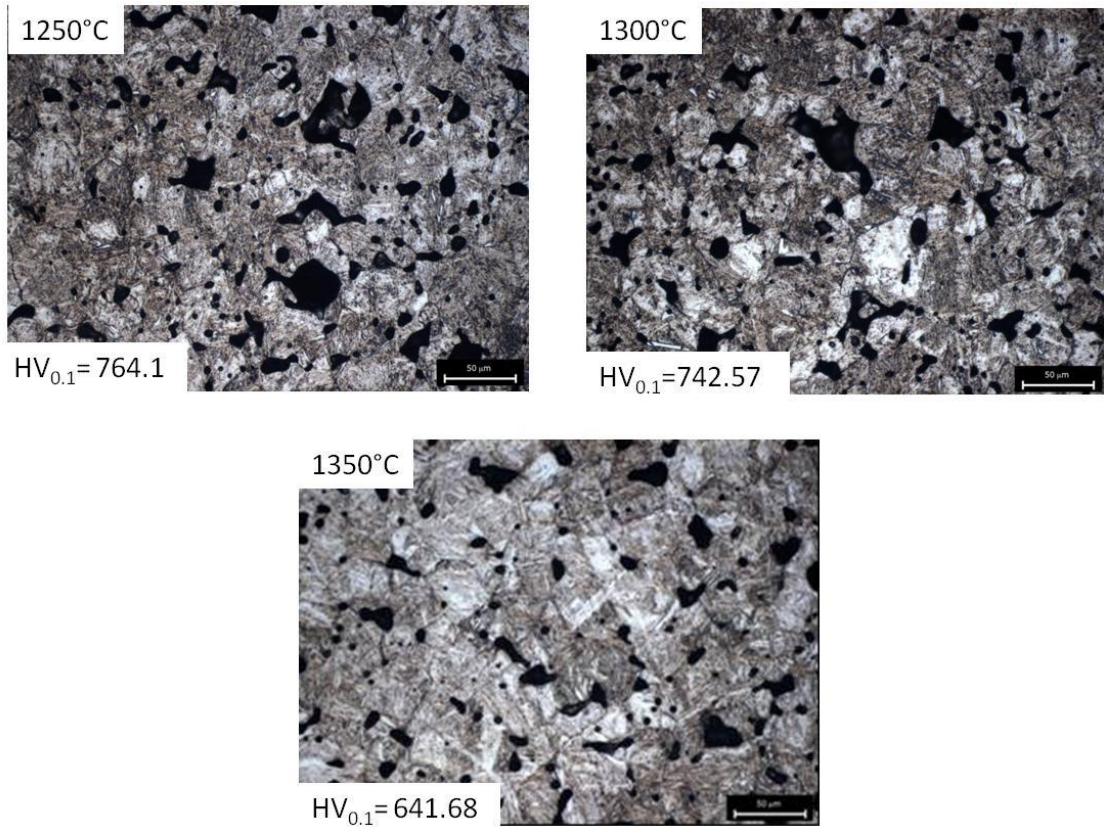


Fig. 4.3.2 microstructure of sinterhardened parts

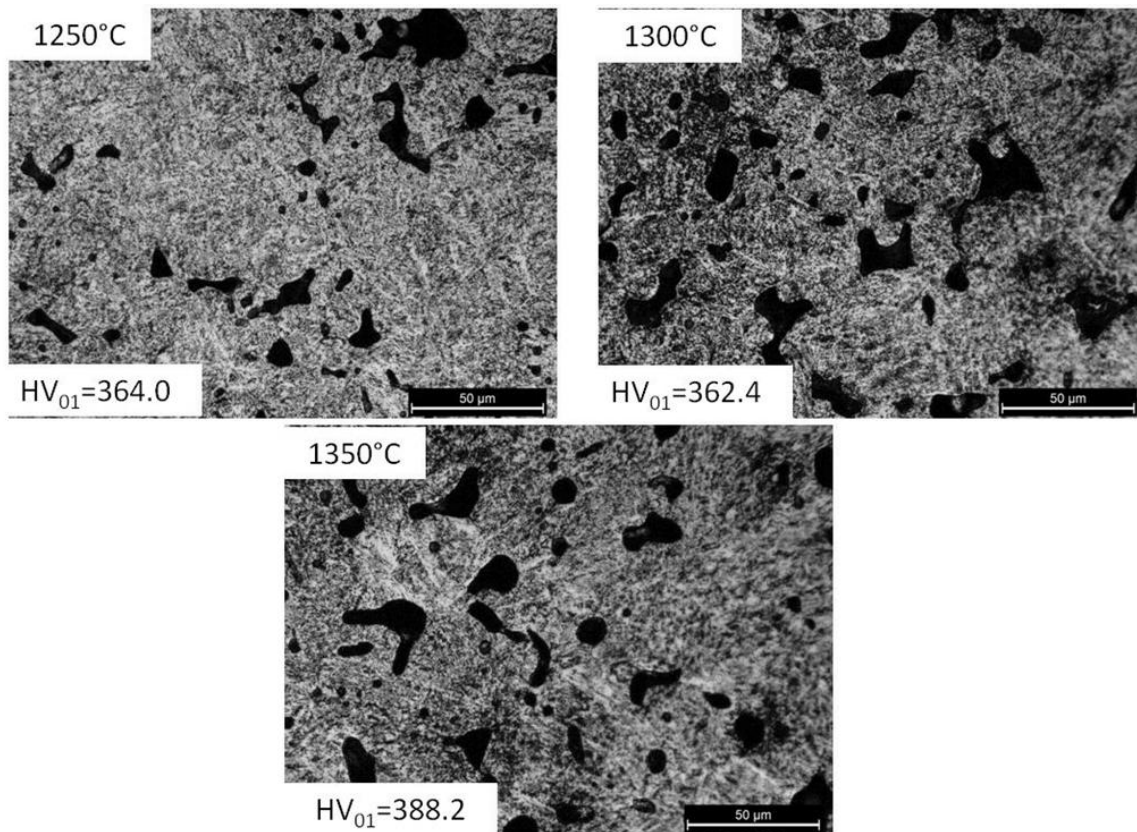


Fig. 4.3.3 microstructure of sintered parts

The microstructure of the sinterhardened parts is martensitic at the two lower temperatures, while a mixture of martensite and bainite is observed at 1350°C.

The microstructure of the sintered parts is upper bainitic in all the cases. As it is well known, the volume increase of the martensite formation is larger than that of the bainite formation, and this accounts for the slightly lower density of the sinterhardened specimens.

On increasing sintering temperature pores become increasingly rounded and slightly smaller, what leads to an increase in the mechanical properties, due to the increase in the fraction of load bearing section.

The fraction of load bearing section may be determined using the following equation [10]:

$$\Phi = [1 - (5.58 - 5.7f_{circle})\varepsilon]^2$$

being ε the fractional porosity and f_{circle} the ore shape parameter defined as $p^2/4\pi A$ where p and A are the perimeter and the area of the pores in the metallographic section, respectively.

On increasing the sintering temperature, the population of experimental points shifts towards higher f_{circle} values and the pore size distribution shifts towards smaller values, as shown in Fig. 4.3.4 relevant to sinterhardened parts. The fraction of load bearing section is reported in each figure; it increases from 0.55 up to 0.69 and a corresponding increase in yield and fatigue strength and an even larger increase in impact toughness are expected [1].

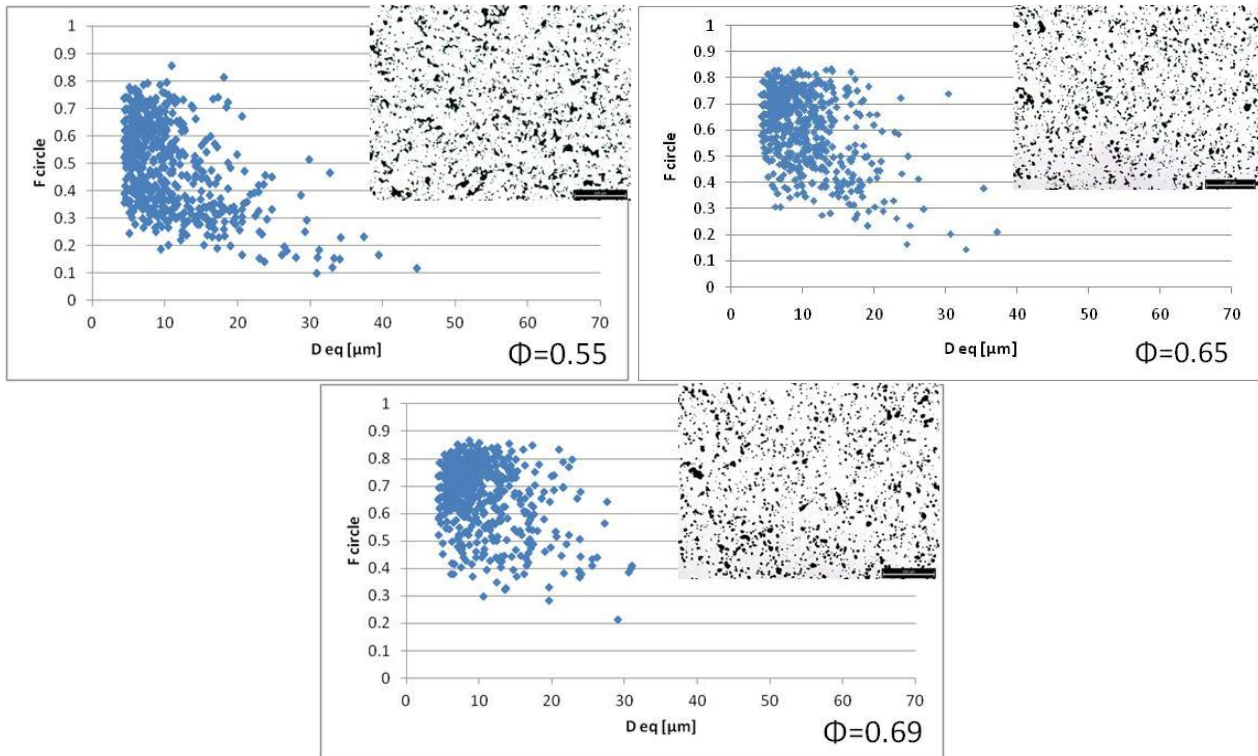


Fig. 4.3.4 Microstructure and pore morphology in the sinterhardened case at different temperatures

The same can be highlighted observing the sintered parts.

4.3.1.2 Dimensions in the green and sintered state, and dimensional variation

The dimensions of the green and sintered parts are shown in the Fig. 4.3.5.

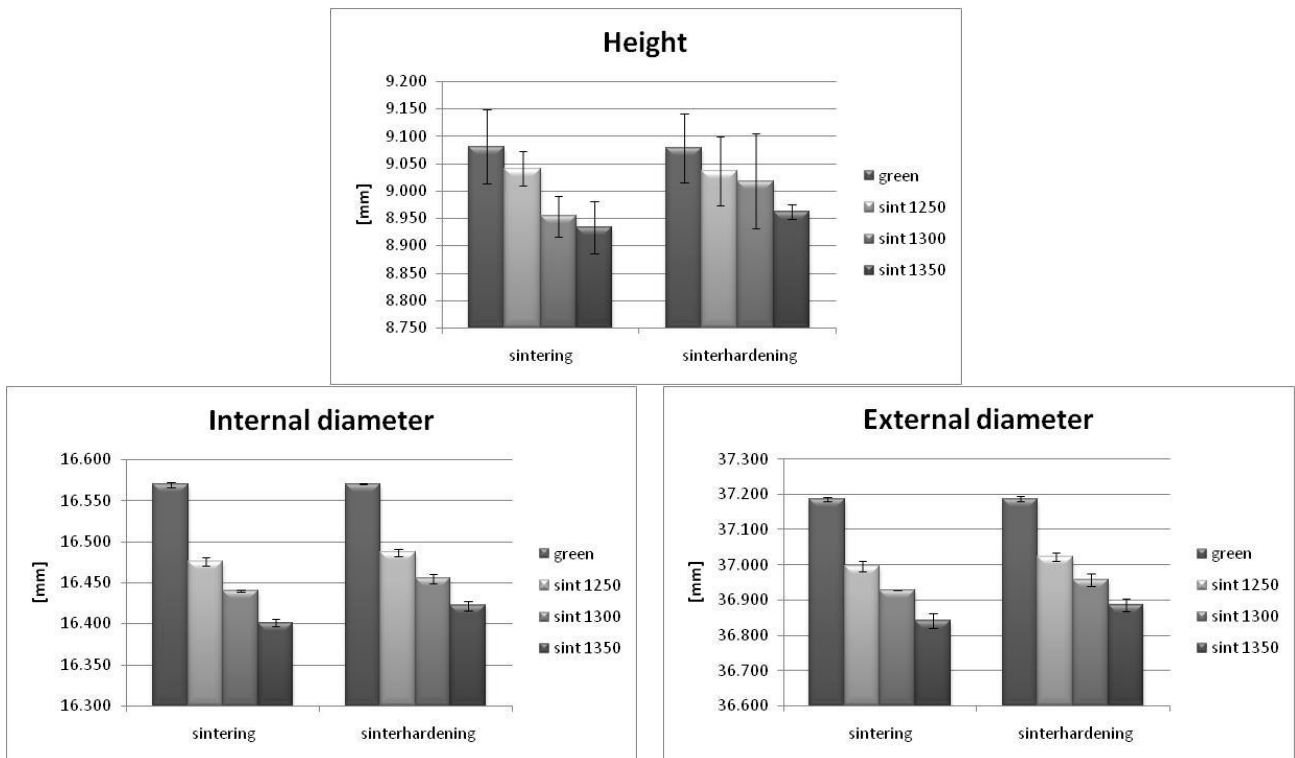


Fig. 4.3.5 dimensions in green and sintered state

The dimensions tend to decrease on increasing the sintering temperature, and the amount of shrinkage is higher after sintering than after sinterhardening, as already observed in the rings discussed in the previous chapter on powders.

With respect to the precision of the dimensions, the height is less accurate than the diameters. In particular, with respect to the ISO IT tolerance classes, the dimensional tolerances of the height correspond to ISO IT 11-12 in green state and ISO IT 12-13 in the sintered and sinterhardened state. For the diameters the dimensional tolerance in the green state may be estimated at ISO IT 5 (internal diameter) and ISO IT 7 (external diameter) in the green state and at ISO IT 7 (internal diameter) ISO IT 7-8 (external diameter) in the sintered and sinterhardened state. As expected, the dimensional precision of the sintered/sinterhardened parts is worse than that of the green ones, but it must be highlighted that it is in all the cases very good, even at very high sintering temperature.

Table 4.3.2 shows the dimensional variation after sintering and sinterhardening.

	2 °C/s (sinterhardening)			0.1 °C/s (sintering)		
Sintering temperature [°C]	1250	1300	1350	1250	1300	1350
$\Delta h/h_g$	-0.48%	-0.65%	-1.24%	-0.8%	-1.28%	-1.39%
$\Delta\phi_i/\phi_{ig}$	-0.51%	-0.7%	-0.9%	-0.57%	-0.78%	-1.02%
$\Delta\phi_e/\phi_{eg}$	-0.45%	-0.63%	-0.82%	-0.51%	-0.7%	-0.92%

Table 4.3.2 Shrinkage during sintering and sinterhardening

The larger dimensional variations observed after sintering can be ascribed to the different transformations occurring during sintering and sinterhardening, as highlighted by the different microstructures obtained (see next paragraph).

4.3.1.3 Geometrical characteristics

In Fig. 4.3.6 the most interesting geometrical characteristics for axi-symmetrical parts are shown.

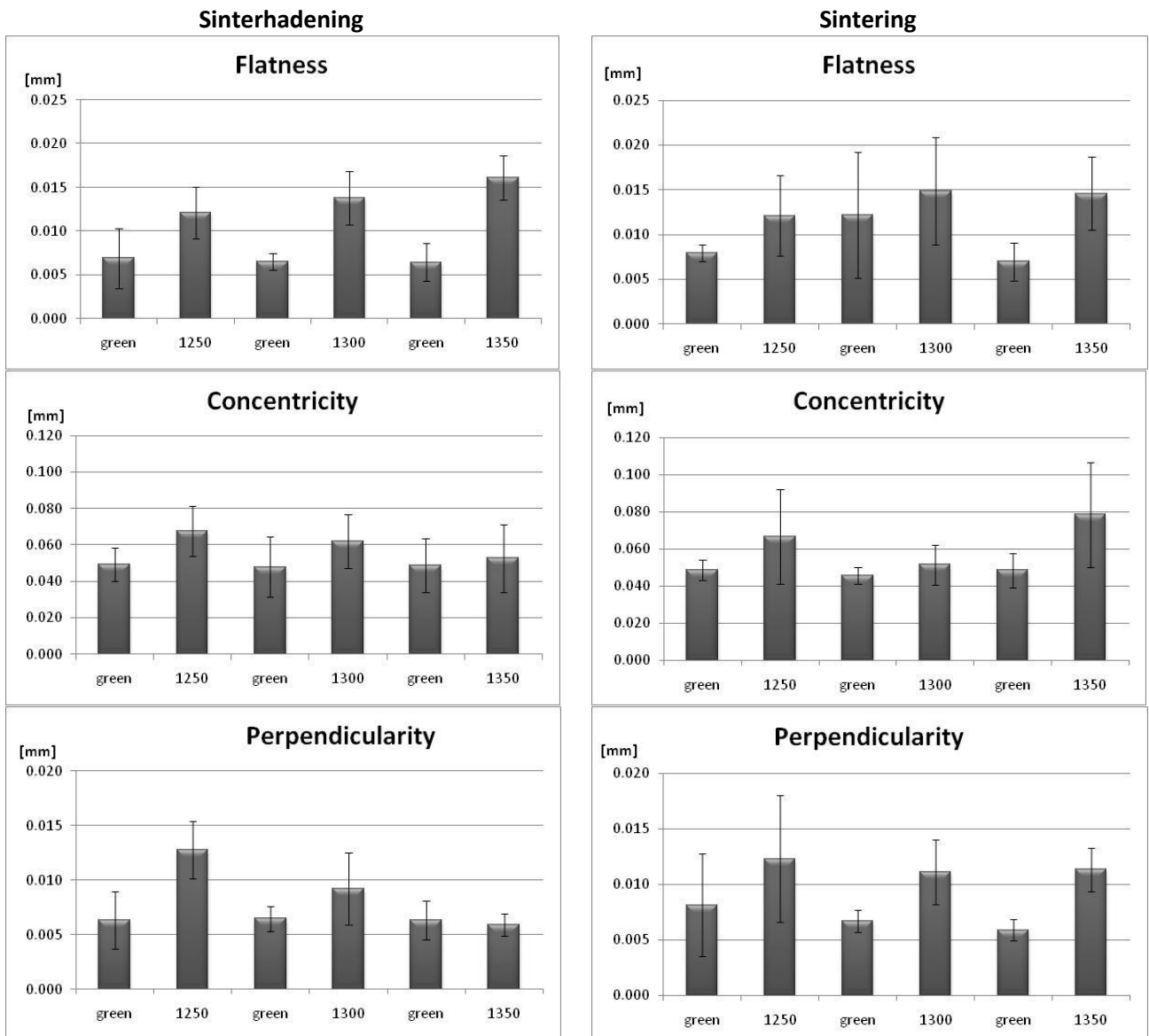


Fig. 4.3.6 Flatness, concentricity and perpendicularity in sinterhardened parts, on the left and sintered part on the right

Flatness increases after sintering/sinterhardening. A slight effect of temperature is observed in sinterhardened parts, which is not confirmed by sintered ones. Since differences are not significant, the effect of temperature may be considered negligible. Concentricity too tends to worsen after sintering/sinterhardening without any systematic effect of temperature and of cooling rate, and the same for perpendicularity. In all the cases, the precision of geometrical features is excellent irrespective to sintering temperature.

An important geometrical characteristic of the investigated parts is the position of the three grooves on the upper side, given by the angle between the relevant median planes (Fig. 4.3.7). The maximum deviation of the three angles formed by the median planes of the grooves from the nominal value (120°) $w = |\vartheta_{\text{measured}} - \vartheta_{\text{nominal}}|_{\text{max}}$ in the green and the sintered state is reported in Table 4.3.3.

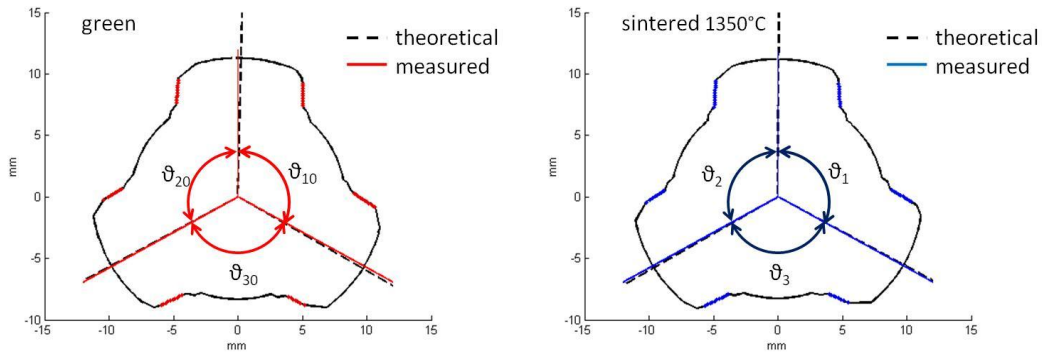


Fig. 4.3.7 Angles between grooves

	2°C/s			0.1°C/s		
	1250°C	1300°C	1350°C	1250°C	1300°C	1350°C
w_0	0.29	0.23	0.76	0.23	0.26	0.23
w	0.86	0.73	0.94	1.31	1.15	1.36

Table 4.3.3 Deviation from the nominal value of the angle between grooves

where:

w_0 = max deviation from 120° in the green state

w = max deviation from 120° in the sintered or sinterhardened state

The maximum deviation from the nominal value, i.e. the precision of the position of the grooves, gets worse after sinterhardening and slightly more after sintering, but no effect of the increase in temperature can be observed. There is no correlation with shrinkage. The variation of the position of the grooves may be described as a rotation of the relevant median planes occurring on sintering/sinterhardening. The maximum rotation was measured on the part sintered at 1350°C , where $w - w_0 = 1.13$; it corresponds to a tangential shift of a point on the median circumference of 0.001, which is one order of magnitude smaller than the tangential shrinkage (-0.01 for the internal circumference, -0.009 for the external circumference). In case of a definitely perfect homogeneity of shrinkage along the circumferences, the three grooves shall keep their original position. In the investigated parts, some inhomogeneity exists since angles change their position, but the effect on precision is virtually negligible.

In conclusion the values of tolerances for diameters keep very small in sintered parts, while those of height are larger in any case, as usual in Powder Metallurgy; however the dimensional precision obtained in all the cases is very good even at very high sintering temperature. All the measured geometrical characteristics show a trend towards a slight worsening on sintering, but again without any systematic and noticeable effect of the sintering temperature. The geometrical precision matches the indications reported in the technical literature for designers even when parts are sintered at very high temperature.

4.3.2 AISI 316L

The second case studied is the stainless steel part shown in Fig. 4.3.8.

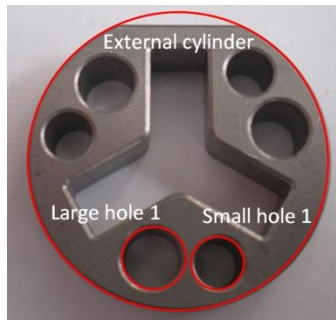


Fig. 4.3.8 AISI 316L part

4.3.2.1 Density and microstructure

The analysis of density was made by water displacement method and the results are shown in Table 4.3.4:

$\rho_{\text{nom}}[\text{g}/\text{cm}^3]$	$\rho_{\text{green}}[\text{g}/\text{cm}^3]$	$\rho_{1250}[\text{g}/\text{cm}^3]$	$\rho_{1300}[\text{g}/\text{cm}^3]$	$\rho_{1350}[\text{g}/\text{cm}^3]$
6.4	6.27	6.55	6.68	6.74
6.6	6.54	6.66	6.97	6.92
6.8	6.73	6.94	7.09	7.10

Table 4.3.4 Density in the green and sintered state

Density increases on increasing the sintering temperature and the densification is higher for the parts with the lowest density. Fig. 4.3.9 shows the microstructure of the parts relevant to the different green density and sintering temperature. Fig. 4.3.10 shows the fraction of load bearing section in function of density and sintering temperature.

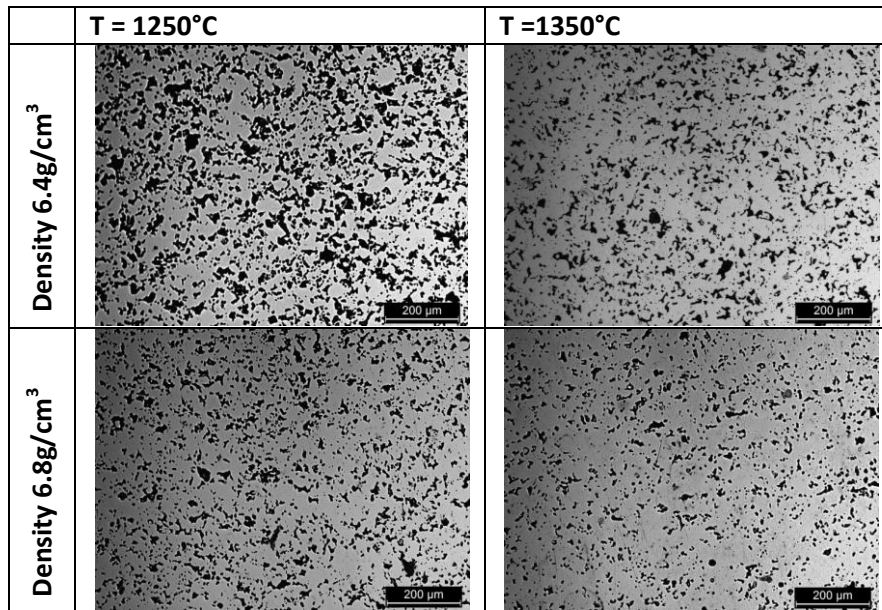


Fig. 4.3.9 Microstructure in function of sintering temperature and green density

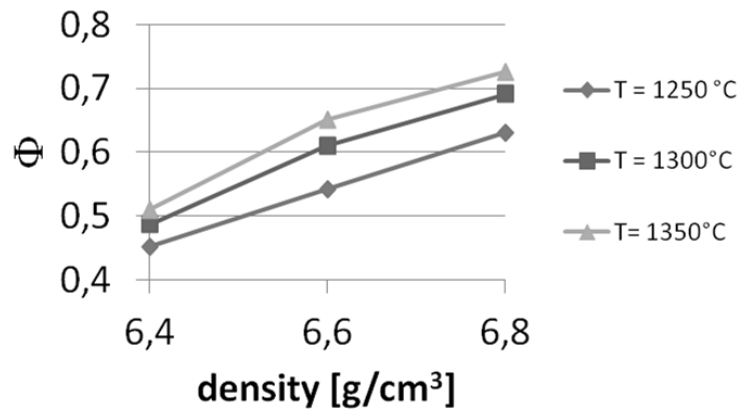


Fig. 4.3.10 Fraction of load bearing section in function of green density and sintering temperature

As expected, the pores become more rounded and the fractional porosity tends to decrease on increasing sintering temperature and increasing green density.

4.3.2.2 Dimensions in green and sintering state, and dimensional variation

With reference to Fig. 4.3.8, the dimensions of some representative features for the different densities and sintering temperatures are shown in Fig. 4.3.11, Fig. 4.3.12, Fig. 4.3.13 and Fig. 4.3.14.

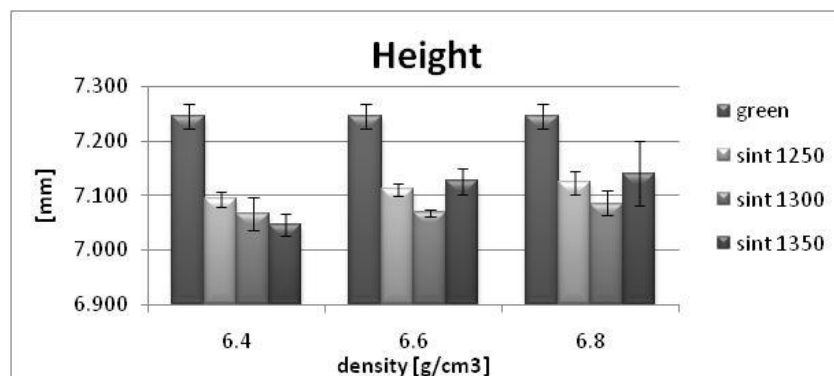


Fig. 4.3.11 Height of green and sintered part

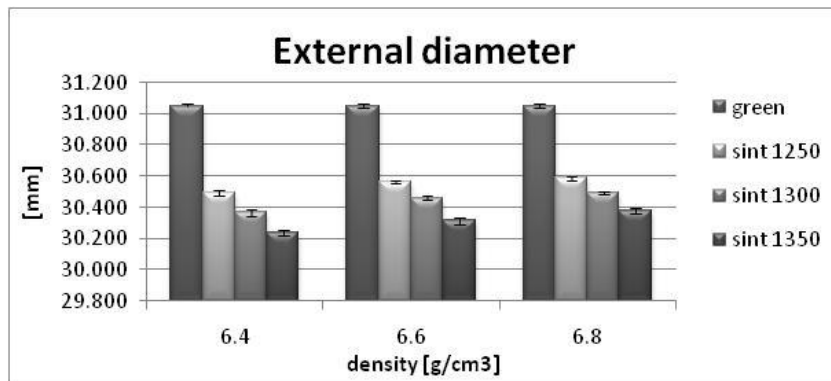


Fig. 4.3.12 External diameter of green and sintered part

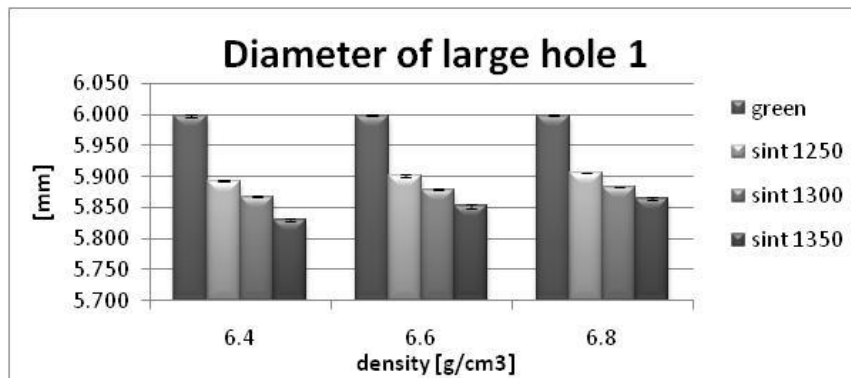


Fig. 4.3.13 Diameter of the large hole in green and sintered part

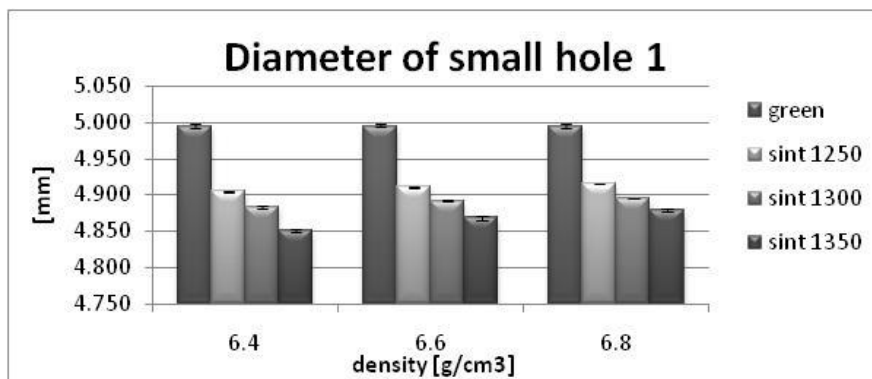


Fig. 4.3.14 Diameter of the small hole in green and sintered part

It is possible to observe that all dimensions shrink on sintering. While height does not reveal a definite trend with respect to the increase in the sintering temperature, for all the dimensions in the compaction plane the shrinkage increases with the sintering temperature.

Scatter bands of dimensions may be related to the ISO IT tolerance classes attainable for the different features after the whole production process, as summarized in Table 4.3.5. It may be highlighted that the best precision is attainable for the dimensions of the internal features in the compaction plane (diameters of holes and width of slots), it decreases for the external feature in the compaction plane (external diameter) and even more for the dimension parallel to the compaction direction (height). In any case the relevant ISO IT classes are lower than that normally associated to PM compaction-sintering process.

		ISO IT classes for the different features								
		Height			External diameter			Internal features		
$T_{\text{sint}} \text{ } ^\circ\text{C}$ ρ_g g/cm^3		6.4	6.6	6.8	6.4	6.6	6.8	6.4	6.6	6.8
	green	IT 8	IT 8	IT 9	IT 6	IT 6	IT 6	IT 4/IT 5	IT 3/IT 4	IT 4
	1250	IT 7	IT 9	IT 9	IT 8	IT 7	IT 8	IT 4	IT 5	IT 4
	1300	IT 9	IT 8	IT 9	IT 8	IT 7	IT 8	IT 4	IT 4/IT 5	IT 5
	1350	IT 8	IT 11	IT 11	IT 8	IT 8	IT 8	IT 5/IT 6	IT 5/IT 6	IT 5/IT 6

Table 4.3.5 ISO IT classes for dimensional tolerances relevant to the different features

Dimensional variations are reported in Table 4.3.6.

	Height			External diameter		
	$\rho=6.4\text{g/cm}^3$	$\rho=6.6\text{ g/cm}^3$	$\rho=6.8\text{ g/cm}^3$	$\rho=6.4\text{ g/cm}^3$	$\rho=6.6\text{ g/cm}^3$	$\rho=6.8\text{ g/cm}^3$
T = 1250 °C	-2.3%	-1.9%	-1.7%	-1.8%	-1.6%	-1.5%
T = 1300 °C	-2.3%	-2.5%	-2.2%	-2.2%	-1.8%	-1.8%
T = 1350 °C	-2.8%	-1.7%	-1.5%	-2.6%	-2.4%	-2.2%

Table 4.3.6 Dimensional variation after sintering in function of density and sintering temperature

As expected, the parts with the lowest green density show the largest dimensional variations, the larger the higher the sintering temperature.

4.3.2.3 Geometrical characteristics

In Fig. 4.3.15 and Fig. 4.3.16 the geometrical characteristics describing the intrinsic shape of the part, flatness and cylindricity, with respect to the sintering temperature and the green density are shown.

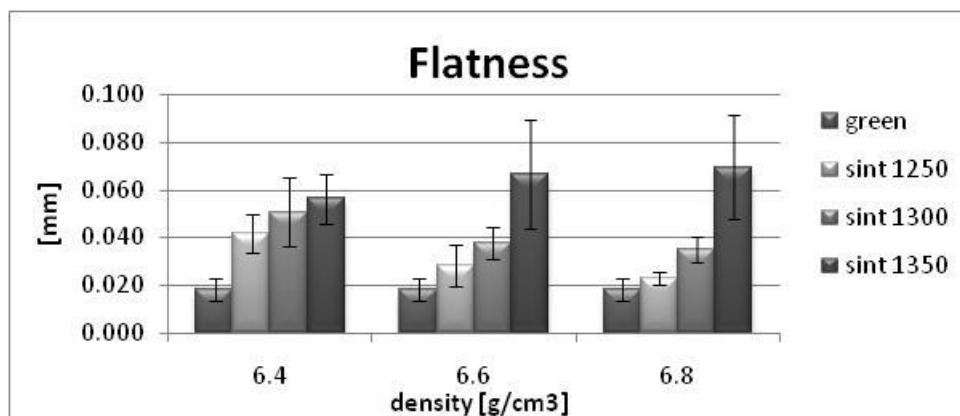


Fig. 4.3.15 Flatness in green and sintered state

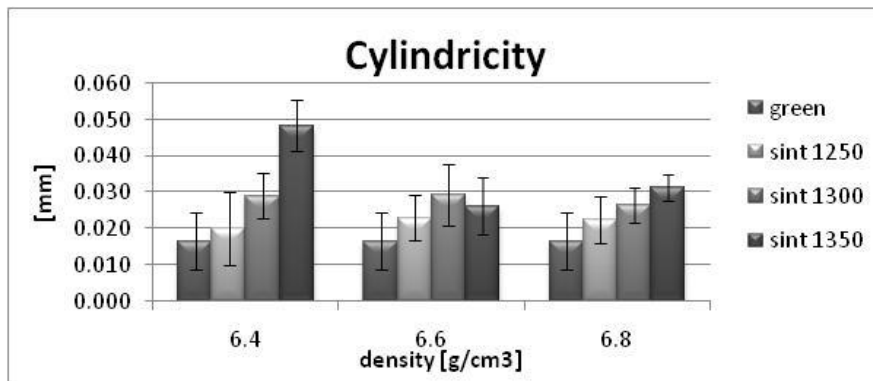


Fig. 4.3.16 Cylindricity of external diameter in green and sintered state

Flatness tends to worsen on increasing sintering temperature, both as mean value and as scatter band. At 1250°C and 1300°C the effect is more pronounced for the 6.4 g/cm³ green density, while at 1350 °C the worsening is generalized on all the green densities. Same trend is observed for cylindricity, but the effect on 6.4 g/cm³ green density parts is more pronounced at all the sintering temperatures. On evaluating cylindricity, it may be observed that on sintering the shape of holes tends to become conical: the effect is enhanced by increasing sintering temperature. The measured values are in any case in the range of values acceptable for PM parts, with the exception of the flatness at the higher sintering temperature.

The relative position of the different features is critical in this kind of parts. Median planes of the slots must be kept at 120°. Fig. 4.3.17 shows as an example the angle between the slot 1 and 2. It may be observed that in the green parts the angle between median planes varies in an interval of 0.1 degrees, irrespective of the green density. After sintering the angle decrease slightly, irrespective of sintering temperature. No significant trend is observed. A slight different behavior is observed in the parts with the lowest green density.

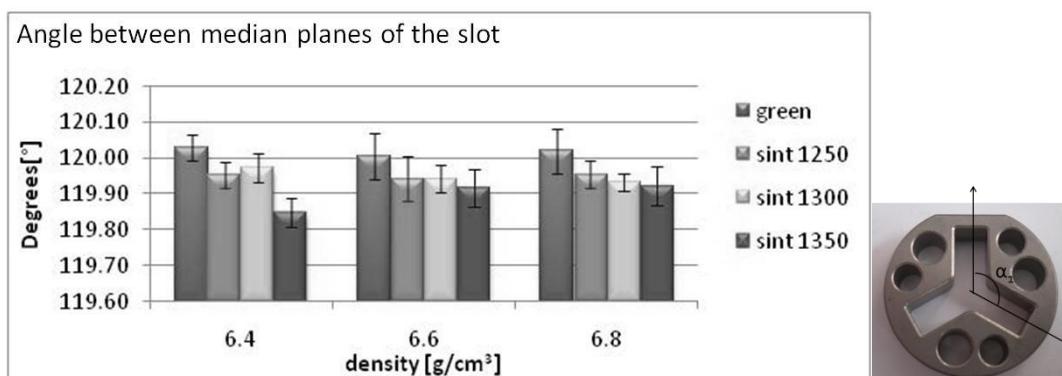


Fig. 4.3.17 Angle between median planes of the slot

Another critical geometrical feature is the position of the holes, which must be controlled both in terms of distance from the axis of the external cylinder and in terms of distance from the other internal features (median planes of the slots, axes of the other holes). Considering the angles between a plane passing through the axis of each holes and the axis of the external cylinder and the median plane of the slot taken as reference, it is observed the same trend of the angles between the median planes of the slots. In Fig. 4.3.23 is shown an example. The angles are kept stable after sintering, the variation is 0.1 degree and it is comparable with the scatter band.

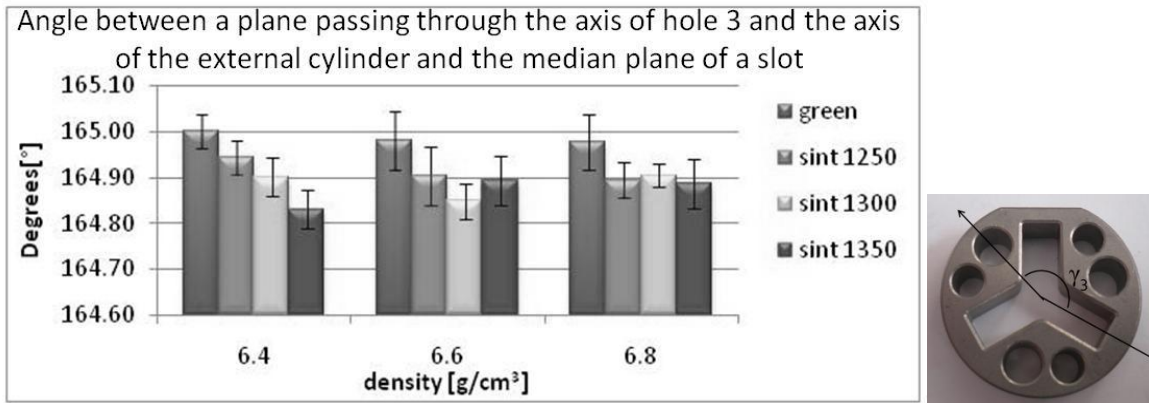


Fig. 4.3.18 Angle between a lane passing through the axis of the hole 3 and the axis of the external cylinder and the median plane of the slot

The distance between the axes of each pair of small-large hole is the same for each pair of hole irrespective to the green density. The mean value decreases on sintering and with the increasing of sintering temperature. This trend is more pronounced in the parts with lower density, but the precision is maintained, as shown in Fig. 4.3.19.

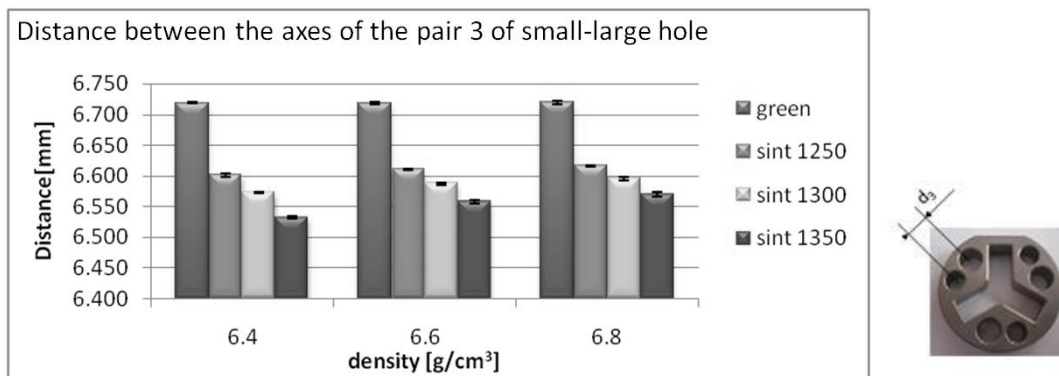


Fig. 4.3.19 Distance between the axes of a pair of small-large hole

The axes of the small and large holes lie on two cylinders that may be concentric with the axis of the external cylinder, so the position of the holes versus the external cylinder is evaluated in terms of concentricity between the axis of the external cylinder and the axis of the cylinder containing the small or large holes and in terms of distance between the axis of the external cylinder and the axis of every holes. For what concern the concentricity in Fig. 4.3.20 is shown the trend. The concentricity worsens with the increasing of sintering temperature only in the specimens with the lowest density, while the behavior for the other density condition is less significant, and is almost the same for each sintering temperature. A large scatter band is however revealed in all the measured value. This trend is confirmed both for large and the small holes.

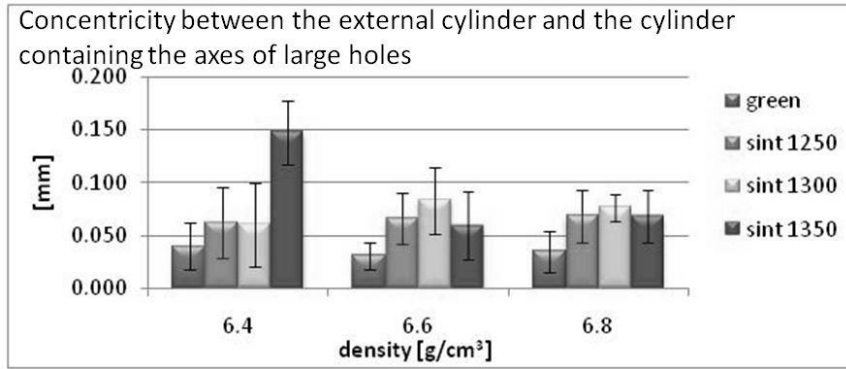


Fig. 4.3.20 Concentricity between the external cylinder and the cylinder containing the axes of large holes

The position of the holes with respect the axis of the external cylinder may be evaluated also in terms of distance between the axis of each hole and the axis of the external cylinder. Fig. 4.3.21 shows the behavior of the distance between the axis of the large hole 1 and the external axis in function of density and sintering temperature. The behavior is the same for all the large and the small holes. The distance decreases on sintering, with no significant effect of temperature, while a slight effect of green density may be highlighted (the decrease is less pronounced in the highest green density parts). The distances are very precise in green parts and maintain this trend after sintering.

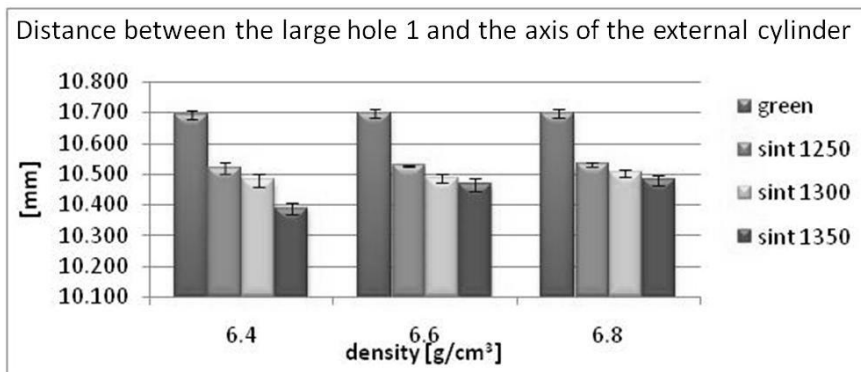


Fig. 4.3.21 Distance between the large hole 1 and the axis of the external cylinder

To compare the results of the different kind of evaluation of the position of the holes (distances or concentricity) Fig. 4.3.23 reports the dimensional variation of the distance between the axes of each large holes and the axis of external cylinder and Fig. 4.3.24 reports the concentricity between the external cylinder and the axis of the cylinder defined by the three axes of the large hole. The case with the highest green density is reported.

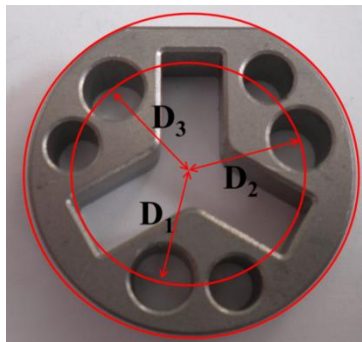


Fig. 4.3.22 dimensions reported in Fig. 1.18

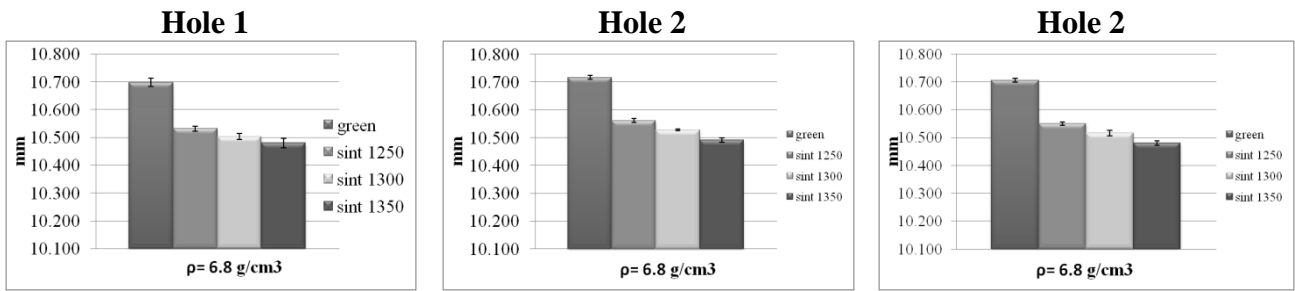


Fig. 4.3.23 Distance between the axis hole and the axis of the external cylinder

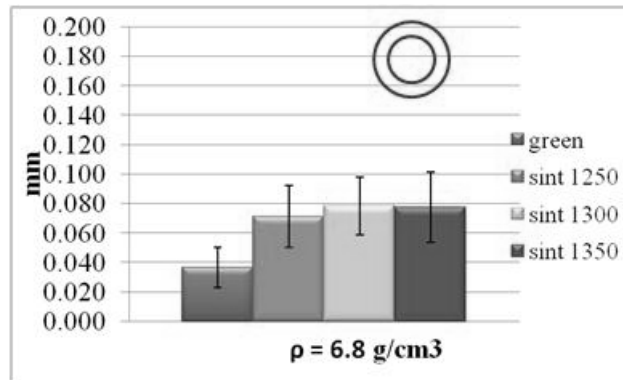


Fig. 4.3.24 Concentricity of large holes with respect to the external diameter

Even if the decrease of the distance between the axis of the hole and the external axis decrease on increasing of sintering temperature, the value of the concentricity remains almost the same, very good even at higher sintering temperature. This is due to the fact that the decreasing of the dimension during sintering is always in the radial direction, so the different decreases do not affect the worsening of the concentricity.

4.3.2.4 Study of the flatness

Flatness of the upper surface worsens on sintering. It may be justified by an inhomogeneous shrinkage in height, due to an uneven filling of the narrow sections. To verify this hypothesis, height was measured in the fifteen different positions shown in Fig. 4.3.25 in the part with green density 6.8g/cm^3 sintered at 1250°C which, due to the smallest shrinkage, is the most similar to the green parts a different local height can be related to a different density distribution.

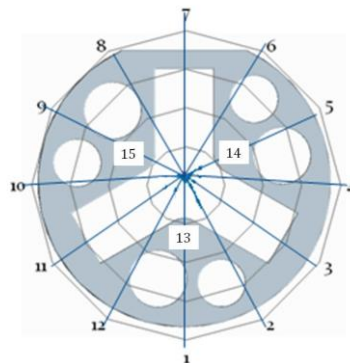


Fig. 4.3.25 Measured section

The measure of the 15 section made the following data, in Table 4.3.7.

section	Height in green state [mm]	Height in sintered state [mm]
1	7.60	7.45
2	7.60	7.44
3	7.59	7.43
4	7.57	7.41
5	7.57	7.42
6	7.57	7.43
7	7.59	7.44
8	7.62	7.45
9	7.63	7.47
10	7.64	7.48
11	7.64	7.48
12	7.63	7.46
13	7.59	7.45
14	7.57	7.42
15	7.58	7.44

Table 4.3.7 Height relevant to 15 different positions, in the green and sintered state, for the part sintered at 1250°C, green density 6.8g/cm³

The results are presented in Fig. 4.3.26: different levels of green refer to different heights (two consecutive levels in the scale of colors correspond to a difference in height 0.01 mm).

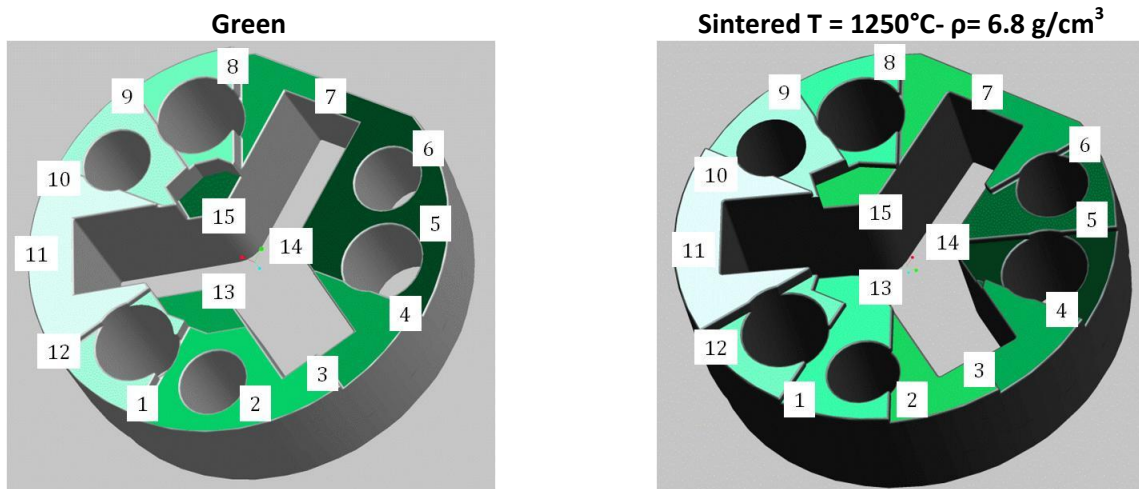


Fig. 4.3.26 Height of the samples in green and sintered state

In the sections 1-12, the fractional porosity was measured by Image Analysis, and the results are reported in Fig. 4.3.27; porosity was measured at five different heights in each section.

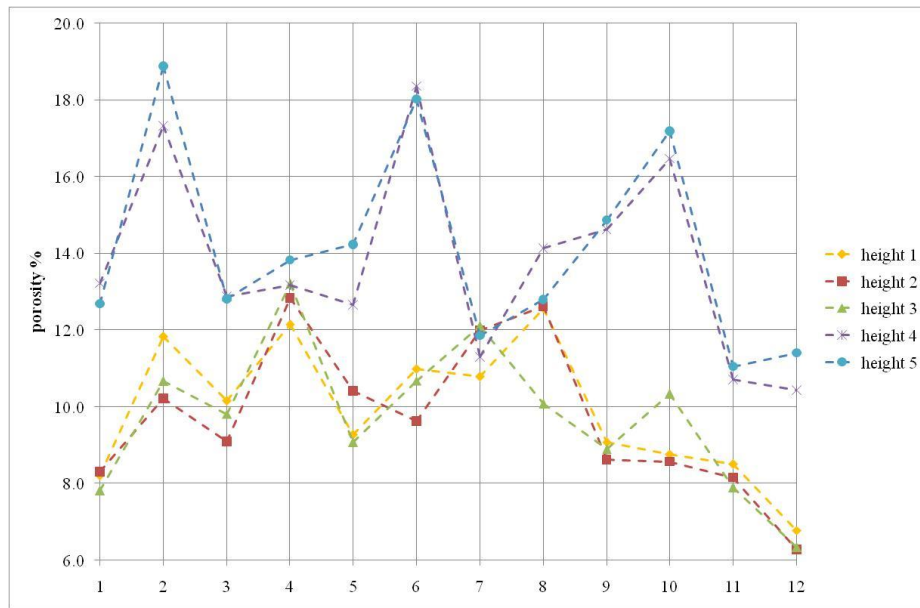


Fig. 4.3.27 Fractional porosity in height

Porosity is not homogeneously distributed in the different positions and the positions corresponding to the lower height have a higher porosity than those corresponding to the higher height. This has to be ascribed to an inhomogeneous filling of the powder in the different positions, due to the geometrical complexity of the part.

In conclusion the dimensions are very precise in the green parts, irrespective to green density. As expected, the best precision is found considering the dimensions in the compaction plane, but also the height of the parts is just slightly scattered around a mean value. Although significant dimensional variations can be observed, precision does not significantly worsen on sintering, even at the highest sintering temperature. The characteristics describing orientation and position are directly related to the dimensional change in the compaction plane.

Dimensional and geometrical precision are good even if sintering at very high temperature (1350 °C), particularly in the specimens with high green density (6.8 g/cm³). The inhomogeneous filling of the powder may lead to a lack of geometrical precision, which increases with the sintering temperature.

4.3.3 Conclusions

The two parts investigated show unambiguously that sintering temperature may be increased up to very high values to improve the fraction of the load bearing section without preventing the dimensional and geometrical precision. The critical issue is the quality of the green parts, in terms of green density distribution. An important element is the homogeneous filling of the die cavity during compaction.

The parts investigated are characterized by quite a high geometrical complexity, therefore the results are very promising in relation to a broad range of parts.

4.3.4 References

1. R. M. German, "Powder Metallurgy of Iron and Steel", Eds. John Wiley & Sons Inc., pp 205-209, 1998.
2. M. Puscas et al, Materials Characterization, 50(1)(2003) 1-10.

3. V. Stoyanova et al, 4(2)(2004) 79-87.
4. J. Tengzelius et al, Eds. Metal Powder Industries Federation, (1990) 217-228.
5. A. Pietrowski et al, Powder Metallurgy, 41(2)(1998) 109-114.
6. M. Azadbeh et al, Powder Metallurgy Progress, 6(1)(2006) 1-10.
7. H. Danninger et al, 40 (2008) 33-46.
8. S. Hatami et al, Journal of Materials Processing Technology, 210 (2010) 1180–1189.
9. A. Molinari et al, Advances in Powder Metallurgy & Particulate Materials, 5(2009) 79-86.
10. A. Molinari, et al, Powder Metallurgy Progress, 11(1-2)(2011) 12-20.

4.4 Post-sintering operation

Sizing is a post-sintering operation which can be characterized by different goals: to increase the density of the sintered part, to improve the dimensional and geometrical precision to match the design requirements, to improve surface finishing. In all the cases, the goal is attained by plastic deformation of the parts within a die. The extent of plastic deformation depends on the aim of the operation and, in particular, on the extent of change in density and/or in dimensional and geometrical characteristics required. Plastic deformation depends on size and shape of the part and on the force applied by the punches. The following study analyzes the sizing of the sintered gear shown in Fig. 4.4.1 aimed at improving the dimensional and geometrical characteristics; an hydraulic press is used for sizing.

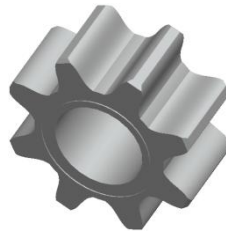


Fig. 4.4.1 Part studied

The demanding requirement for this parts conicity < 0.05%, which is not reachable at the end of the sintering process, The main characteristics of the part are following summarized.

- ✓ Material: Fe-2%Cu-0.55%C;
- ✓ Density: 6.9 g/cm³;

During the sizing cycle the force and the movement of the punches, the die and the core rod were continuously recorded.

The study of sizing condition was divided in two part, the first one is the sizing in displacement control, the second one the sizing in force control. The displacement control sizing was performed to set a reference point comparable to a mechanical press sizing. On the basis of these results, the values of force to be used in force control sizing were set. The force control sizing was firstly performed with die movement, this allows to obtain a more homogeneous distribution of pressure along the sizing direction. The value of force was then adjusted to provide force control sizing without the die movement. The main sizing conditions studied are shown in Table 4.4.1.

Displacement control	Position [mm]	Force control with die movement	Force [kN]	Force control without die movement	Force [kN]
	17.85		260		290
17.90	290	320			
17.95	320				
18.00					

Table 4.4.1 Sizing condition

4.4.1 Displacement control sizing

4.4.1.1 Dimensions and conicity

The dimensions and conicity for the sintered and displacement control sized parts is shown in Table 4.4.2.

Position [mm]		h [mm]	Φ_{ext} [mm]	Φ_{int} [mm]	Conicity %
17.85	sintered	18.478 ± 0.019	41.912 ± 0.003	14.876 ± 0.001	0.165 ± 0.022
	sized	18.410 ± 0.018	41.951 ± 0.002	14.882 ± 0.001	-0.074 ± 0.010
17.90	sintered	18.488 ± 0.014	41.911 ± 0.002	14.879 ± 0.001	0.161 ± 0.012
	sized	18.428 ± 0.010	41.944 ± 0.005	14.882 ± 0.001	-0.063 ± 0.008
17.95	sintered	18.480 ± 0.008	41.910 ± 0.003	14.879 ± 0.001	0.169 ± 0.024
	sized	18.442 ± 0.003	41.931 ± 0.004	14.881 ± 0.001	-0.041 ± 0.012
18.00	sintered	18.482 ± 0.008	41.910 ± 0.003	14.878 ± 0.001	0.168 ± 0.018
	sized	18.454 ± 0.003	41.921 ± 0.003	14.880 ± 0.001	-0.023 ± 0.008

Table 4.4.2 Dimensions and conicity of sintered and sized part

The values of the dimensions and the conicity of the sintered parts are homogeneously distributed, the trend of the variations after sizing is the one expected: on increasing the position (the displacement decreases) the decrease in height and conicity, as well as the increase in the external diameter, are less pronounced, while the internal diameter does not show significant variations. It is possible to observe that the required conicity is only obtained when the sizing condition implies a position of 18.00 mm. In Fig. 4.4.2 is shown the conicity versus the position, the straight line represents the required conicity.

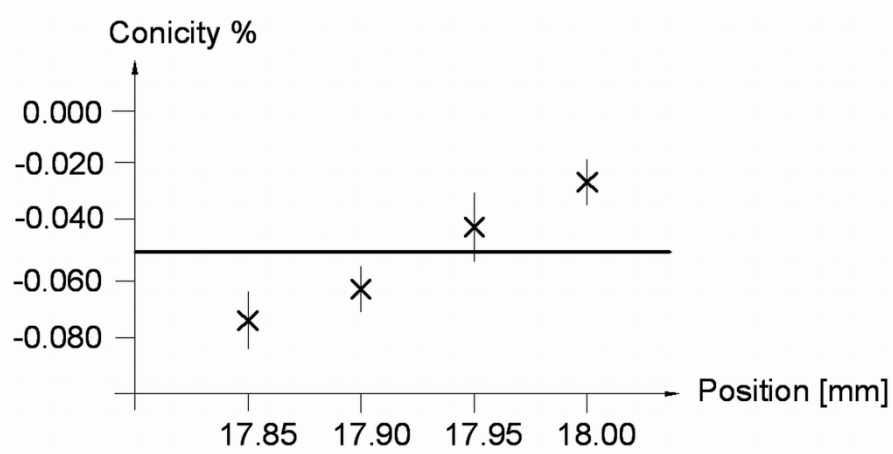


Fig. 4.4.2 Conicity of parts sized in displacement control versus position

The values of force corresponding to the different displacements were recorded and used to define the value of force in force control sizing.

4.4.2 Force control sizing

4.4.2.1 Dimensions and conicity

A very low variation in volume was measured, to which a negligible densification corresponds, as confirmed by the microstructural analysis. A slight strain hardening was also observed: microhardness increases from 210 HV01 for the sintered part to 240-250 HV01 for sized parts. The microstructure is shown in Fig. 4.4.3.

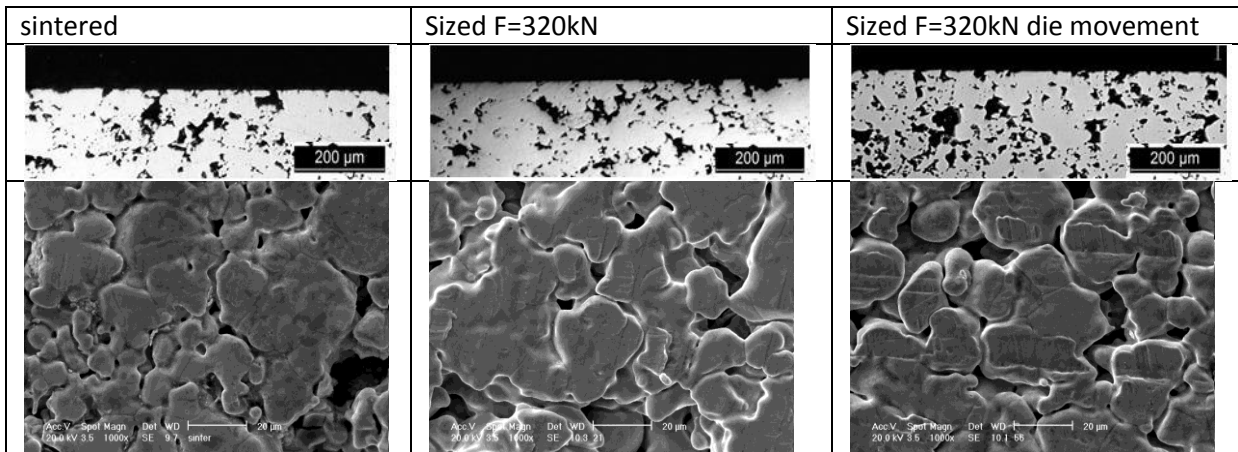


Fig. 4.4.3 Microstructures of sintered and force control sized parts

Table 4.4.3 summarizes the values of dimensions and conicity for the sintered and the force control sized parts.

Force [kN]		h [mm]	Φ_{ext} [mm]	Φ_{int} [mm]	Conicity %
260 + die mov.	sintered	18.481 ± 0.030	41.911 ± 0.003	14.882 ± 0.001	0.175 ± 0.016
	sized	18.445 ± 0.033	41.937 ± 0.003	14.881 ± 0.001	-0.013 ± 0.026
290 + die mov.	sintered	18.484 ± 0.020	41.911 ± 0.003	14.871 ± 0.001	0.189 ± 0.024
	sized	18.432 ± 0.020	41.947 ± 0.004	14.882 ± 0.001	-0.011 ± 0.019
320 + die mov.	sintered	18.465 ± 0.019	41.914 ± 0.003	14.876 ± 0.001	0.182 ± 0.016
	sized	18.392 ± 0.018	41.954 ± 0.004	14.884 ± 0.001	-0.015 ± 0.012
290	sintered	18.472 ± 0.013	41.909 ± 0.004	14.881 ± 0.001	0.140 ± 0.023
	sized	18.419 ± 0.019	41.948 ± 0.005	14.882 ± 0.001	-0.042 ± 0.043
320	sintered	18.479 ± 0.013	41.912 ± 0.005	14.881 ± 0.002	0.167 ± 0.025
	sized	18.413 ± 0.016	41.955 ± 0.002	14.882 ± 0.001	-0.061 ± 0.019
350	sintered	18.480 ± 0.025	41.913 ± 0.002	14.880 ± 0.001	0.185 ± 0.018
	sized	18.390 ± 0.030	41.960 ± 0.003	14.883 ± 0.001	-0.055 ± 0.012

Table 4.4.3 Dimensions and conicity of sintered and force control sized parts

The trend of the variations after sizing is that expected: on increasing the force, the decrease in height and the increase in the external diameter, are more pronounced, no significant variations of the internal diameter are observed. The trend in the conicity variations is significantly affected by the occurrence of die movement: without die movement, the requirement is never met, nevertheless reasonably lower values of force could be helpful in this sense. However, no definite trend may be derived, due to the noticeable effect of the conicity values of the sintered parts. Considering the height of the sintered parts, in fact, the values are quite scattered, and this also affects the distribution of the values of conicity of sintered parts.

If die movement is provided the required conicity is always met, irrespective to the applied force and the scatter in the conicity value of the sintered parts, as shown in Fig. 4.4.4.

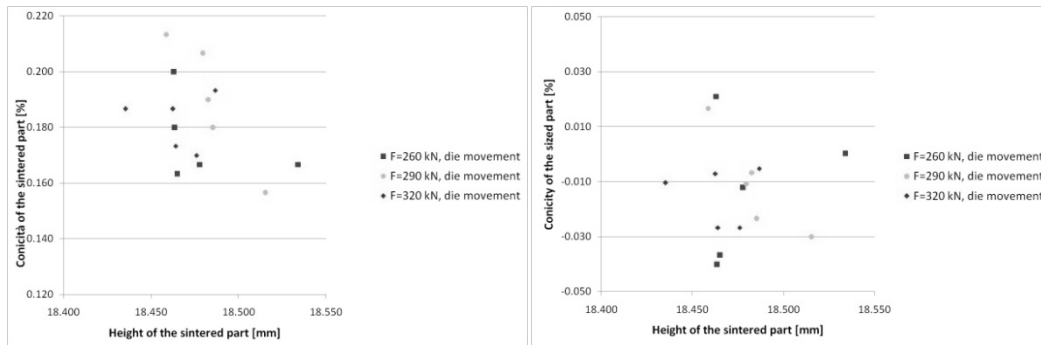


Fig. 4.4.4 Conicity of the sintered parts and of the force control considering the die movement sized parts vs the height of the sintered parts

This results, from an industrial point of view, is particularly interesting. It means that force control sizing with die movement allows to control the conicity of the parts irrespective from the height of the sintered parts, thus improving the effectiveness of the process.

The force control die movement sized parts meet the required conicity for any value of applied force, but the reliability of the process increases on increasing the applied force, as shown in Fig. 4.4.5, where the decreasing scatter of the conicity vs. force is reported.

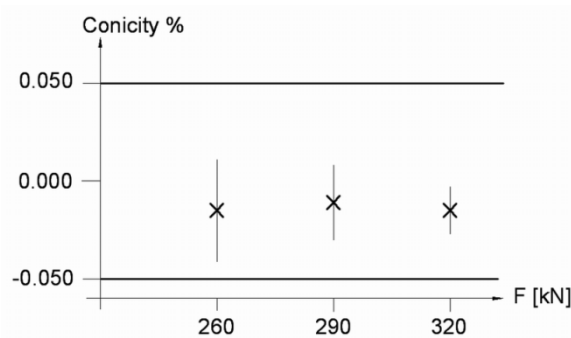


Fig. 4.4.5 Conicity of sized parts versus force applied in force control die movement

4.4.2.2 Geometrical characteristics

The influence of the applied force on the most significant geometrical characteristics was also studied. As an example, in Fig. 4.4.6 are shown the cylindricity of the hole and the cylindricity of the envelope of the external surface.

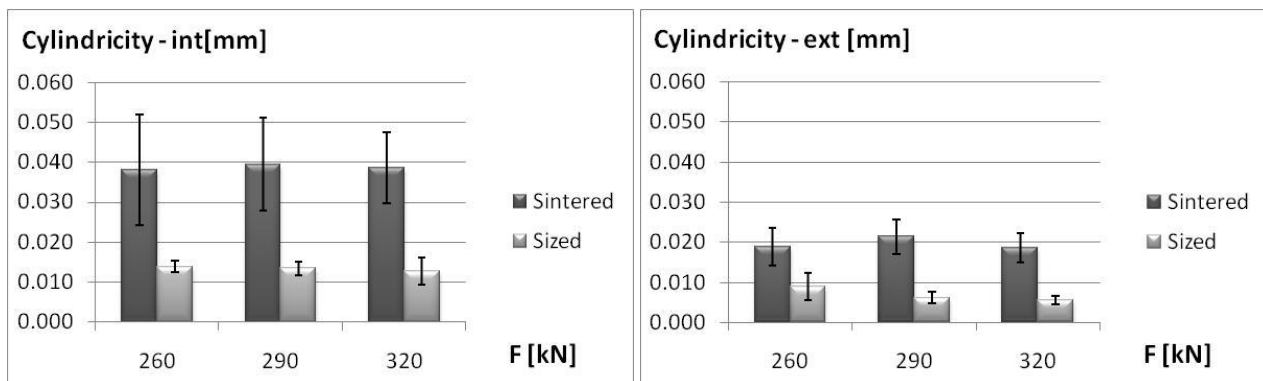


Fig. 4.4.6 Cylindricity of internal and external cylinder measured on sintered and sized parts in force control with die movement

The cylindricity decreases after sizing, and it may be observed that these values are very low. The mean value of cylindricity tends to decrease on increasing the applied force. The concentricity

between the cylindrical envelope of the external surface and the surface of the hole is shown in Fig. 4.4.7.

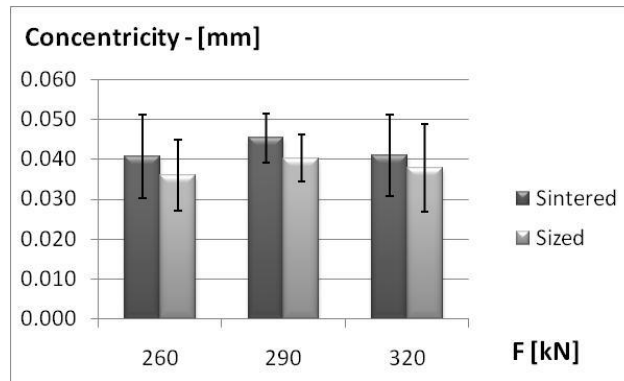


Fig. 4.4.7 Concentricity of sintered and sized parts - force control with die movement

Concentricity is scarcely affected by sizing, being low both in the sintered as in the sized parts. The flatness of the upper and lower planes is shown in Fig. 4.4.8.

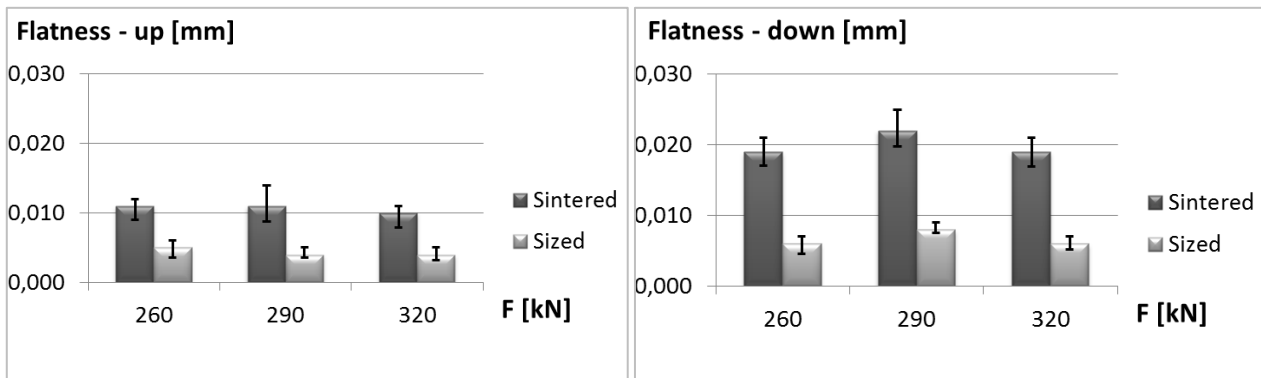


Fig. 4.4.8 Flatness of upper and lower plane of sintered and sized parts - force control with die movement

Flatness decreases after sizing, and the mean value is very low, moreover the difference in flatness between the upper and lower surfaces tends to disappear.

4.4.2.3 Dimensional precision

Although sizing is performed to obtain the required geometrical characteristics, dimensional precision has also to be guaranteed, as by the dimensional tolerances shown in Fig. 4.4.9.

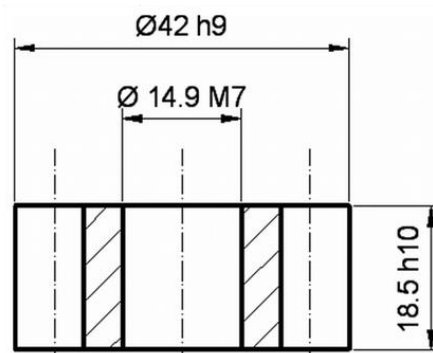


Fig. 4.4.9 Dimension tolerances

To this point, comparing the conditions which allow to guarantee the requested conicity, the highest force in the interval considered ensures the best reliability of the process (smallest scatter in the measured conicity values), as well as the best control of the geometry of the part. A different trend may be observed considering the dimensional precision of height and diameters. Fig. 4.4.10 reports the measured height and diameters of sintered and sized parts - force control with die movement.

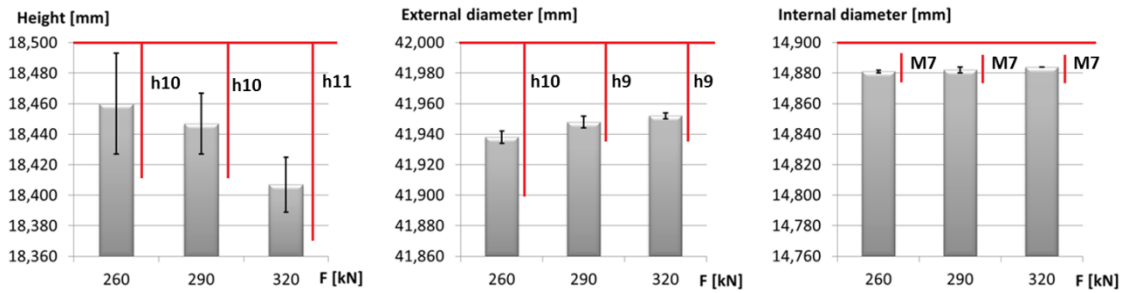


Fig. 4.4.10 Dimensions in sintered and sized parts vs force - force control with die movement sizing

Comparing the measured values to the requirements on drawing (see Fig. 4.4.9), it is highlighted that height does not meet the requirements at the highest value of sizing force, while it does in the other cases, as shown in Fig. 4.4.10. On the other hand, the external diameter does not meet the requirements at the lowest value of sizing force, while it does in the other cases; the internal diameter meets the requirements in any case. It may thus be concluded that, aiming at guaranteeing the requested dimensional precision, the intermediate value for sizing force must be chosen, ensuring the best compromise between the modifications due to sizing and to springback.

4.4.3 Conclusions

This work highlights how the precision of the sized part, considered in terms of the whole of the dimensional and geometrical characteristics, strongly depends on the possibility of precisely controlling the force. Therefore the direct control of force is more effective than its indirect control through the displacement.

5 Conclusion

The results of the work have been discussed in the previous paragraphs and the conclusive remarks have been drawn consequently. Here a general conclusion related to the aim of the work is proposed.

The experimental approach used in this work, based on the measurement and on the characterization of the parts, allowed to highlight the correlation among the chemical and physical characteristics of the materials, the processing parameters, the characteristics of the green parts, the dimensional changes on sintering and the final geometrical features.

The two powders investigated, characterized by a different dimensional behavior on sintering in dependence on the composition and on the processing parameters, allow an excellent control of the dimensional and geometrical precision to be obtained. The simple geometry of the disks utilized promotes a homogeneous distribution of density in the green parts. It may be expected that the same results will be obtained on complex geometry, provided that compaction parameters and strategy lead to a similarly homogeneous green density distribution, within the limits allowed by the geometrical complexity. The use of the modern lubricant systems and of diffusion bonded powders enhances the dimensional and geometrical control, and this will be particularly important in the manufacturing of complex parts.

As far as compaction is concerned, the two case studies investigated demonstrate the importance of the compaction strategy. The use of hydraulic presses allows to precisely monitor the force and the movements of the independent axes, and this has to be utilized to carefully set up the compaction strategy. Even small changes in the movements of the axes may determine modifications of the powder distribution in the different columns and/or a different effect of the post-compaction on dimensional and geometrical precision.

In case of sintering, the most important result is that the sintering temperature may be increased up to 1350°C (which has never been used in the industrial production) without preventing dimensional and geometrical precision even in complex parts, provided that green density distribution is the best attainable within the technical limits related to the parts geometry. Powder filling has a great importance to this purpose. The modification in the shape of the parts, which determines geometrical precision, is correlated to dimensional changes in the axial and transversal direction.

When geometrical precision has to be corrected by a post-sintering sizing, hydraulic presses, which allow to control the applied force, perform better than mechanical presses working in displacement control.

The above remarks have a great technological interest. The work cannot be considered as conclusive, since the experimentation has to be extended to other materials used in the industrial production, as the Ni-Cu-Mo steels and the modern Cr-Mn-Si steels, just for examples. Other different geometries have to be considered, as those characterized by both a large and a small H/D ratio and by square compaction sections. An important development of the project might be related to the prediction of the variations of geometry on the basis of dimensional changes in the axial and transversal directions. Finally, the work highlighted the anisotropy of dimensional change. This subject was also investigated, even if the results have been not included in the present thesis. The

study of the correlation among the material composition, the geometry of the parts and the anisotropy of dimensional changes will further contribute to the dimensional and geometrical control of the sintered parts and generate data and procedures for the part designers.

All these issues need for an accurate experimental methodology, in particular for what concerns the measurement of the parts. The procedure implemented here represents the most reliable methodology, which however might not be applicable in the industrial practice, being rather time consuming. Nevertheless, in the present step of the research the proposed procedure is the one which can generate reliable data and give the possibility of a geometrical representation of the parts in order to interpret how they evolve during the whole of the processes in terms of both dimensions and geometry.

6 Publications

6.1 Journals

I.Cristofolini, M.Pilla, A.Molinari, C.Menapace, M.Larsson, “DOE investigation of anisotropic dimensional change during sintering of Iron-Copper-Carbon” *International Journal of Powder Metallurgy*, 48(4)(2012) 33-44

I.Cristofolini, M. Pilla, M. Larsson, A.Molinari, “A DOE analysis of dimensional change on sintering of a 3%Cr-0.5%Mo-X%C steel and its effect on dimensional and geometric precision” , *Powder Metallurgy Progress* ,12(2012) 127-143

I.Cristofolini, M.Pilla, A.Rao, S.Libardi, A.Molinari, “Dimensional and geometrical precision of powder metallurgy parts sintered and sinterhardened at high temperature”, *International Journal of Precision Engineering and Manufacturing* 14(10)(2013) 1735-1742.

I.Cristofolini, N.Corsentino, M.Pilla, A.Molinari, M.Larsson, “Anisotropy of dimensional change on sintering of PM parts - the influence of material and geometry”, submitted to *Journal of Materials and Processing Technologies* (2013)

P. V. Muterle , I. Cristofolini, M. Pilla, W. Pahl, A. Molinari, ”Surface durability and design criteria for graphite-bronze sintered composites in dry sliding applications”, *Materials and Design*, 32(2011) 3756-3764

I.Cristofolini, M.Pilla, G.Strafellini, A.Molinari, “Design guidelines for PM parts subject to dry rolling-sliding wear”, *Powder Metallurgy* , volume 56(2)(2013). 124-134

6.2 Proceedings

I. Cristofolini, M. Pilla, A. Rao, A. Molinari, S. Libardi, “Dimensional and geometrical control of PM parts sintered at low and high temperatures”, *Advances in Powder Metallurgy and Particulate Materials* 1(2010) 19-26

I. Cristofolini ,M. Pilla ,A. Rao ,G. Pederzini ,A. Salemi ,R. Crosa, A. Molinari, “Optimisation of powder compaction to improve the dimensional characteristics of PM steel parts”, *World PM 2010 World Congress & Exhibition, Florence 10-14 oct 2010*, ed. EPMA Shrewsbury, UK 1(2010) 441-448

I.Cristofolini, M.Pilla, A.Molinari, “Optimization of PM parts for wear resistance design criteria for dry rolling-sliding wear”, *Advances in Powder Metallurgy and Particulate Materials*, 9(2011)47-56

I. Cristofolini, M. Pilla, A. Molinari, M. Larsson, “Study of the effect of powder mixture on the geometrical characteristics of PM copper steel parts by DOE analysis”, *Proceeding Euro PM2011 Congress & Exhibition, Barcelona 9-12 Oct 2011*, ed. EPMA Shrewsbury, UK, 3(2011) 405-410

M. Pilla, I. Cristofolini, G. Pederzini, A. Molinari, “Influence of the compaction speed on the dimensional and geometrical precision of Cr-Mo steel multilevel parts”, *Proceeding Euro PM2011 Congress & Exhibition, Barcelona 9-12 Oct 2011*, ed. EPMA Shrewsbury, UK, 3(2011) 27-32

- I. Cristofolini, F. Selber, C. Menapace, M. Pilla, A. Molinari, S. Libardi, “Anisotropia nelle variazioni dimensionali e suoi effetti sulla precisione di pezzi sinterizzati”, 2° Congresso Nazionale del Coordinamento della Meccanica Italiana Ancona, 25-26 Giugno 2012
- I. Cristofolini, F. Selber, C. Menapace, M. Pilla, A. Molinari, S. Libardi, “Anisotropy of Dimensional Variation and its Effect on Precision of Sintered Parts”, Proceedings Euro PM2012 Congress & Exhibition, Basel 16-19 Sep. 2012, ed. EPMA, Shrewsbury (UK), 1(2012) 519-524
- I. Cristofolini, M. Pilla, D. Belluzzi, M. Crocetti, A. Molinari “Experimental Study of Sizing of Gears by a Hydraulic Press”, Proceedings Euro PM2012 Congress & Exhibition, Basel 16-19 Sep. 2012, ed. EPMA, Shrewsbury (UK), 1(2012) 501-506
- I. Cristofolini, M. Pilla, G. Pederzini, A. Rambelli, S. Libardi, A. Molinari, “Influence of the Green characteristics on the Geometrical Features of Stainless Steel Parts Sintered at High Temperature”, Proceedings World PM2012 World Congress & Exhibition, Yokohama (Japan) Oct. 2012 14-18 , cd-rom, Japan Society of Powder and Powder Metallurgy, ISBN 978-4-9900214-9-8
- M. Pilla, I. Cristofolini, D. Belluzzi, M. Crocetti, Alberto Molinari, “Calibratura di sinterizzati ferrosi con pressa idraulica”, 34° Convegno nazionale AIM, 7-9 novembre 2012
- I. Cristofolini, M. Pilla, D. Belluzzi, G. Pederzini, M. Crocetti, A. Molinari, “Influence of the Scatter of Sintered Height on the Precision of Parts Sized by a Hydraulic Press”, Proceedings Euro PM2013 Congress & Exhibition, Gotheborg 15-18 September 2013, ed. EPMA, Shrewsbury (UK), 2(2013) 1-6
- I. Cristofolini, N. Corsentino, M. Pilla, A. Molinari, M. Larsson “Influence of geometry on the anisotropic dimensional change on sintering of PM parts”, Advances in Powder Metallurgy and Particulate Materials 11(2013)49-61

7 Acknowledgements

The path that took me to the conclusion of the three years of graduate studies has been long and demanding, so I would like to thank all those people who have helped me.

First of all, I would like to thank my tutors Ilaria Cristofolini and Alberto Molinari, who have shown a passion for the subject of my doctorate studies that fascinated and made me really fond of it. I would like to thank them also for the trust they have always had in me. I hope I have never disappointed them.

I would like dedicate this work to my father, whose passion for life and research has always pushed me to fully commit myself, and even now that he is not here anymore, his memories help me in hard times.

I would like to thank with all my heart my mother and my brother who have always supported me in my choices. You have allowed me to reach my goals, putting up with me, sometimes even too much. I hope I'll have the opportunity of rewarding you.

To all those who in these years have been working in the laboratory, I always think of them with pleasure. We have worked hard but we have had a great time too.

To all my friends, those near and those far away, who have always helped and supported me.

8 Appendix A

PART NAME: AISI 316 L

REV NUMBER: 1

SER NUMBER:

STATS COUNT: 1

STARTUP= ALIGNMENT/START,RECALL:,LIST=YES

ALIGNMENT/END

MODE/MANUAL

PREHIT/1.5

RETRACT/1.5

CHECK/5,1

SCANSPEED/4

MOVESPEED/ 100

FLY/ON,3

FORMAT/TEXT,OPTIONS,ID,HEADINGS,SYMBOLS, ;NOM,MEAS,TOL,DEV,OUTTOL, ,

LOADPROBE/DIM2

TIP/T1A0B0, SHANKIJK=0, 0, 1, ANGLE=0

PLANE1= FEAT/PLANE,CARTESIAN,TRIANGLE

THEO/<-6.163,145.042,-748.889>,<-0.999998,-0.0018055,-0.0008969>

ACTL/<-6.163,145.042,-748.889>,<-0.999998,-0.0018055,-0.0008969>

MEAS/PLANE,4

ENDMEAS/

A1= ALIGNMENT/START,RECALL:STARTUP,LIST=YES

ALIGNMENT/LEVEL,XMINUS,PIANO1

ALIGNMENT/TRANS,XAXIS,PIANO1

ALIGNMENT/END

PLANE2= FEAT/PLANE,CARTESIAN,TRIANGLE

THEO/<27.488,119.354,-748.101>,<0.0000434,-0.9999996,-0.0008637>

ACTL/<27.488,119.354,-748.101>,<0.0000434,-0.9999996,-0.0008637>

MEAS/PLANE,4

ENDMEAS/

A2= ALIGNMENT/START,RECALL:A1,LIST=YES

ALIGNMENT/TRANS,YAXIS,PIANO2

ALIGNMENT/LEVEL,YMINUS,PIANO2

ALIGNMENT/END

PIONT1= FEAT/POINT,CARTESIAN

THEO/<6.806,6.282,-741.42>,<0,0,1>

ACTL/<6.806,6.282,-741.42>,<0,0,1>

MEAS/POINT,1

ENDMEAS/

A3= ALIGNMENT/START,RECALL:A2,LIST=YES

ALIGNMENT/TRANS,ZAXIS,PUNTO1

ALIGNMENT/END

CLEARP/ZPLUS,25,ZPLUS,25,ON

MODE/DCC

CIRCLE1=FEAT/CIRCLE,CARTESIAN,OUT,LEAST_SQR

THEO/<75.005,54.031,7.755>,<0,0,1>,30.496,0

ACTL/<75.011,53.978,7.755>,<0,0,1>,30.451,0

MEAS/CIRCLE,7,ZPLUS

ENDMEAS/

A4= ALIGNMENT/START,RECALL:A3,LIST=YES

ALIGNMENT/TRANS,XAXIS,CERCHIO1

```

ALIGNMENT/TRANS,YAXIS,CERCHIO1
ALIGNMENT/END
PLANE3= FEAT/PLANE,CARTESIAN,TRIANGLE
THEO/<0.117,0.086,9.84>,<0.0020766,0.0006656,0.9999976>
ACTL/<0.126,0.076,10.242>,<0.0006431,0.0012361,0.999999>
MEAS/PLANE,9
ENDMEAS/
A5= ALIGNMENT/START,RECALL:A4,LIST=YES
ALIGNMENT/TRANS,ZAXIS,PIANO3
ALIGNMENT/END
MOVE/CLEARPLANE
SCN1= BASICSCAN/LINE,NUMBER OF HITS=60,SHOW HITS=NO,SHOWALLPARAMS=NO
MEAS/SCAN
BASICSCAN/LINE,NUMBER OF HITS=60,SHOW HITS=NO,SHOWALLPARAMS=NO
ENDSCAN
ENDMEAS/
SCN2= BASICSCAN/LINE,NUMBER OF HITS=58,SHOW HITS=NO,SHOWALLPARAMS=NO
MEAS/SCAN
BASICSCAN/LINE,NUMBER OF HITS=58,SHOW HITS=NO,SHOWALLPARAMS=NO
ENDSCAN
ENDMEAS/
SCN3= BASICSCAN/LINE,NUMBER OF HITS=59,SHOW HITS=NO,SHOWALLPARAMS=NO
MEAS/SCAN
BASICSCAN/LINE,NUMBER OF HITS=59,SHOW HITS=NO,SHOWALLPARAMS=NO
ENDSCAN
ENDMEAS/
SCN4= BASICSCAN/LINE,NUMBER OF HITS=50,SHOW HITS=NO,SHOWALLPARAMS=NO
MEAS/SCAN
BASICSCAN/LINE,NUMBER OF HITS=50,SHOW HITS=NO,SHOWALLPARAMS=NO
ENDSCAN
ENDMEAS/
SCN5= BASICSCAN/LINE,NUMBER OF HITS=55,SHOW HITS=NO,SHOWALLPARAMS=NO
MEAS/SCAN
BASICSCAN/LINE,NUMBER OF HITS=55,SHOW HITS=NO,SHOWALLPARAMS=NO
ENDSCAN
ENDMEAS/
SCN6= BASICSCAN/LINE,NUMBER OF HITS=45,SHOW HITS=NO,SHOWALLPARAMS=NO
MEAS/SCAN
BASICSCAN/LINE,NUMBER OF HITS=45,SHOW HITS=NO,SHOWALLPARAMS=NO
ENDSCAN
ENDMEAS/
SCN7= BASICSCAN/LINE,NUMBER OF HITS=53,SHOW HITS=NO,SHOWALLPARAMS=NO
MEAS/SCAN
BASICSCAN/LINE,NUMBER OF HITS=3SHOW HITS=NO,SHOWALLPARAMS=NO
ENDSCAN
ENDMEAS/
SCN8= BASICSCAN/LINE,NUMBER OF HITS=53,SHOW HITS=NO,SHOWALLPARAMS=NO
MEAS/SCAN
BASICSCAN/LINE,NUMBER OF HITS=53,SHOW HITS=NO,SHOWALLPARAMS=NO
ENDSCAN
ENDMEAS/

```

PLANE4= FEAT/PLANE,CARTESIAN,TRIANGLE,NO
 THEO/<6.606,-0.405,-3.808>,<-0.5085082,-0.8610271,-0.0072024>
 ACTL/<6.579,-0.41,-3.661>,<-0.5091036,-0.8606685,-0.0079513>
 CONSTR/PLANE,BF,SCN1,SCN2,SCN3,SCN4,,
 OUTLIER_REMOVAL/OFF,3
 FILTER/OFF,WAVELENGTH=0

PLANE5= FEAT/PLANE,CARTESIAN,TRIANGLE,NO
 THEO/<4.678,-6.219,-3.727>,<0.5070644,0.861899,-0.0039822>
 ACTL/<4.718,-6.265,-3.753>,<0.5069203,0.8619664,-0.0067561>
 CONSTR/PLANE,BF,SCN5,SCN6,SCN7,SCN8,,
 OUTLIER_REMOVAL/OFF,3
 FILTER/OFF,WAVELENGTH=0

PIANO6= FEAT/PLANE,CARTESIAN,TRIANGLE,NO
 THEO/<5.604,-3.325,-3.657>,<-0.509156,-0.8606711,0.0023363>
 ACTL/<5.648,-3.338,-3.707>,<-0.5080261,-0.8613415,-0.0005976>
 CONSTR/PLANE,MID,PIANO4,PIANO5

A6= ALIGNMENT/START,RECALL:A5,LIST=YES
 ALIGNMENT/ROTATE,YMINUS,TO,PIANO6,ABOUT,ZPLUS
 ALIGNMENT/END
 MOVE/CLEARPLANE

SCN9= BASICSCAN/CIRCLE,NUMBER OF HITS=785,SHOW HITS=NO,SHOWALLPARAMS=YES
 MEAS/SCAN
 BASICSCAN/LINE,NUMBER OF HITS=785,SHOW HITS=NO,SHOWALLPARAMS=NO
 ENDSCAN
 ENDMEAS/
 MOVE/CLEARPLANE

SCN10= FEAT/SCAN,LINEAROPEN,NUMBER OF HITS=165,SHOW HITS=NO,SHOWALLPARAMS=NO
 MEAS/SCAN
 BASICSCAN/LINE,NUMBER OF HITS=165,SHOW HITS=NO,SHOWALLPARAMS=NO
 ENDSCAN
 ENDMEAS/
 MOVE/CLEARPLANE

SCN11= FEAT/SCAN,LINEAROPEN,NUMBER OF HITS=165,SHOW HITS=NO,SHOWALLPARAMS=NO
 MEAS/SCAN
 BASICSCAN/LINE,NUMBER OF HITS=165,SHOW HITS=NO,SHOWALLPARAMS=NO
 ENDSCAN
 ENDMEAS/
 MOVE/CLEARPLANE

SCN12= FEAT/SCAN,LINEAROPEN,NUMBER OF HITS=101,SHOW HITS=NO,SHOWALLPARAMS=NO
 MEAS/SCAN
 BASICSCAN/LINE,NUMBER OF HITS=101,SHOW HITS=NO,SHOWALLPARAMS=NO
 ENDSCAN
 ENDMEAS/
 MOVE/CLEARPLANE

SCN13= FEAT/SCAN,LINEAROPEN,NUMBER OF HITS=101,SHOW HITS=NO,SHOWALLPARAMS=NO
 MEAS/SCAN
 BASICSCAN/LINE,NUMBER OF HITS=101,SHOW HITS=NO,SHOWALLPARAMS=NO
 ENDSCAN
 ENDMEAS/

CYL1= FEAT/CYLINDER,CARTESIAN,OUT,LEAST_SQR,NO
 THEO/<-0.022,0.036,-1.98>,<-0.0150731,0.0243292,-0.9995904>,30.42,2.831

ACTL/<-0.007,0.014,-1.973>,<-0.0125028,0.0248727,-0.9996124>,30.42,2.803

CONSTR/CYLINDER,BF,SCN9,SCN10,SCN11,SCN12,SCN13,,

FCFCYLTA1=CYLINDRICITY OF CIL1

FEATCTRLFRAME/SHOWPARAMS=YES,SHOWEXPANDED=YES

CADGRAPH=OFF,REPORTGRAPH=OFF,TEXT=OFF,MULT=1000.00,ARROWDENSITY=100,OUTPUT=

BOTH,UNITS=MM

DIMENSION/CYLINDRICITY,0.01

NOTE/FCFCILTA1

FEATURES/CYL1,,

CIRCLE2=FEAT/CIRCLE,CARTESIAN,OUT,LEAST_SQR,NO

THEO/<0,0,-1>,<0,0,1>,30.4

ACTL/<0.006,-0.009,-1>,<0,0,1>,30.431

CONSTR/CIRCLE,BF,2D,SCN9,,

CIRCLE3=FEAT/CIRCLE,CARTESIAN,OUT,LEAST_SQR,NO

THEO/<-0.011,0.006,-2>,<0,0,1>,30.49

ACTL/<-0.027,0.055,-2.002>,<0,0,1>,30.385

CONSTR/CIRCLE,BF,2D,SCN10,SCN13,,

CIRCLE4=FEAT/CIRCLE,CARTESIAN,OUT,LEAST_SQR,NO

THEO/<-0.008,0,-3>,<0,0,1>,30.491

ACTL/<-0.024,0.047,-3.001>,<0,0,1>,30.397

CONSTR/CIRCLE,BF,2D,SCN11,SCN12,,

FCFCIRTA1=CIRCULARITY OF CIRCLE2

FEATCTRLFRAME/SHOWPARAMS=YES,SHOWEXPANDED=YES

CADGRAPH=OFF,REPORTGRAPH=OFF,TEXT=OFF,MULT=1000.00,ARROWDENSITY=100,OUTPUT=

BOTH,UNITS=MM

DIMENSION/CIRCULARITY,0.01

NOTE/FCFCIRTA1

FEATURES/ CIRCLE2,,

FCFCIRTA2=CIRCULARITY OF CERCHIO3

FEATCTRLFRAME/SHOWPARAMS=YES,SHOWEXPANDED=YES

CADGRAPH=OFF,REPORTGRAPH=OFF,TEXT=OFF,MULT=1000.00,ARROWDENSITY=100,OUTPUT=

BOTH,UNITS=MM

DIMENSION/CIRCULARITY,0.01

NOTE/FCFCIRTA2

FEATURES/ CIRCLE3,,

FCFCIRTA3=CIRCULARITY OF CIRCLE4

FEATCTRLFRAME/SHOWPARAMS=YES,SHOWEXPANDED=YES

CADGRAPH=OFF,REPORTGRAPH=OFF,TEXT=OFF,MULT=1000.00,ARROWDENSITY=100,OUTPUT=

BOTH,UNITS=MM

DIMENSION/CIRCULARITY,0.01

NOTE/FCFCIRTA3

FEATURES/ CIRCLE4,,

FINAL_ALL=ALIGNMENT/START,RECALL:A6,LIST=YES

ALIGNMENT/TRANS,XAXIS,CIL1

ALIGNMENT/TRANS,YAXIS,CIL1

ALIGNMENT/END

MOVE/CLEARPLANE

SCN14= FEAT/SCAN,LINEARCLOSE,NUMBER OF HITS=122,SHOW HITS=NO,SHOWALLPARAMS=NO

MEAS/SCAN

BASICSCAN/LINE,NUMBER OF HITS=122,SHOW HITS=NO,SHOWALLPARAMS=NO

ENDSCAN

ENDMEAS/
 SCN15= FEAT/SCAN,LINEARCLOSE,NUMBER OF HITS=124,SHOW HITS=NO,SHOWALLPARAMS=NO
 MEAS/SCAN
 BASICSCAN/LINE,NUMBER OF HITS=124,SHOW HITS=NO,SHOWALLPARAMS=NO
 ENDSCAN
 ENDMEAS/
 SCN16= FEAT/SCAN,LINEARCLOSE,NUMBER OF HITS=124,SHOW HITS=NO,SHOWALLPARAMS=NO
 MEAS/SCAN
 BASICSCAN/LINE,NUMBER OF HITS=124,SHOW HITS=NO,SHOWALLPARAMS=NO
 ENDSCAN
 ENDMEAS/
 SCN17= FEAT/SCAN,LINEARCLOSE,NUMBER OF HITS=125,SHOW HITS=NO,SHOWALLPARAMS=NO
 MEAS/SCAN
 BASICSCAN/LINE,NUMBER OF HITS=125,SHOW HITS=NO,SHOWALLPARAMS=NO
 ENDSCAN
 ENDMEAS/
 CYL2= FEAT/CYLINDER,CARTESIAN,IN,LEAST_SQR,NO
 THEO/<8.67,-7.284,-3.75>,<-0.0019076,-0.0004892,-0.9999981>,4.905,4.506
 ACTL/<8.665,-7.295,-3.75>,<-0.0021383,0.0018861,-0.9999959>,4.896,4.536
 CONSTR/CYLINDER,BFRE,SCN14,SCN15,SCN16,SCN17,,
 CIRCLE5= FEAT/CIRCLE,CARTESIAN,IN,LEAST_SQR,NO
 THEO/<8.673,-7.282,-1.5>,<0,0,1>,4.905
 ACTL/<8.669,-7.299,-1.504>,<0,0,1>,4.895
 CONSTR/CIRCLE,BF,2D,SCN14,,
 CIRCLE6= FEAT/CIRCLE,CARTESIAN,IN,LEAST_SQR,NO
 THEO/<8.671,-7.283,-3>,<0,0,1>,4.906
 ACTL/<8.667,-7.298,-3.004>,<0,0,1>,4.897
 CONSTR/CIRCLE,BF,2D,SCN15,,
 CIRCLE7= FEAT/CIRCLE,CARTESIAN,IN,LEAST_SQR,NO
 THEO/<8.669,-7.283,-4.5>,<0,0,1>,4.905
 ACTL/<8.664,-7.295,-4.503>,<0,0,1>,4.898
 CONSTR/CIRCLE,BF,2D,SCN16,,
 CIRCLE8= FEAT/CIRCLE,CARTESIAN,IN,LEAST_SQR,NO
 THEO/<8.664,-7.285,-6>,<0,0,1>,4.904
 ACTL/<8.66,-7.29,-6.001>,<0,0,1>,4.895
 CONSTR/CIRCLE,BF,2D,SCN17,,
 FCFCILTÁ2=CYLINDRICITY OF CYL2
 FEATCTRLFRAME/SHOWPARAMS=YES,SHOWEXPANDED=YES
 CADGRAPH=OFF,REPORTGRAPH=OFF,TEXT=OFF,MULT=1000.00,ARROWDENSITY=100,OUTPUT=
 BOTH,UNITS=MM
 DIMENSION/CYLINDRICITY,0.01
 NOTE/FCFCILTÁ2
 FEATURES/CYL2,,
 FCFCIRTÁ4=CIRCULARITY OF CIRCLE5
 FEATCTRLFRAME/SHOWPARAMS=YES,SHOWEXPANDED=YES
 CADGRAPH=OFF,REPORTGRAPH=OFF,TEXT=OFF,MULT=1000.00,ARROWDENSITY=100,OUTPUT=
 BOTH,UNITS=MM
 DIMENSION/CIRCULARITY,0.01
 NOTE/FCFCIRTÁ4
 FEATURES/CIRCLE5,,
 FCFCIRTÁ5=CIRCULARITY OF CIRCLE6

FEATCTRLFRAME/SHOWPARAMS=YES,SHOWEXPANDED=YES

CADGRAPH=OFF,REPORTGRAPH=OFF,TEXT=OFF,MULT=1000.00,ARROWDENSITY=100,OUTPUT=BOTH,UNITS=MM

DIMENSION/CIRCULARITY,0.01

NOTE/FCFCIRTÁ5

FEATURES/CIRCLE6,,

FCFCIRTÁ6=CIRCULARITY OF CIRCLE7

FEATCTRLFRAME/SHOWPARAMS=YES,SHOWEXPANDED=YES

CADGRAPH=OFF,REPORTGRAPH=OFF,TEXT=OFF,MULT=1000.00,ARROWDENSITY=100,OUTPUT=BOTH,UNITS=MM

DIMENSION/CIRCULARITY,0.01

NOTE/FCFCIRTÁ6

FEATURES/CIRCLE7,,

FCFCIRTÁ7=CIRCULARITY OF CIRCLE8

FEATCTRLFRAME/SHOWPARAMS=YES,SHOWEXPANDED=YES

CADGRAPH=OFF,REPORTGRAPH=OFF,TEXT=OFF,MULT=1000.00,ARROWDENSITY=100,OUTPUT=BOTH,UNITS=MM

DIMENSION/CIRCULARITY,0.01

NOTE/FCFCIRTÁ7

FEATURES/CIRCLE8,,

MOVE/CLEARPLANE

SCN18= FEAT/SCAN,LINEARCLOSE,NUMBER OF HITS=154,SHOW HITS=NO,SHOWALLPARAMS=NO

MEAS/SCAN

BASICSCAN/LINE,NUMBER OF HITS=154,SHOW HITS=NO,SHOWALLPARAMS=NO

ENDSCAN

ENDMEAS/

SCN19= FEAT/SCAN,LINEARCLOSE,NUMBER OF HITS=158,SHOW HITS=NO,SHOWALLPARAMS=NO

MEAS/SCAN

BASICSCAN/LINE,NUMBER OF HITS=158,SHOW HITS=NO,SHOWALLPARAMS=NO

ENDSCAN

ENDMEAS/

SCN20= FEAT/SCAN,LINEARCLOSE,NUMBER OF HITS=91,SHOW HITS=NO,SHOWALLPARAMS=NO

MEAS/SCAN

BASICSCAN/LINE,NUMBER OF HITS=91,SHOW HITS=NO,SHOWALLPARAMS=NO

ENDSCAN

ENDMEAS/

SCN21= FEAT/SCAN,LINEARCLOSE,NUMBER OF HITS=151,SHOW HITS=NO,SHOWALLPARAMS=NO

MEAS/SCAN

BASICSCAN/LINE,NUMBER OF HITS=151,SHOW HITS=NO,SHOWALLPARAMS=NO

ENDSCAN

ENDMEAS/

CYL3= FEAT/CYLINDER,CARTESIAN,IN,LEAST_SQR,NO

THEO/<2.72,-10.178,-3.75>,<-0.002177,-0.0014461,-0.9999966>,5.895,4.51

ACTL/<2.746,-10.185,-3.75>,<-0.0030114,-0.0007341,-0.9999952>,5.887,4.533

CONSTR/CYLINDER,BFRE,SCN18,SCN19,SCN20,SCN21,,

CIRCLE9= FEAT/CIRCLE,CARTESIAN,IN,LEAST_SQR,NO

THEO/<2.724,-10.175,-1.5>,<0,0,1>,5.894

ACTL/<2.752,-10.183,-1.501>,<0,0,1>,5.883

CONSTR/CIRCLE,BF,2D,SCN18,,

CIRCLE10= FEAT/CIRCLE,CARTESIAN,IN,LEAST_SQR,NO

THEO/<2.722,-10.175,-3>,<0,0,1>,5.893

ACTL/<2.748,-10.185,-2.999>,<0,0,1>,5.887
 CONSTR/CIRCLE,BF,2D,SCN19,,
 CIRCLE11= FEAT/CIRCLE,CARTESIAN,IN,LEAST_SQR,NO
 THEO/<2.719,-10.179,-4.5>,<0,0,1>,5.895
 ACTL/<2.744,-10.187,-4.5>,<0,0,1>,5.889
 CONSTR/CIRCLE,BF,2D,SCN20,,
 CIRCLE12= FEAT/CIRCLE,CARTESIAN,IN,LEAST_SQR,NO
 THEO/<2.714,-10.181,-6>,<0,0,1>,5.897
 ACTL/<2.739,-10.186,-6.002>,<0,0,1>,5.889
 CONSTR/CIRCLE,BF,2D,SCN21,,
 FCFCILTÁ3=CYLINDRICITY OF CYL3
 FEATCTRLFRAME/SHOWPARAMS=YES,SHOWEXPANDED=YES
 CADGRAPH=OFF,REPORTGRAPH=OFF,TEXT=OFF,MULT=1000.00,ARROWDENSITY=100,OUTPUT=
 BOTH,UNITS=MM
 DIMENSION/CYLINDRICITY,0.01
 NOTE/FCFCILTÁ3
 FEATURES/CIL3,,
 FCFCIRTÁ8=CIRCULARITY OF CIRCLE9
 FEATCTRLFRAME/SHOWPARAMS=YES,SHOWEXPANDED=YES
 CADGRAPH=OFF,REPORTGRAPH=OFF,TEXT=OFF,MULT=1000.00,ARROWDENSITY=100,OUTPUT=
 BOTH,UNITS=MM
 DIMENSION/CIRCULARITY,0.01
 NOTE/FCFCIRTÁ8
 FEATURES/CIRCLE9,,
 FCFCIRTÁ9=CIRCULARITY OF CIRCLE10
 FEATCTRLFRAME/SHOWPARAMS=YES,SHOWEXPANDED=YES
 CADGRAPH=OFF,REPORTGRAPH=OFF,TEXT=OFF,MULT=1000.00,ARROWDENSITY=100,OUTPUT=
 BOTH,UNITS=MM
 DIMENSION/CIRCULARITY,0.01
 NOTE/FCFCIRTÁ9
 FEATURES/CERCHIO10,,
 FCFCIRTÁ10=CIRCULARITY OF CIRCLE11
 FEATCTRLFRAME/SHOWPARAMS=YES,SHOWEXPANDED=YES
 CADGRAPH=OFF,REPORTGRAPH=OFF,TEXT=OFF,MULT=1000.00,ARROWDENSITY=100,OUTPUT=
 BOTH,UNITS=MM
 DIMENSION/CIRCULARITY,0.01
 NOTE/FCFCIRTÁ10
 FEATURES/CIRCLE11,,
 FCFCIRTÁ11=CIRCULARITY OF CIRCLE12
 FEATCTRLFRAME/SHOWPARAMS=YES,SHOWEXPANDED=YES
 CADGRAPH=OFF,REPORTGRAPH=OFF,TEXT=OFF,MULT=1000.00,ARROWDENSITY=100,OUTPUT=
 BOTH,UNITS=MM
 DIMENSION/CIRCULARITY,0.01
 NOTE/FCFCIRTÁ11
 FEATURES/CIRCLE12,,
 MOVE/CLEARPLANE
 SCN22= FEAT/SCAN,LINEARCLOSE,NUMBER OF HITS=120,SHOW HITS=NO,SHOWALLPARAMS=NO
 MEAS/SCAN
 BASICSCAN/LINE,NUMBER OF HITS=120,SHOW HITS=NO,SHOWALLPARAMS=NO
 ENDSCAN
 ENDMEAS/

SCN23= FEAT/SCAN,LINEARCLOSE,NUMBER OF HITS=114,SHOW HITS=NO,SHOWALLPARAMS=NO
 MEAS/SCAN
 BASICSCAN/LINE,NUMBER OF HITS=114,SHOW HITS=NO,SHOWALLPARAMS=NO
 ENDSCAN
 ENDMEAS/

SCN24= FEAT/SCAN,LINEARCLOSE,NUMBER OF HITS=114,SHOW HITS=NO,SHOWALLPARAMS=NO
 MEAS/SCAN
 BASICSCAN/LINE,NUMBER OF HITS=114,SHOW HITS=NO,SHOWALLPARAMS=NO
 ENDSCAN
 ENDMEAS/

SCN25= FEAT/SCAN,LINEARCLOSE,NUMBER OF HITS=84,SHOW HITS=NO,SHOWALLPARAMS=NO
 MEAS/SCAN
 BASICSCAN/LINE,NUMBER OF HITS=84,SHOW HITS=NO,SHOWALLPARAMS=NO
 ENDSCAN
 ENDMEAS/

CYL4= FEAT/CYLINDER,CARTESIAN,IN,LEAST_SQR,NO
 THEO/<2,11.177,-3.75>,<0.0013878,-0.0020412,-0.999997>,4.906,4.507
 ACTL/<1.967,11.153,-3.75>,<0.0026051,-0.0005256,-0.9999965>,4.895,4.529
 CONSTR/CYLINDER,BFRE,SCN22,SCN23,SCN24,SCN25,,

CIRCLE13=FEAT/CIRCLE,CARTESIAN,IN,LEAST_SQR,NO
 THEO/<1.997,11.183,-1.5>,<0,0,1>,4.907
 ACTL/<1.961,11.154,-1.5>,<0,0,1>,4.893
 CONSTR/CIRCLE,BF,2D,SCN22,,

CIRCLE14=FEAT/CIRCLE,CARTESIAN,IN,LEAST_SQR,NO
 THEO/<2,11.177,-3>,<0,0,1>,4.909
 ACTL/<1.966,11.155,-3>,<0,0,1>,4.895
 CONSTR/CIRCLE,BF,2D,SCN23,,

CIRCLE15= FEAT/CIRCLE,CARTESIAN,IN,LEAST_SQR,NO
 THEO/<2,11.175,-4.5>,<0,0,1>,4.904
 ACTL/<1.97,11.154,-4.502>,<0,0,1>,4.896
 CONSTR/CIRCLE,BF,2D,SCN24,,

CIRCLE16= FEAT/CIRCLE,CARTESIAN,IN,LEAST_SQR,NO
 THEO/<2.004,11.173,-6>,<0,0,1>,4.906
 ACTL/<1.972,11.151,-6.006>,<0,0,1>,4.896
 CONSTR/CIRCLE,BF,2D,SCN25,,

FCFCILTÁ4=CYLINDRICITY OF CYL4
 FEATCTRLFRAME/SHOWPARAMS=YES,SHOWEXPANDED=YES
 CADGRAPH=OFF,REPORTGRAPH=OFF,TEXT=OFF,MULT=1000.00,ARROWDENSITY=100,OUTPUT=
 BOTH,UNITS=MM
 DIMENSION/CYLINDRICITY,0.01
 NOTE/FCFCILTÁ4
 FEATURES/CyL4,,

FCFCIRTÁ12=CIRCULARITY OF CIRCLE13
 FEATCTRLFRAME/SHOWPARAMS=YES,SHOWEXPANDED=YES
 CADGRAPH=OFF,REPORTGRAPH=OFF,TEXT=OFF,MULT=1000.00,ARROWDENSITY=100,OUTPUT=
 BOTH,UNITS=MM
 DIMENSION/CIRCULARITY,0.01
 NOTE/FCFCIRTÁ12
 FEATURES/CIRCLE13,,

FCFCIRTÁ13=CIRCULARITY OF CIRCLE14
 FEATCTRLFRAME/SHOWPARAMS=YES,SHOWEXPANDED=YES

CADGRAPH=OFF,REPORTGRAPH=OFF,TEXT=OFF,MULT=1000.00,ARROWDENSITY=100,OUTPUT= BOTH,UNITS=MM

DIMENSION/CIRCULARITY,0.01

NOTE/FCFCIRTA13

FEATURES/CIRCLE14,,

FCFCIRTA14=CIRCULARITY OF CIRCLE15

FEATCTRLFRAME/SHOWPARAMS=YES,SHOWEXPANDED=YES

CADGRAPH=OFF,REPORTGRAPH=OFF,TEXT=OFF,MULT=1000.00,ARROWDENSITY=100,OUTPUT= BOTH,UNITS=MM

DIMENSION/CIRCULARITY,0.01

NOTE/FCFCIRTA14

FEATURES/CIRCLE15,,

FCFCIRTA15=CIRCULARITY OF CIRCLE16

FEATCTRLFRAME/SHOWPARAMS=YES,SHOWEXPANDED=YES

CADGRAPH=OFF,REPORTGRAPH=OFF,TEXT=OFF,MULT=1000.00,ARROWDENSITY=100,OUTPUT= BOTH,UNITS=MM

DIMENSION/CIRCULARITY,0.01

NOTE/FCFCIRTA15

FEATURES/CIRCLE16,,

MOVE/CLEARPLANE

SCN26= FEAT/SCAN,LINEARCLOSE,NUMBER OF HITS=106,SHOW HITS=NO,SHOWALLPARAMS=NO

MEAS/SCAN

BASICSCAN/LINE,NUMBER OF HITS=106,SHOW HITS=NO,SHOWALLPARAMS=NO

ENDSCAN

ENDMEAS/

SCN27= FEAT/SCAN,LINEARCLOSE,NUMBER OF HITS=143,SHOW HITS=NO,SHOWALLPARAMS=NO

MEAS/SCAN

BASICSCAN/LINE,NUMBER OF HITS=143,SHOW HITS=NO,SHOWALLPARAMS=NO

ENDSCAN

ENDMEAS/

SCN28= FEAT/SCAN,LINEARCLOSE,NUMBER OF HITS=93,SHOW HITS=NO,SHOWALLPARAMS=NO

MEAS/SCAN

BASICSCAN/LINE,NUMBER OF HITS=93,SHOW HITS=NO,SHOWALLPARAMS=NO

ENDSCAN

ENDMEAS/

SCN29= FEAT/SCAN,LINEARCLOSE,NUMBER OF HITS=107,SHOW HITS=NO,SHOWALLPARAMS=NO

MEAS/SCAN

BASICSCAN/LINE,NUMBER OF HITS=107,SHOW HITS=NO,SHOWALLPARAMS=NO

ENDSCAN

ENDMEAS/

CYL5= FEAT/CYLINDER,CARTESIAN,IN,LEAST_SQR,NO

THEO/<7.48,7.472,-3.75>,<0.0019488,-0.0008184,-0.9999978>,5.895,4.508

ACTL/<7.424,7.449,-3.747>,<0.0033591,0.0014951,-0.9999932>,5.883,4.539

CONSTR/CYLINDER,BFRE,SCN26,SCN27,SCN28,SCN29,,

CIRCLE17= FEAT/CIRCLE,CARTESIAN,IN,LEAST_SQR,NO

THEO/<7.477,7.474,-1.5>,<0,0,1>,5.894

ACTL/<7.417,7.445,-1.504>,<0,0,1>,5.883

CONSTR/CIRCLE,BF,2D,SCN26,,

CIRCLE18= FEAT/CIRCLE,CARTESIAN,IN,LEAST_SQR,NO

THEO/<7.477,7.473,-3>,<0,0,1>,5.893

ACTL/<7.422,7.448,-3.001>,<0,0,1>,5.884

CONSTR/CIRCLE,BF,2D,SCN27,,
 CIRCLE19= FEAT/CIRCLE,CARTESIAN,IN,LEAST_SQR,NO
 THEO/<7.481,7.472,-4.5>,<0,0,1>,5.896
 ACTL/<7.427,7.45,-4.504>,<0,0,1>,5.884
 CONSTR/CIRCLE,BF,2D,SCN28,,
 CIRCLE20= FEAT/CIRCLE,CARTESIAN,IN,LEAST_SQR,NO
 THEO/<7.485,7.47,-6>,<0,0,1>,5.898
 ACTL/<7.432,7.452,-6.004>,<0,0,1>,5.882
 CONSTR/CIRCLE,BF,2D,SCN29,,
 FCFCILTÁ5=CYLINDRICITY OF CYL5
 FEATCTRLFRAME/SHOWPARAMS=YES,SHOWEXPANDED=YES
 CADGRAPH=OFF,REPORTGRAPH=OFF,TEXT=OFF,MULT=1000.00,ARROWDENSITY=100,OUTPUT=
 BOTH,UNITS=MM
 DIMENSION/CYLINDRICITY,0.01
 NOTE/FCFCILTÁ5
 FEATURES/CYL5,,
 FCFCIRTÁ16=CIRCULARITY OF CIRCLE17
 FEATCTRLFRAME/SHOWPARAMS=YES,SHOWEXPANDED=YES
 CADGRAPH=OFF,REPORTGRAPH=OFF,TEXT=OFF,MULT=1000.00,ARROWDENSITY=100,OUTPUT=
 BOTH,UNITS=MM
 DIMENSION/CIRCULARITY,0.01
 NOTE/FCFCIRTÁ16
 FEATURES/CIRCLE17,,
 FCFCIRTÁ17=CIRCULARITY OF CIRCLE18
 FEATCTRLFRAME/SHOWPARAMS=YES,SHOWEXPANDED=YES
 CADGRAPH=OFF,REPORTGRAPH=OFF,TEXT=OFF,MULT=1000.00,ARROWDENSITY=100,OUTPUT=
 BOTH,UNITS=MM
 DIMENSION/CIRCULARITY,0.01
 NOTE/FCFCIRTÁ17
 FEATURES/CIRCLE18,,
 FCFCIRTÁ18=CIRCULARITY OF CIRCLE19
 FEATCTRLFRAME/SHOWPARAMS=YES,SHOWEXPANDED=YES
 CADGRAPH=OFF,REPORTGRAPH=OFF,TEXT=OFF,MULT=1000.00,ARROWDENSITY=100,OUTPUT=
 BOTH,UNITS=MM
 DIMENSION/CIRCULARITY,0.01
 NOTE/FCFCIRTÁ18
 FEATURES/CIRCLE19,,
 FCFCIRTÁ19=CIRCULARITY OF CIRCLE20
 FEATCTRLFRAME/SHOWPARAMS=YES,SHOWEXPANDED=YES
 CADGRAPH=OFF,REPORTGRAPH=OFF,TEXT=OFF,MULT=1000.00,ARROWDENSITY=100,OUTPUT=
 BOTH,UNITS=MM
 DIMENSION/CIRCULARITY,0.01
 NOTE/FCFCIRTÁ19
 FEATURES/CIRCLE20,,
 MOVE/CLEARPLANE
 SCN30= FEAT/SCAN,LINEARCLOSE,NUMBER OF HITS=79,SHOW HITS=NO,SHOWALLPARAMS=NO
 MEAS/SCAN
 BASICSCAN/LINE,NUMBER OF HITS=79,SHOW HITS=NO,SHOWALLPARAMS=NO
 ENDSCAN
 ENDMEAS/
 SCN31= FEAT/SCAN,LINEARCLOSE,NUMBER OF HITS=86,SHOW HITS=NO,SHOWALLPARAMS=NO

```

MEAS/SCAN
BASICSCAN/LINE,NUMBER OF HITS=86,SHOW HITS=NO,SHOWALLPARAMS=NO
ENDSCAN
ENDMEAS/
SCN32= FEAT/SCAN,LINEARCLOSE,NUMBER OF HITS=92,SHOW HITS=NO,SHOWALLPARAMS=NO
MEAS/SCAN
BASICSCAN/LINE,NUMBER OF HITS=92,SHOW HITS=NO,SHOWALLPARAMS=NO
ENDSCAN
ENDMEAS/
SCN33= FEAT/SCAN,LINEARCLOSE,NUMBER OF HITS=94,SHOW HITS=NO,SHOWALLPARAMS=NO
MEAS/SCAN
BASICSCAN/LINE,NUMBER OF HITS=94,SHOW HITS=NO,SHOWALLPARAMS=NO
ENDSCAN
ENDMEAS/
CYL6= FEAT/CYLINDER,CARTESIAN,IN,LEAST_SQR,NO
THEO/<-10.68,-3.856,-3.75>,<0.0010739,0.0022225,-0.999997>,4.906,4.507
ACTL/<-10.628,-3.85,-3.748>,<-0.0030936,-0.0030548,-0.9999905>,4.897,4.542
CONSTR/CYLINDER,BFRE,SCN30,SCN31,SCN32,SCN33,,
CIRCLE21= FEAT/CIRCLE,CARTESIAN,IN,LEAST_SQR,NO
THEO/<-10.683,-3.862,-1.5>,<0,0,1>,4.907
ACTL/<-10.621,-3.842,-1.501>,<0,0,1>,4.894
CONSTR/CIRCLE,BF,2D,SCN30,,
CIRCLE22=FEAT/CIRCLE,CARTESIAN,IN,LEAST_SQR,NO
THEO/<-10.679,-3.856,-3>,<0,0,1>,4.909
ACTL/<-10.626,-3.848,-3>,<0,0,1>,4.897
CONSTR/CIRCLE,BF,2D,SCN31,,
CIRCLE23= FEAT/CIRCLE,CARTESIAN,IN,LEAST_SQR,NO
THEO/<-10.678,-3.855,-4.5>,<0,0,1>,4.904
ACTL/<-10.631,-3.853,-4.505>,<0,0,1>,4.9
CONSTR/CIRCLE,BF,2D,SCN32,,
CIRCLE24= FEAT/CIRCLE,CARTESIAN,IN,LEAST_SQR,NO
THEO/<-10.678,-3.851,-6>,<0,0,1>,4.906
ACTL/<-10.635,-3.857,-6.007>,<0,0,1>,4.899
CONSTR/CIRCLE,BF,2D,SCN33,,
FCFCILTÁ6=CYLINDRICITY OF CYL6
FEATCTRLFRAME/SHOWPARAMS=YES,SHOWEXPANDED=YES
CADGRAPH=OFF,REPORTGRAPH=OFF,TEXT=OFF,MULT=1000.00,ARROWDENSITY=100,OUTPUT=
BOTH,UNITS=MM
DIMENSION/CYLINDRICITY,0.01
NOTE/FCFCILTÁ6
FEATURES/CYL6,,
FCFCIRTÁ20=CIRCULARITY OF CIRCLE21
FEATCTRLFRAME/SHOWPARAMS=YES,SHOWEXPANDED=YES
CADGRAPH=OFF,REPORTGRAPH=OFF,TEXT=OFF,MULT=1000.00,ARROWDENSITY=100,OUTPUT=
BOTH,UNITS=MM
DIMENSION/CIRCULARITY,0.01
NOTE/FCFCIRTÁ20
FEATURES/CIRCLE21,,
FCFCIRTÁ21=CIRCULARITY OF CIRCLE22
FEATCTRLFRAME/SHOWPARAMS=YES,SHOWEXPANDED=YES

```

CADGRAPH=OFF,REPORTGRAPH=OFF,TEXT=OFF,MULT=1000.00,ARROWDENSITY=100,OUTPUT= BOTH,UNITS=MM

DIMENSION/CIRCULARITY,0.01

NOTE/FCFCIRTÁ21

FEATURES/CIRCLE22,,

FCFCIRTÁ22=CIRCULARITY OF CIRCLE23

FEATCTRLFRAME/SHOWPARAMS=YES,SHOWEXPANDED=YES

CADGRAPH=OFF,REPORTGRAPH=OFF,TEXT=OFF,MULT=1000.00,ARROWDENSITY=100,OUTPUT= BOTH,UNITS=MM

DIMENSION/CIRCULARITY,0.01

NOTE/FCFCIRTÁ22

FEATURES/CIRCLE23,,

FCFCIRTÁ23=CIRCULARITY OF CIRCLE24

FEATCTRLFRAME/SHOWPARAMS=YES,SHOWEXPANDED=YES

CADGRAPH=OFF,REPORTGRAPH=OFF,TEXT=OFF,MULT=1000.00,ARROWDENSITY=100,OUTPUT= BOTH,UNITS=MM

DIMENSION/CIRCULARITY,0.01

NOTE/FCFCIRTÁ23

FEATURES/CIRCLE24,,

MOVE/CLEARPLANE

SCN34= FEAT/SCAN,LINEARCLOSE,NUMBER OF HITS=138,SHOW HITS=NO,SHOWALLPARAMS=NO

MEAS/SCAN

BASICSCAN/LINE,NUMBER OF HITS=138,SHOW HITS=NO,SHOWALLPARAMS=NO

ENDSCAN

ENDMEAS/

SCN35= FEAT/SCAN,LINEARCLOSE,NUMBER OF HITS=142,SHOW HITS=NO,SHOWALLPARAMS=NO

MEAS/SCAN

BASICSCAN/LINE,NUMBER OF HITS=142,SHOW HITS=NO,SHOWALLPARAMS=NO

ENDSCAN

ENDMEAS/

SCN36= FEAT/SCAN,LINEARCLOSE,NUMBER OF HITS=88,SHOW HITS=NO,SHOWALLPARAMS=NO

MEAS/SCAN

BASICSCAN/LINE,NUMBER OF HITS=88,SHOW HITS=NO,SHOWALLPARAMS=NO

ENDSCAN

ENDMEAS/

SCN37= FEAT/SCAN,LINEARCLOSE,NUMBER OF HITS=124,SHOW HITS=NO,SHOWALLPARAMS=NO

MEAS/SCAN

BASICSCAN/LINE,NUMBER OF HITS=124,SHOW HITS=NO,SHOWALLPARAMS=NO

ENDSCAN

ENDMEAS/

CYL7= FEAT/CYLINDER,CARTESIAN,IN,LEAST_SQR,NO

THEO/<-10.211,2.742,-3.75>,<-0.0002657,0.0020969,-0.9999978>,5.895,4.508

ACTL/<-10.164,2.735,-3.748>,<-0.0017518,-0.0022119,-0.999996>,5.884,4.536

CONSTR/CYLINDER,BFRE,SCN34,SCN35,SCN36,SCN37,,

CIRCLE25= FEAT/CIRCLE,CARTESIAN,IN,LEAST_SQR,NO

THEO/<-10.211,2.738,-1.5>,<0,0,1>,5.894

ACTL/<-10.159,2.74,-1.502>,<0,0,1>,5.882

CONSTR/CIRCLE,BF,2D,SCN34,,

CIRCLE26= FEAT/CIRCLE,CARTESIAN,IN,LEAST_SQR,NO

THEO/<-10.21,2.739,-3>,<0,0,1>,5.893

ACTL/<-10.163,2.737,-3>,<0,0,1>,5.884

CONSTR/CIRCLE,BF,2D,SCN35,,
 CIRCLE27= FEAT/CIRCLE,CARTESIAN,IN,LEAST_SQR,NO
 THEO/<-10.212,2.743,-4.5>,<0,0,1>,5.896
 ACTL/<-10.166,2.734,-4.502>,<0,0,1>,5.886
 CONSTR/CIRCLE,BF,2D,SCN36,,
 CIRCLE28= FEAT/CIRCLE,CARTESIAN,IN,LEAST_SQR,NO
 THEO/<-10.212,2.747,-6>,<0,0,1>,5.898
 ACTL/<-10.167,2.73,-6.004>,<0,0,1>,5.885
 CONSTR/CIRCLE,BF,2D,SCN37,,
 FCFCILTÁ7=CYLINDRICITY OF CYL7
 FEATCTRLFRAME/SHOWPARAMS=YES,SHOWEXPANDED=YES
 CADGRAPH=OFF,REPORTGRAPH=OFF,TEXT=OFF,MULT=1000.00,ARROWDENSITY=100,OUTPUT=
 BOTH,UNITS=MM
 DIMENSION/CYLINDRICITY,0.01
 NOTE/FCFCILTÁ7
 FEATURES/CYL7,,
 FCFCIRTÁ24=CIRCULARITY OF CIRCLE25
 FEATCTRLFRAME/SHOWPARAMS=YES,SHOWEXPANDED=YES
 CADGRAPH=OFF,REPORTGRAPH=OFF,TEXT=OFF,MULT=1000.00,ARROWDENSITY=100,OUTPUT=
 BOTH,UNITS=MM
 DIMENSION/CIRCULARITY,0.01
 NOTE/FCFCIRTÁ24
 FEATURES/CIRCLE25,,
 FCFCIRTÁ25=CIRCULARITY OF CIRCLE26
 FEATCTRLFRAME/SHOWPARAMS=YES,SHOWEXPANDED=YES
 CADGRAPH=OFF,REPORTGRAPH=OFF,TEXT=OFF,MULT=1000.00,ARROWDENSITY=100,OUTPUT=
 BOTH,UNITS=MM
 DIMENSION/CIRCULARITY,0.01
 NOTE/FCFCIRTÁ25
 FEATURES/CIRCLE26,,
 FCFCIRTÁ26=CIRCULARITY OF CIRCLE27
 FEATCTRLFRAME/SHOWPARAMS=YES,SHOWEXPANDED=YES
 CADGRAPH=OFF,REPORTGRAPH=OFF,TEXT=OFF,MULT=1000.00,ARROWDENSITY=100,OUTPUT=
 BOTH,UNITS=MM
 DIMENSION/CIRCULARITY,0.01
 NOTE/FCFCIRTÁ26
 FEATURES/CIRCLE27,,
 FCFCIRTÁ27=CIRCULARITY OF CIRCLE28
 FEATCTRLFRAME/SHOWPARAMS=YES,SHOWEXPANDED=YES
 CADGRAPH=OFF,REPORTGRAPH=OFF,TEXT=OFF,MULT=1000.00,ARROWDENSITY=100,OUTPUT=
 BOTH,UNITS=MM
 DIMENSION/CIRCULARITY,0.01
 NOTE/FCFCIRTÁ27
 FEATURES/CIRCLE28,,
 MOVE/CLEARPLANE
 SCN38= BASICSCAN/LINE,NUMBER OF HITS=62,SHOW HITS=NO,SHOWALLPARAMS=NO
 MEAS/SCAN
 BASICSCAN/LINE,NUMBER OF HITS=62,SHOW HITS=NO,SHOWALLPARAMS=NO
 ENDSCAN
 ENDMEAS/
 SCN39= BASICSCAN/LINE,NUMBER OF HITS=61,SHOW HITS=NO,SHOWALLPARAMS=NO

```

MEAS/SCAN
BASICSCAN/LINE,NUMBER OF HITS=61,SHOW HITS=NO,SHOWALLPARAMS=NO
ENDSCAN
ENDMEAS/
SCN40= BASICSCAN/LINE,NUMBER OF HITS=57,SHOW HITS=NO,SHOWALLPARAMS=NO
MEAS/SCAN
BASICSCAN/LINE,NUMBER OF HITS=57,SHOW HITS=NO,SHOWALLPARAMS=NO
ENDSCAN
ENDMEAS/
SCN41= BASICSCAN/LINE,NUMBER OF HITS=58,SHOW HITS=NO,SHOWALLPARAMS=NO
MEAS/SCAN
BASICSCAN/LINE,NUMBER OF HITS=58,SHOW HITS=NO,SHOWALLPARAMS=NO
ENDSCAN
ENDMEAS/
SCN42= BASICSCAN/LINE,NUMBER OF HITS=49,SHOW HITS=NO,SHOWALLPARAMS=NO
MEAS/SCAN
BASICSCAN/LINE,NUMBER OF HITS=49,SHOW HITS=NO,SHOWALLPARAMS=NO
ENDSCAN
ENDMEAS/
SCN43= BASICSCAN/LINE,NUMBER OF HITS=52,SHOW HITS=NO,SHOWALLPARAMS=NO
MEAS/SCAN
BASICSCAN/LINE,NUMBER OF HITS=52,SHOW HITS=NO,SHOWALLPARAMS=NO
ENDSCAN
ENDMEAS/
SCN44= BASICSCAN/LINE,NUMBER OF HITS=53,SHOW HITS=NO,SHOWALLPARAMS=NO
MEAS/SCAN
BASICSCAN/LINE,NUMBER OF HITS=53,SHOW HITS=NO,SHOWALLPARAMS=NO
ENDSCAN
ENDMEAS/
SCN45= BASICSCAN/LINE,NUMBER OF HITS=48,SHOW HITS=NO,SHOWALLPARAMS=YES
MEAS/SCAN
BASICSCAN/LINE,NUMBER OF HITS=48,SHOW HITS=NO,SHOWALLPARAMS=NO
ENDSCAN
ENDMEAS/
PLANE7= FEAT/PLANE,CARTESIAN,TRIANGLE,NO
THEO/<-5.834,4.164,-3.717>,<0.8653663,0.5011311,-0.0029697>
ACTL/<-5.842,4.144,-3.708>,<0.8654476,0.5008899,-0.0104786>
CONSTR/PLANE,BF,SCN38,SCN39,SCN40,SCN41,,
PLANE8= FEAT/PLANE,CARTESIAN,TRIANGLE,NO
THEO/<-0.886,7.513,-3.754>,<-0.8664289,-0.4993004,0.0000468>
ACTL/<-0.944,7.586,-3.745>,<-0.867164,-0.4979281,-0.0097054>
CONSTR/PLANE,BF,SCN42,SCN43,SCN44,SCN45,,
PLANE9= FEAT/PLANE,CARTESIAN,TRIANGLE,NO
THEO/<-3.231,5.685,-3.657>,<0.866023,0.4999986,0.0023363>
ACTL/<-3.393,5.865,-3.727>,<0.8663512,0.4994352,-0.0003866>
CONSTR/PLANE,MID,PIANO7,PIANO8
MOVE/CLEARPLANE
SCN46= BASICSCAN/LINE,NUMBER OF HITS=48,SHOW HITS=NO,SHOWALLPARAMS=NO
MEAS/SCAN
BASICSCAN/LINE,NUMBER OF HITS=48,SHOW HITS=NO,SHOWALLPARAMS=NO
ENDSCAN

```

```

ENDMEAS/
SCN47= BASICSCAN/LINE,NUMBER OF HITS=27,SHOW HITS=NO,SHOWALLPARAMS=NO
      MEAS/SCAN
      BASICSCAN/LINE,NUMBER OF HITS=27,SHOW HITS=NO,SHOWALLPARAMS=NO
      ENDSCAN
      ENDMEAS/
SCN48= BASICSCAN/LINE,NUMBER OF HITS=53,SHOW HITS=NO,SHOWALLPARAMS=NO
      MEAS/SCAN
      BASICSCAN/LINE,NUMBER OF HITS=53,SHOW HITS=NO,SHOWALLPARAMS=NO
      ENDSCAN
      ENDMEAS/
SCN49= BASICSCAN/LINE,NUMBER OF HITS=49,SHOW HITS=NO,SHOWALLPARAMS=NO
      MEAS/SCAN
      BASICSCAN/LINE,NUMBER OF HITS=49,SHOW HITS=NO,SHOWALLPARAMS=NO
      ENDSCAN
      ENDMEAS/
SCN50= BASICSCAN/LINE,NUMBER OF HITS=47,SHOW HITS=NO,SHOWALLPARAMS=NO
      MEAS/SCAN
      BASICSCAN/LINE,NUMBER OF HITS=47,SHOW HITS=NO,SHOWALLPARAMS=NO
      ENDSCAN
      ENDMEAS/
SCN51= BASICSCAN/LINE,NUMBER OF HITS=54,SHOW HITS=NO,SHOWALLPARAMS=NO
      MEAS/SCAN
      BASICSCAN/LINE,NUMBER OF HITS=54,SHOW HITS=NO,SHOWALLPARAMS=NO
      ENDSCAN
      ENDMEAS/
SCN52= BASICSCAN/LINE,NUMBER OF HITS=54,SHOW HITS=NO,SHOWALLPARAMS=NO
      MEAS/SCAN
      BASICSCAN/LINE,NUMBER OF HITS=54,SHOW HITS=NO,SHOWALLPARAMS=NO
      ENDSCAN
      ENDMEAS/
SCN53= BASICSCAN/LINE,NUMBER OF HITS=53,SHOW HITS=NO,SHOWALLPARAMS=NO
      MEAS/SCAN
      BASICSCAN/LINE,NUMBER OF HITS=53,SHOW HITS=NO,SHOWALLPARAMS=NO
      ENDSCAN
      ENDMEAS/
PLANE10= FEAT/PLANE,CARTESIAN,TRIANGLE,NO
        THEO/<-0.749,-7.292,-3.753>,<-0.8655871,0.5007117,0.0068399>
        ACTL/<-0.7,-7.237,-3.882>,<-0.866559,0.499027,-0.0068911>
        CONSTR/PLANE,BF,SCN46,SCN47,SCN48,SCN49,,
PLANE11= FEAT/PLANE,CARTESIAN,TRIANGLE,NO
        THEO/<-5.77,-4.042,-3.642>,<0.8668178,-0.4984742,-0.0122625>
        ACTL/<-5.857,-4.171,-3.691>,<0.8664572,-0.4991852,-0.0081311>
        CONSTR/PLANE,BF,SCN50,SCN51,SCN52,SCN53,,
PLANE12= FEAT/PLANE,CARTESIAN,TRIANGLE,NO
        THEO/<-3.308,-5.641,-3.657>,<-0.866023,0.4999986,0.0023363>
        ACTL/<-3.279,-5.704,-3.786>,<-0.8665325,0.4991202,0.00062>
        CONSTR/PLANE,MID,PIANO10,PIANO11
CIRCLE29= FEAT/CIRCLE,CARTESIAN,IN,LEAST_SQR,NO
        THEO/<0,0,-3.75>,<0,0,1>,21.150
        ACTL/<0,-0.019,-3.748>,<0,0,1>,21.06

```

CONSTR/CIRCLE,BF,2D,CYL3,CYL5,CYL7,,
 CIRCLE30= FEAT/CIRCLE,CARTESIAN,IN,LEAST_SQR,NO
 THEO/<0,0,-3.75>,<0,0,1>,22.700
 ACTL/<0.015,0.004,-3.749>,<0,0,1>,22.638
 CONSTR/CIRCLE,BF,2D,CYL2,CYL4,CYL6,,
 MOVE/CLEARPLANE
 SCN54= FEAT/SCAN,LINEAROPEN,NUMBER OF HITS=182,SHOW HITS=NO,SHOWALLPARAMS=NO
 MEAS/SCAN
 BASICSCAN/LINE,NUMBER OF HITS=182,SHOW HITS=NO,SHOWALLPARAMS=NO
 ENDSCAN
 ENDMEAS/
 MOVE/CLEARPLANE

SCN55=FEAT/SCAN,LINEAROPEN,NUMBER OF HITS=80,SHOW HITS=NO,SHOWALLPARAMS=NO
 MEAS/SCAN
 BASICSCAN/LINE,NUMBER OF HITS=80,SHOW HITS=NO,SHOWALLPARAMS=NO
 ENDSCAN
 ENDMEAS/

PIANO13= FEAT/PLANE,CARTESIAN,TRIANGLE,NO
 THEO/<2.572,38.428,-7.300>,<0.5560411,0.8311543,-0.0009755>
 ACTL/<2.583,38.402,-7.287>,<0.5479745,0.8364945,-0.000987>
 CONSTR/PLANE,MID,SCN54,SCN55

DIM ANG1= 2D ANGLE FROM PLANE PLANE6 TO PLANE PLANE9,\$
 GRAPH=OFF, TEXT=OFF, MULT=1000.00, OUTPUT=BOTH

AX	NOMINAL	MEAS	+TOL	-TOL	DEV	OUTTOL
α	-120°	-119.963	0.05	-0.05	0.037	0

DIM ANG2= 2D ANGLE FROM PLANE PIANO6 TO PLANE PIANO12,\$
 GRAPH=OFF, TEXT=OFF, MULT=1000.00, OUTPUT=BOTH

AX	NOMINAL	MEAS	+TOL	-TOL	DEV	OUTTOL
α	120°	119.942	0.05	-0.05	0.058	-0.008

DATDEF/FEATURE=PLANE3,A
 DATDEF/FEATURE=CYL1,B

FCFPERP1=PERPENDICULARITY OF CyL1
 FEATCTRLFRAME/SHOWNOMS=NO,SHOWPARAMS=YES,SHOWEXPANDED=YES
 CADGRAPH=OFF,REPORTGRAPH=OFF,TEXT=OFF,MULT=1000.00,ARROWDENSITY=100,OUTPUT=
 BOTH,UNITS=MM
 SIZE TOLERANCES/1,DIAMETER,30.42,0.01,-0.01
 DIMENSION/PERPENDICULARITY,0.01,<PZ>,<len>,A,<dat>,<dat>
 NOTE/FCFPERP1
 FEATURES/CYL1,,

FCFPERP2=PERPENDICULARITY OF CYL2
 FEATCTRLFRAME/SHOWNOMS=NO,SHOWPARAMS=YES,SHOWEXPANDED=YES
 CADGRAPH=OFF,REPORTGRAPH=OFF,TEXT=OFF,MULT=1000.00,ARROWDENSITY=100,OUTPUT=
 BOTH,UNITS=MM
 SIZE TOLERANCES/1,DIAMETER,4.906,0.01,-0.01
 DIMENSION/PERPENDICULARITY,0.01,<PZ>,<len>,A,<dat>,<dat>
 NOTE/FCFPERP2
 FEATURES/CYL2,,

FCFPERP3=PERPENDICULARITY OF CYL3
 FEATCTRLFRAME/SHOWNOMS=NO,SHOWPARAMS=YES,SHOWEXPANDED=YES
 CADGRAPH=OFF,REPORTGRAPH=OFF,TEXT=OFF,MULT=1000.00,ARROWDENSITY=100,OUTPUT=
 BOTH,UNITS=MM

SIZE TOLERANCES/1,DIAMETER,5.895,0.01,-0.01
DIMENSION/PERPENDICULARITY,0.01,<PZ>,<len>,A,<dat>,<dat>
NOTE/FCFPERP3
FEATURES/CYL3,,

FCFPERP4=PERPENDICULARITY OF CYL4

FEATCTRLFRAME/SHOWNOMS=NO,SHOWPARAMS=YES,SHOWEXPANDED=YES
CADGRAPH=OFF,REPORTGRAPH=OFF,TEXT=OFF,MULT=1000.00,ARROWDENSITY=100,OUTPUT=
BOTH,UNITS=MM
SIZE TOLERANCES/1,DIAMETER,4.906,0.01,-0.01
DIMENSION/PERPENDICULARITY,0.01,<PZ>,<len>,A,<dat>,<dat>
NOTE/FCFPERP4
FEATURES/CYL4,,

FCFPERP5=PERPENDICULARITY OF CYL5

FEATCTRLFRAME/SHOWNOMS=NO,SHOWPARAMS=YES,SHOWEXPANDED=YES
CADGRAPH=OFF,REPORTGRAPH=OFF,TEXT=OFF,MULT=1000.00,ARROWDENSITY=100,OUTPUT=
BOTH,UNITS=MM
SIZE TOLERANCES/1,DIAMETER,5.895,0.01,-0.01
DIMENSION/PERPENDICULARITY,0.01,<PZ>,<len>,A,<dat>,<dat>
NOTE/FCFPERP5
FEATURES/CYL5,,

FCFPERP6=PERPENDICULARITY OF CYL6

FEATCTRLFRAME/SHOWNOMS=NO,SHOWPARAMS=YES,SHOWEXPANDED=YES
CADGRAPH=OFF,REPORTGRAPH=OFF,TEXT=OFF,MULT=1000.00,ARROWDENSITY=100,OUTPUT=
BOTH,UNITS=MM
SIZE TOLERANCES/1,DIAMETER,4.906,0.01,-0.01
DIMENSION/PERPENDICULARITY,0.01,<PZ>,<len>,A,<dat>,<dat>
NOTE/FCFPERP6
FEATURES/CYL6,,

FCFPERP7=PERPENDICULARITY OF CYL7

FEATCTRLFRAME/SHOWNOMS=NO,SHOWPARAMS=YES,SHOWEXPANDED=YES
CADGRAPH=OFF,REPORTGRAPH=OFF,TEXT=OFF,MULT=1000.00,ARROWDENSITY=100,OUTPUT=
BOTH,UNITS=MM
SIZE TOLERANCES/1,DIAMETER,5.895,0.01,-0.01
DIMENSION/PERPENDICULARITY,0.01,<PZ>,<len>,A,<dat>,<dat>
NOTE/FCFPERP7
FEATURES/CYL7,,

FCFCONCEN1=CONCENTRICITY OF CIRCLE29

FEATCTRLFRAME/SHOWPARAMS=YES,SHOWEXPANDED=YES
CADGRAPH=OFF,REPORTGRAPH=OFF,TEXT=OFF,MULT=1000.00,ARROWDENSITY=100,OUTPUT=
BOTH,UNITS=MM
CUSTOMIZED DRF=NO
DIMENSION/CONCENTRICITY,DIAMETER,0.01,B
NOTE/FCFCONCEN1
FEATURES/CIRCLE29,,

FCFCONCEN2=CONCENTRICITY OF CIRCLE30

FEATCTRLFRAME/SHOWPARAMS=YES,SHOWEXPANDED=YES
CADGRAPH=OFF,REPORTGRAPH=OFF,TEXT=OFF,MULT=1000.00,ARROWDENSITY=100,OUTPUT=
BOTH,UNITS=MM
CUSTOMIZED DRF=NO
DIMENSION/CONCENTRICITY,DIAMETER,0.01,B
NOTE/FCFCONCEN2

FEATURES/CIRLCE30,,

DIM DIST1= 3D DISTANCE FROM PLANE PLANE4 TO PLANE PLANE5, SHORTEST=OFF, NO_RADIUS
UNITS=MM GRAPH=OFFTEXT=OFFMULT=1000.00 OUTPUT=BOTH

AX	NOMINAL	MEAS	+TOL	-TOL	DEV	OUTTOL
H	6.00	5.990	0.01	-0.01	-0.010	0.000

DIM DIST2= 3D DISTANCE FROM PLANE PLANE7 TO PLANE PLANE8 SHORTEST=OFF, NO_RADIUS
UNITS=MM GRAPH=OFFTEXT=OFFMULT=1000.00 OUTPUT=BOTH

AX	NOMINAL	MEAS	+TOL	-TOL	DEV	OUTTOL
H	6.00	5.960	0.01	-0.01	-0.04	-0.03

DIM DIST3= 3D DISTANCE FROM PLANE PLANE10 TO PLANE PLANE11 SHORTEST=OFF, NO_RADIUS
UNITS=MM GRAPH=OFFTEXT=OFFMULT=1000.00 OUTPUT=BOTH

AX	NOMINAL	MEAS	+TOL	-TOL	DEV	OUTTOL
H	6.00	6.001	0.01	-0.01	+0.001	0.000

DIM DIST4= 3D DISTANCE FROM CYLINDER CYL1 TO CYLINDER CYL2 SHORTEST=OFF, NO_RADIUS
UNITS=MM GRAPH=OFFTEXT=OFFMULT=1000.00 OUTPUT=BOTH

AX	NOMINAL	MEAS	+TOL	-TOL	DEV	OUTTOL
D	11.500	11.332	0.2	-0.2	-0.168	0.000

DIM DIST5= 3D DISTANCE FROM CYLINDER CYL1 TO CYLINDER CYL3 SHORTEST=OFF, NO_RADIUS
UNITS=MM GRAPH=OFFTEXT=OFFMULT=1000.00 OUTPUT=BOTH

AX	NOMINAL	MEAS	+TOL	-TOL	DEV	OUTTOL
D	10.700	10.549	0.2	-0.2	-0.151	0.000

DIM DIST6= 3D DISTANCE FROM CYLINDER CYL1 TO CYLINDER CYL4 SHORTEST=OFF, NO_RADIUS
UNITS=MM GRAPH=OFFTEXT=OFFMULT=1000.00 OUTPUT=BOTH

AX	NOMINAL	MEAS	+TOL	-TOL	DEV	OUTTOL
D	11.500	11.326	0.2	-0.2	-0.174	0.000

DIM DIST7= 3D DISTANCE FROM CYLINDER CYL1 TO CYLINDER CYL5 SHORTEST=OFF, NO_RADIUS
UNITS=MM GRAPH=OFFTEXT=OFFMULT=1000.00 OUTPUT=BOTH

AX	NOMINAL	MEAS	+TOL	-TOL	DEV	OUTTOL
D	10.700	10.511	0.2	-0.2	-0.189	0.000

DIM DIST8= 3D DISTANCE FROM CYLINDER CYL1 TO CYLINDER CYL6 SHORTEST=OFF, NO_RADIUS
UNITS=MM GRAPH=OFFTEXT=OFFMULT=1000.00 OUTPUT=BOTH

AX	NOMINAL	MEAS	+TOL	-TOL	DEV	OUTTOL
D	11.500	11.297	0.2	-0.2	-0.203	-0.003

DIM DIST9= 3D DISTANCE FROM CYLINDER CYL1 TO CYLINDER CYL7 SHORTEST=OFF, NO_RADIUS
UNITS=MM GRAPH=OFFTEXT=OFFMULT=1000.00 OUTPUT=BOTH

AX	NOMINAL	MEAS	+TOL	-TOL	DEV	OUTTOL
D	10.700	10.523	0.2	-0.2	-0.177	0.000

DIM DIST10= 3D DISTANCE FROM CYLINDER CYL2 TO CYLINDER CYL3 SHORTEST=OFF, NO_RADIUS
UNITS=MM GRAPH=OFFTEXT=OFFMULT=1000.00 OUTPUT=BOTH

AX	NOMINAL	MEAS	+TOL	-TOL	DEV	OUTTOL
D	6.600	6.587	0.2	-0.2	-0.013	0.000

DIM DIST11= 3D DISTANCE FROM CYLINDER CYL4 TO CYLINDER CYL5 SHORTEST=OFF, NO_RADIUS
UNITS=MM GRAPH=OFFTEXT=OFFMULT=1000.00 OUTPUT=BOTH

AX	NOMINAL	MEAS	+TOL	-TOL	DEV	OUTTOL
D	6.600	6.596	0.2	-0.2	-0.003	0.000

DIM DIST12= 3D DISTANCE FROM CYLINDER CYL6 TO CYLINDER CYL7 SHORTEST=OFF, NO_RADIUS
UNITS=MM GRAPH=OFFTEXT=OFFMULT=1000.00 OUTPUT=BOTH

AX	NOMINAL	MEAS	+TOL	-TOL	DEV	OUTTOL
D	6.600	6.601	0.2	-0.2	+0.001	0.000

DIM DIST13= 3D DISTANCE FROM PLANE PLANE13 TO PLANE PLANE3, SHORTEST=OFF, NO_RADIUS
UNITS=MM GRAPH=OFFTEXT=OFFMULT=1000.00 OUTPUT=BOTH

AX	NOMINAL	MEAS	+TOL	-TOL	DEV	OUTTOL
H	7.25	7.264	0.01	-0.01	+0.014	0.000

DIM POS1= LOCATION OF CYLINDER CYL1, UNITS=MM, GRAPH=OFF, TEXT=OFF, MULT=1000.00,
OUTPUT=BOTH, HALF ANGLE=NO

AX	NOMINAL	MEAS	+TOL	-TOL	DEV	OUTTOL
Φ	30.400	30.420	0.2	-0.2	+0.020	0.000

END OF DIMENSION POS1

DIM POS2= LOCATION OF CYLINDER CYL2, UNITS=MM, GRAPH=OFF, TEXT=OFF, MULT=1000.00,
OUTPUT=BOTH, HALF ANGLE=NO

AX	NOMINAL	MEAS	+TOL	-TOL	DEV	OUTTOL
PA	40.000°	40.094	0.1	-0.1	0.094	0.000
Φ	4.900	4.896	0.1	-0.1	-0.004	0.000

END OF DIMENSION POS2

DIM POS3= LOCATION OF CYLINDER CYL3, UNITS=MM, GRAPH=OFF, TEXT=OFF, MULT=1000.00,
OUTPUT=BOTH, HALF ANGLE=NO

AX	NOMINAL	MEAS	+TOL	-TOL	DEV	OUTTOL
PA	-75.000	-74.911	0.1	-0.1	-0.089	0.000
Φ	5.900	5.887	0.1	-0.1	-0.013	0.000

END OF DIMENSION POS3

DIM POS4= LOCATION OF CYLINDER CYL4, UNITS=MM, GRAPH=OFF, TEXT=OFF, MULT=1000.00,
OUTPUT=BOTH, HALF ANGLE=NO

AX	NOMINAL	MEAS	+TOL	-TOL	DEV	OUTTOL
PA	-80.000	-79.997	0.1	-0.1	-0.003	0.000
Φ	4.900	4.895	0.1	-0.1	-0.015	0.000

END OF DIMENSION POS4

DIM POS5= LOCATION OF CYLINDER CYL5, UNITS=MM, GRAPH=OFF, TEXT=OFF, MULT=1000.00,
OUTPUT=BOTH, HALF ANGLE=NO

AX	NOMINAL	MEAS	+TOL	-TOL	DEV	OUTTOL
PA	45.00	45.094	0.1	-0.1	0.094	0.000
Φ	5.900	5.887	0.1	-0.1	-0.013	0.000

END OF DIMENSION POS5

DIM POS6= LOCATION OF CYLINDER CYL6, UNITS=MM, GRAPH=OFF, TEXT=OFF, MULT=1000.00,
OUTPUT=BOTH, HALF ANGLE=NO

AX	NOMINAL	MEAS	+TOL	-TOL	DEV	OUTTOL
PA	-160.00	-160.087	0.1	-0.1	+0.087	0.000
Φ	4.900	4.897	0.1	-0.1	-0.003	0.000

END OF DIMENSION POS6

DIM POS7= LOCATION OF CYLINDER CY7, UNITS=MM, GRAPH=OFF, TEXT=OFF, MULT=1000.00,
OUTPUT=BOTH, HALF ANGLE=NO

AX	NOMINAL	MEAS	+TOL	-TOL	DEV	OUTTOL
PA	165.00	164.939	0.1	-0.1	0.061	0.000
Φ	5.900	5.887	0.1	-0.1	-0.013	0.000

END OF DIMENSION POS7

DIM POS8= LOCATION OF CIRCLE CIRCLE2, UNITS=MM, GRAPH=OFF, TEXT=OFF, MULT=1000.00,
OUTPUT=BOTH, HALF ANGLE=NO

AX	NOMINAL	MEAS	+TOL	-TOL	DEV	OUTTOL
Φ	30.400	30.431	0.2	-0.2	+0.031	0.000

END OF DIMENSION POS8

DIM POS9= LOCATION OF CIRCLE CIRCLE3, UNITS=MM, GRAPH=OFF, TEXT=OFF, MULT=1000.00,
OUTPUT=BOTH, HALF ANGLE=NO

AX	NOMINAL	MEAS	+TOL	-TOL	DEV	OUTTOL
Φ	30.400	30.385	0.2	-0.2	-0.015	0.000

END OF DIMENSION POS9

DIM POS10= LOCATION OF CIRCLE CIRCLE4, UNITS=MM, GRAPH=OFF, TEXT=OFF, MULT=1000.00,
OUTPUT=BOTH, HALF ANGLE=NO

AX	NOMINAL	MEAS	+TOL	-TOL	DEV	OUTTOL
Φ	30.400	30.397	0.2	-0.2	-0.003	0.000

END OF DIMENSION POS10

DIM POS11= LOCATION OF CIRCLE CIRCLE5, UNITS=MM, GRAPH=OFF, TEXT=OFF, MULT=1000.00,
OUTPUT=BOTH, HALF ANGLE=NO

AX	NOMINAL	MEAS	+TOL	-TOL	DEV	OUTTOL
Φ	4.900	4.895	0.1	-0.1	-0.005	0.000

END OF DIMENSION POS11

DIM POS12= LOCATION OF CIRCLE CIRCLE6, UNITS=MM, GRAPH=OFF, TEXT=OFF, MULT=1000.00,
OUTPUT=BOTH, HALF ANGLE=NO

AX	NOMINAL	MEAS	+TOL	-TOL	DEV	OUTTOL
Φ	4.900	4.897	0.1	-0.1	-0.003	0.000

END OF DIMENSION POS12

DIM POS13= LOCATION OF CIRCLE CIRCLE7, UNITS=MM, GRAPH=OFF, TEXT=OFF, MULT=1000.00,
OUTPUT=BOTH, HALF ANGLE=NO

AX	NOMINAL	MEAS	+TOL	-TOL	DEV	OUTTOL
Φ	4.900	4.898	0.1	-0.1	-0.002	0.000

END OF DIMENSION POS13

DIM POS14= LOCATION OF CIRCLE CIRCLE8, UNITS=MM, GRAPH=OFF, TEXT=OFF, MULT=1000.00,
OUTPUT=BOTH, HALF ANGLE=NO

AX	NOMINAL	MEAS	+TOL	-TOL	DEV	OUTTOL
Φ	4.900	4.895	0.1	-0.1	-0.005	0.000

END OF DIMENSION POS14

DIM POS15= LOCATION OF CIRCLE CIRCLE9, UNITS=MM, GRAPH=OFF, TEXT=OFF, MULT=1000.00,
OUTPUT=BOTH, HALF ANGLE=NO

AX	NOMINAL	MEAS	+TOL	-TOL	DEV	OUTTOL
Φ	5.900	5.883	0.1	-0.1	-0.017	0.000

END OF DIMENSION POS15

DIM POS16= LOCATION OF CIRCLE CIRCLE10, UNITS=MM, GRAPH=OFF, TEXT=OFF, MULT=1000.00,
OUTPUT=BOTH, HALF ANGLE=NO

AX	NOMINAL	MEAS	+TOL	-TOL	DEV	OUTTOL
Φ	5.900	5.887	0.1	-0.1	-0.013	0.000

END OF DIMENSION POS16

DIM POS17= LOCATION OF CIRCLE CIRCLE11, UNITS=MM, GRAPH=OFF, TEXT=OFF, MULT=1000.00,
OUTPUT=BOTH, HALF ANGLE=NO

AX	NOMINAL	MEAS	+TOL	-TOL	DEV	OUTTOL
Φ	5.900	5.889	0.1	-0.1	-0.011	0.000

END OF DIMENSION POS17

DIM POS18= LOCATION OF CIRCLE CIRCLE12, UNITS=MM, GRAPH=OFF, TEXT=OFF, MULT=1000.00,
OUTPUT=BOTH, HALF ANGLE=NO

AX	NOMINAL	MEAS	+TOL	-TOL	DEV	OUTTOL
Φ	5.900	5.889	0.1	-0.1	-0.011	0.000

END OF DIMENSION POS18

DIM POS19= LOCATION OF CIRCLE CIRCLE13, UNITS=MM, GRAPH=OFF, TEXT=OFF, MULT=1000.00,
OUTPUT=BOTH, HALF ANGLE=NO

AX	NOMINAL	MEAS	+TOL	-TOL	DEV	OUTTOL
Φ	4.900	4.893	0.1	-0.1	-0.007	0.000

END OF DIMENSION POS19

DIM POS20= LOCATION OF CIRCLE CIRCLE14, UNITS=MM, GRAPH=OFF, TEXT=OFF, MULT=1000.00,
OUTPUT=BOTH, HALF ANGLE=NO

AX	NOMINAL	MEAS	+TOL	-TOL	DEV	OUTTOL
Φ	4.900	4.895	0.1	-0.1	-0.005	0.000

END OF DIMENSION POS20

DIM POS21= LOCATION OF CIRCLE CIRCLE15, UNITS=MM, GRAPH=OFF, TEXT=OFF, MULT=1000.00,
OUTPUT=BOTH, HALF ANGLE=NO

AX	NOMINAL	MEAS	+TOL	-TOL	DEV	OUTTOL
Φ	4.900	4.896	0.1	-0.1	-0.004	0.000

END OF DIMENSION POS21

DIM POS22= LOCATION OF CIRCLE CIRCLE16, UNITS=MM, GRAPH=OFF, TEXT=OFF, MULT=1000.00,
OUTPUT=BOTH, HALF ANGLE=NO

AX	NOMINAL	MEAS	+TOL	-TOL	DEV	OUTTOL
Φ	4.900	4.896	0.1	-0.1	-0.004	0.000

END OF DIMENSION POS22

DIM POS23= LOCATION OF CIRCLE CIRCLE17, UNITS=MM, GRAPH=OFF, TEXT=OFF, MULT=1000.00,
OUTPUT=BOTH, HALF ANGLE=NO

AX	NOMINAL	MEAS	+TOL	-TOL	DEV	OUTTOL
Φ	5.900	5.883	0.1	-0.1	-0.017	0.000

END OF DIMENSION POS23

DIM POS24= LOCATION OF CIRCLE CIRCLE18, UNITS=MM, GRAPH=OFF, TEXT=OFF, MULT=1000.00,
OUTPUT=BOTH, HALF ANGLE=NO

AX	NOMINAL	MEAS	+TOL	-TOL	DEV	OUTTOL
Φ	5.900	5.884	0.1	-0.1	-0.016	0.000

END OF DIMENSION POS24

DIM POS25= LOCATION OF CIRCLE CIRCLE19, UNITS=MM, GRAPH=OFF, TEXT=OFF, MULT=1000.00,
OUTPUT=BOTH, HALF ANGLE=NO

AX	NOMINAL	MEAS	+TOL	-TOL	DEV	OUTTOL
Φ	5.900	5.884	0.1	-0.1	-0.016	0.000

END OF DIMENSION POS25

DIM POS26= LOCATION OF CIRCLE CIRCLE20, UNITS=MM, GRAPH=OFF, TEXT=OFF, MULT=1000.00,
OUTPUT=BOTH, HALF ANGLE=NO

AX	NOMINAL	MEAS	+TOL	-TOL	DEV	OUTTOL
Φ	5.900	5.882	0.1	-0.1	-0.018	0.000

END OF DIMENSION POS26

DIM POS27= LOCATION OF CIRCLE CIRCLE21, UNITS=MM, GRAPH=OFF, TEXT=OFF, MULT=1000.00,
OUTPUT=BOTH, HALF ANGLE=NO

AX	NOMINAL	MEAS	+TOL	-TOL	DEV	OUTTOL
Φ	4.900	4.893	0.1	-0.1	-0.007	0.000

END OF DIMENSION POS27

DIM POS28= LOCATION OF CIRCLE CIRCLE22, UNITS=MM, GRAPH=OFF, TEXT=OFF, MULT=1000.00,
OUTPUT=BOTH, HALF ANGLE=NO

AX	NOMINAL	MEAS	+TOL	-TOL	DEV	OUTTOL
Φ	4.900	4.897	0.1	-0.1	-0.003	0.000

END OF DIMENSION POS20

DIM POS29= LOCATION OF CIRCLE CIRCLE23, UNITS=MM, GRAPH=OFF, TEXT=OFF, MULT=1000.00,
OUTPUT=BOTH, HALF ANGLE=NO

AX	NOMINAL	MEAS	+TOL	-TOL	DEV	OUTTOL
Φ	4.900	4.899	0.1	-0.1	-0.001	0.000

END OF DIMENSION POS29

DIM POS30= LOCATION OF CIRCLE CIRCLE24, UNITS=MM, GRAPH=OFF, TEXT=OFF, MULT=1000.00,
OUTPUT=BOTH, HALF ANGLE=NO

AX	NOMINAL	MEAS	+TOL	-TOL	DEV	OUTTOL
Φ	4.900	4.899	0.1	-0.1	-0.001	0.000

END OF DIMENSION POS30

DIM POS31= LOCATION OF CIRCLE CIRCLE25, UNITS=MM, GRAPH=OFF, TEXT=OFF, MULT=1000.00,
OUTPUT=BOTH, HALF ANGLE=NO

AX	NOMINAL	MEAS	+TOL	-TOL	DEV	OUTTOL
Φ	5.900	5.882	0.1	-0.1	-0.018	0.000

END OF DIMENSION POS31

DIM POS32= LOCATION OF CIRCLE CIRCLE26, UNITS=MM, GRAPH=OFF, TEXT=OFF, MULT=1000.00,
OUTPUT=BOTH, HALF ANGLE=NO

AX	NOMINAL	MEAS	+TOL	-TOL	DEV	OUTTOL
Φ	5.900	5.884	0.1	-0.1	-0.016	0.000

END OF DIMENSION POS32

DIM POS33= LOCATION OF CIRCLE CIRCLE27, UNITS=MM, GRAPH=OFF, TEXT=OFF, MULT=1000.00,
OUTPUT=BOTH, HALF ANGLE=NO

AX	NOMINAL	MEAS	+TOL	-TOL	DEV	OUTTOL
Φ	5.900	5.886	0.1	-0.1	-0.014	0.000

END OF DIMENSION POS33

DIM POS34= LOCATION OF CIRCLE CIRCLE28, UNITS=MM, GRAPH=OFF, TEXT=OFF, MULT=1000.00,
OUTPUT=BOTH, HALF ANGLE=NO

AX	NOMINAL	MEAS	+TOL	-TOL	DEV	OUTTOL
Φ	5.900	5.885	0.1	-0.1	-0.015	0.000

END OF DIMENSION POS34

DIM POS35= LOCATION OF CIRCLE CIRCLE29, UNITS=MM, GRAPH=OFF, TEXT=OFF, MULT=1000.00,
OUTPUT=BOTH, HALF ANGLE=NO

AX	NOMINAL	MEAS	+TOL	-TOL	DEV	OUTTOL
Φ	21.400	21.060	0.4	-0.4	-0.340	0.000

END OF DIMENSION POS35

DIM POS36= LOCATION OF CIRCLE CIRCLE30, UNITS=MM, GRAPH=OFF, TEXT=OFF, MULT=1000.00,
OUTPUT=BOTH, HALF ANGLE=NO

AX	NOMINAL	MEAS	+TOL	-TOL	DEV	OUTTOL
Φ	23.000	22.638	0.4	-0.4	-0.362	0.000

END OF DIMENSION POS36